A Szilikátipari Tudományos Egyesület lapja

építőanyag

Journal of Silicate Based and Composite Materials

A TARTALOMBÓL:

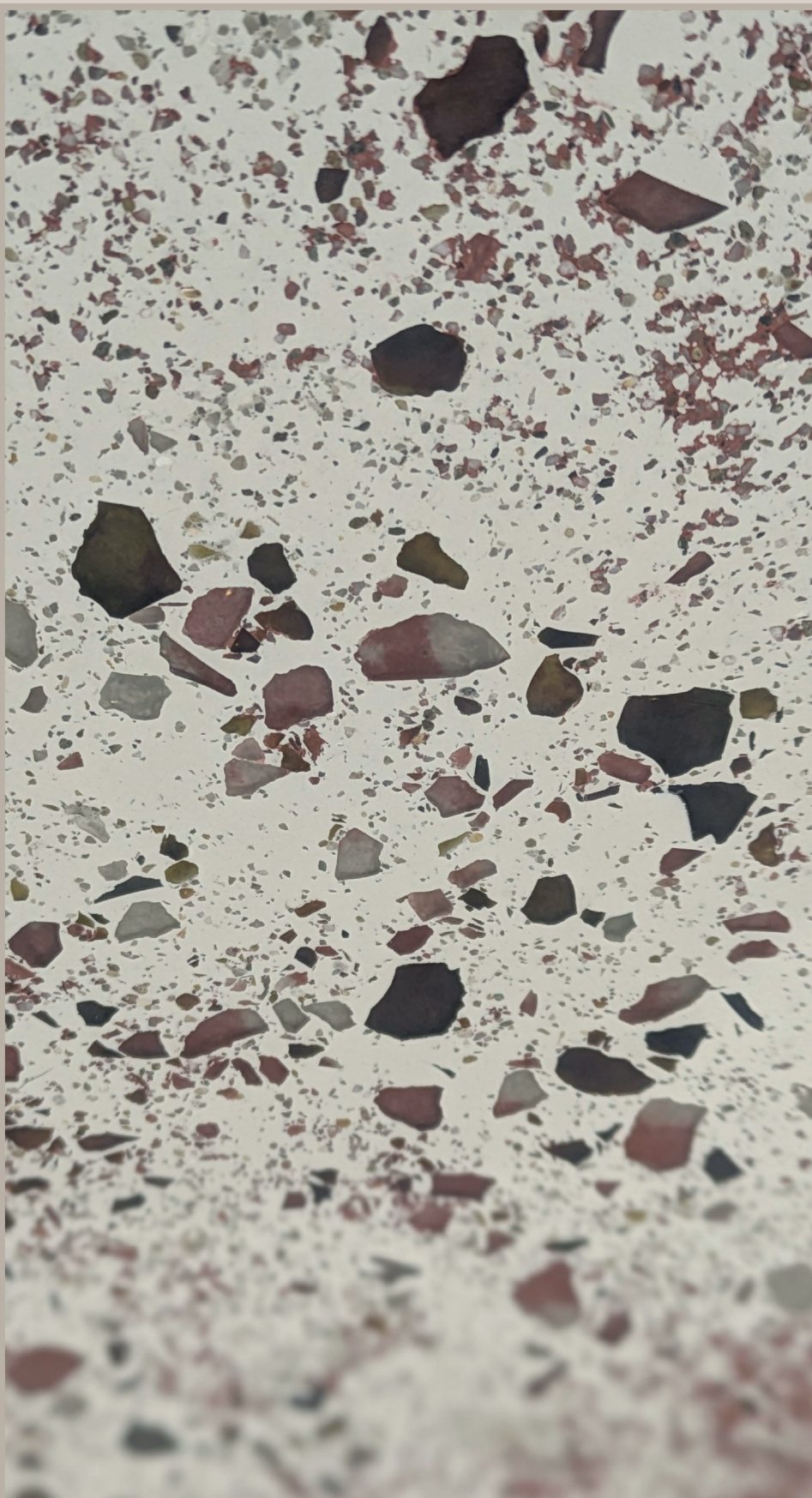

2025/3

Central European Congress on Concrete Engineering

vodiCCCe 2026

15th Central European Congress on Concrete Engineering
Vodice, Croatia
5-7/10/2026

We are pleased to announce the upcoming 15th Central European Congress on Concrete Engineering, to be held in the beautiful coastal town of Vodice in Croatia. This year's theme "Sustainable and Innovative Engineering Solutions for Concrete Design Challenges and Practices" will bring together experts, researchers, academics, and industry professionals to explore advanced approaches, share experiences, and inspire future developments. Whether you are involved in design, construction, research, or policy-making, this congress is an excellent opportunity to connect, collaborate, and contribute to the advancement of concrete engineering across Central Europe and beyond.

We look forward to welcoming you to Vodice for an engaging and inspiring event!

CONGRESS TOPICS

1. Materials
2. Concrete structures, including precast and composite structures
3. Design and analysis of concrete structures
4. Technology and construction methods
5. Sustainability, life cycle assessment and climate change adaptation
6. Maintenance, protection, rehabilitation and strengthening
7. Hazards (explosion, floods, earthquake, fire, storms, landslides, winds)
8. Advances in concrete structures (automation, digital fabrication, robotics, additive manufacturing, design process optimization, AI and BIM)

https://sites.google.com/arhitekt.hr/ccc-2026-vodice/home

aci fib CEB-FIP rilem

ACI-*fib*-RILEM Workshop Call

September 28 to 30, 2026
Budapest, Hungary

ACI-*fib*-RILEM 2026 FRC WORKSHOP BUDAPEST

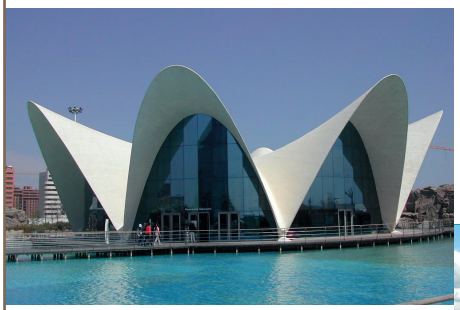

Steel fiber reinforced concrete thin shell structure
Oceanographic Park Restaurant. *City of Arts and Sciences*, Valencia (2002)
Based on blueprint of Felix Candela, by: A. Domingo, C. Lázaro, P. Serna

fib CEB-FIP Hungary

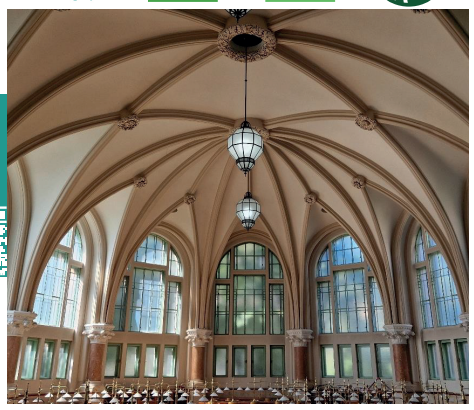

Library of the Budapest University of Tecnology and Ecconomics

Venue – BME Budapest

Budapest University of Technology and Economics was founded in 1782 and it has been regarded as Hungary's number one technical higher education institution for more than 240 years.

Budapest, resting gracefully along the Danube, harmonizes centuries of history with a vibrant present. Landmarks like Buda Castle and Matthias Church echo tales of the past, while District VII's lively atmosphere embodies modern creativity in its eclectic bars and cafes. Art and culture thrive here, from the grandeur of the Hungarian State Opera House to the avant-garde exhibitions at the Ludwig Museum.

Topics

1. Design specifications for applications
   - A. *fib* Model Code 2020
   - B. Standards and design specifications
   - C. Enhanced material behaviour and modelling
   - D. Enhanced structural behaviour and modelling in reinforced and in prestressed concrete members
2. Structural applications
   - A. Buildings, Bridges, Foundations
   - B. Tunnels
   - C. Prefabrication
   - D. Concrete industrial floors
3. Sustainability, Durability, Serviceability
   - A. Design aspects for sustainability and durability. Life Cycle Assessment.
   - B. Serviceability aspects: cracking, ~~first crack,~~ crack pattern, spacing of cracks, crack widths, increase of crack width
4. Design aspects for long term and extreme loads
   - A. Long term behaviour and modelling for shrinkage, creep, fatigue
   - B. FRC under fire, impact or blast loading.
5. Retrofitting and strengthening of existing structures
6. Fibres in new types of concretes and in 3D printed concretes

Sponsorship opportunities

We offer levels of sponsorship: Diamond (8,000 EUR), Gold (5,000 EUR), Silver (2,500 EUR), and Standard (1,000 EUR). Diamond and Gold sponsors receive exhibition space (larger for diamond). Diamond, Gold and Silver receive complimentary workshop registrations (4 for Diamond, 3 for Gold and 2 for Silver). All sponsors will have their logo displayed and name acknowledged during the opening and closing ceremonies, in the workshop proceedings, and on-site materials such as flyers and roll-ups. To become a sponsor, please provide your company details, and the sponsorship fee must be transferred prior to the workshop.
Additionally a Platinum sponsorship level is also considerded and prize is assigned on special topic proposed by the Sponsor.

Contact information

Official website:
https://frcworkshop2026.bme.hu
Műegyetem 3, Budapest, H-1111 Hungary
frcworkshop2026@emk.bme.hu

építőanyag
Journal of Silicate Based and Composite Materials
2025/3

TARTALOM

CONTENT

A finomkerámia-, üveg-, cement-, mész-, beton-, tégla- és cserép-, kő- és kavics-, tűzállóanyag-, szigetelőanyag-iparágak szakmai lapja
Scientific journal of ceramics, glass, cement, concrete, clay products, stone and gravel, insulating and fireproof materials and composites

A folyóiratot referálja · The journal is referred by:
A folyóiratban lektorált cikkek jelennek meg.
All published papers are peer-reviewed.
Kiadó · Publisher: Szilikátipari Tudományos Egyesület (SZTE)
Elnök · President: ASZTALOS István
1034 Budapest, Bécsi út 120.
Tel.: +36-1/201-9360 ▪ E-mail: epitoanyag@szte.org.hu
Tördelő szerkesztő · Layout editor: NÉMETH Hajnalka
Címlapfotó · Cover photo: BIRÓ András

WWW.EPITOANYAG.ORG.HU
EN.EPITOANYAG.ORG.HU

Online ISSN: 2064-4477
Print ISSN: 0013-970x
INDEX: 2 52 50 ▪ 77 (2025) 61-99

Predictive modeling of concrete split tensile strength using Scheffe's simplex lattice design with reclaimed asphalt pavement as coarse aggregates

Michael T. TIZA ▪ Physical Planning Unit, Federal Polytechnic Wannune, Benue State, Nigeria ▪ tizamichael@gmail.com
Justin Nsobundu EGBEBIKE ▪ Civil Engineering Department, Rivers State University
Collins ONUZULIKE ▪ Civil Engineering Department, Air Force Institute of Technology, Kaduna, Nigeria
Ezekwesili OKECHUKWU ▪ Highways Materials, Geotechnics, and Quality Control, Federal Ministry of Works, Abuja
Ebenezer O. AKANDE ▪ Civil Engineering Department, Bells University of Technology, Nigeria
Emmanuel OGUNLEYE ▪ Civil Engineering Department, Federal University of Technology Akure, Nigeria

Érkezett: 2025. 06. 02. ▪ Received: 02. 06. 2025. ▪ https://doi.org/10.14382/epitoanyag-jsbcm.2025.9

Abstract

This study employs Scheffe's Simplex Lattice Design to predict and optimize the split tensile strength of concrete incorporating reclaimed asphalt pavement (RAP) as a partial replacement for natural coarse aggregates. A {5,2} augmented Simplex Lattice, executed in Minitab 22, generated 21 experimental runs to evaluate the effects of cement, sand, water, natural coarse aggregates, and RAP. Pseudo-components were transformed into real ratios using a matrix-based approach, ensuring accurate mixture proportion representation. A quadratic regression model, with an R^2 of 92.89% and a significant F-value of 0.98 ($p = 0.049$), demonstrated strong predictive accuracy. All main components exhibited significant effects, with low variance inflation factors (VIF ≈ 1.59) indicating minimal multicollinearity. Optimal split tensile strength (3.14 N/mm^2) was observed in a sand-dominated mixture (Run 18), closely matching the predicted 3.118 N/mm^2. Experimental results highlighted that a 75% RAP replacement maximized 28-day split tensile strength (3.05 N/mm^2), suggesting RAP's viability as a sustainable aggregate. Residual analysis and a lack-of-fit p-value of 0.032 confirmed model adequacy. These findings offer a robust framework for optimizing concrete mixtures, advancing sustainable construction practices and predictive modeling in civil engineering.

Keywords: concrete, split tensile strength, scheffe's simplex lattice, reclaimed asphalt pavement, mixture design, predictive modeling
Kulcsszavak: beton, hasító-húzószilárdság, Scheffe-féle szimplex rács, újrahasznosított aszfaltburkolat (RAP), keveréktervezés, prediktív modellezés

1. Introduction

The split tensile strength of concrete is a critical parameter influencing the durability and structural integrity of concrete members subjected to tensile stresses [1]. Unlike compressive strength, which is more commonly studied, tensile strength is often more challenging to predict due to the heterogeneous and brittle nature of concrete. Accurate modeling of split tensile strength is essential for the design and optimization of concrete mixes, especially when incorporating alternative materials [2]. These materials can alter the microstructure and mechanical behavior of concrete, necessitating robust predictive tools to ensure performance consistency [3], [4].

Scheffe's simplex lattice design has been widely adopted as an effective statistical tool for modeling and optimizing concrete properties involving multiple mixture components. This approach allows researchers to systematically explore the effects of varying proportions of constituents on mechanical properties, including strength parameters [5], [6]. For instance, prior studies have successfully employed Scheffe's method to model compressive strength and modulus of rupture in concretes incorporating waste materials, illustrating the model's adaptability and predictive power [6], [7]. However, there remains a significant research gap

Michael Toryila TIZA, PhD
is a Nigerian civil engineer specializing in highway and transportation engineering, sustainable construction materials, and related innovations. He earned a B.Eng. in Civil Engineering from the University of Agriculture, Makurdi (2015), an M.Tech/M.Eng. in Transportation Engineering (India, 2017), an MBA in Construction Management, and a Ph.D. in Civil Engineering from the University of Nigeria, Nsukka (2024), with focus on reclaimed asphalt pavement (RAP)-optimized concrete. A COREN-registered engineer (R. Engr.), MNSE member, affiliate of ASCE, and fellow of IOASD (India), CIML (USA), and ISDS (Japan), he currently serves as Acting Dean of the School of Environmental Studies and Deputy Director of Research & Development at Federal Polytechnic Wannune, Benue State, Nigeria. With an h-index of 12 and he has authored/co-authored over 80 publications.

Justin Nsobundu EGBEBIKE
is a Senior Structural Engineering Researcher at Rivers State University, Port Harcourt, Nigeria. His research focuses on structural engineering and cement-based materials, with particular emphasis on concrete technology, supplementary cementitious materials, and the mechanical behaviour of normal- and high-strength concrete. His work includes experimental and analytical investigations on metakaolin-modified concrete, strength development, and material optimisation for sustainable structural applications.

Collins Obiora ONUZULIKE
is a Lecturer in Civil & Environmental Engineering at the Air Force Institute of Technology (AFIT), Kaduna, teaching environmental engineering, hydrology, hydrogeology, water supply, and disaster management. He holds an M.Sc. in Disaster Risk Management (University of Port Harcourt) and is completing a PhD in Geography & Environmental Management there. His research centers on disaster risk reduction, climate change, infrastructure resilience, flood risk, and sustainable construction. A prolific author of numerous peer-reviewed articles, conference papers, and book chapters, he is a chartered fellow of several international professional bodies, a climate change ambassador, conference speaker, and faith-based leader committed to resilient communities through multidisciplinary research, teaching, and service.

Ezekwesili OKECHUKWU
is a Nigerian civil engineer, hybrid project manager, sustainable infrastructure specialist, and researcher with over 15 years of experience. He holds a B.Eng. in Civil Engineering from Federal University of Technology Owerri (2004–2009) and an M.Eng. from University of Nigeria, Nsukka (2013–2015), and has completed Ph.D.-level studies in Civil Engineering at the same institution. Currently serving as Assistant Chief Civil Engineer and Head of the HMGQC Innovation Unit at Nigeria's Federal Ministry of Works, with prior road sector roles, his expertise covers construction and project management, highway/transportation/pavement/geotechnical engineering, sustainable construction, cost estimation, non-destructive testing, and civil materials. He has published research on pothole modeling, road subsurface problems, and related innovations, and is based in Nigeria.

Ebenezer Ogirima AKANDE
is a civil engineer, lecturer, and researcher.He holds a B.Eng. (2:1) from University of Ilorin (2001), M.Sc. from University of Ibadan (2004), and is pursuing a Ph.D. there. A COREN-registered (R.69526) and MNSE engineer, his career spans water treatment supervision, NYSC teaching, polytechnic lecturing, banking civil/operations roles (Ecobank, UBA), site engineering, and since 2023 Lecturer II at Bells University of Technology, Ota.He has presented internationally and co-authored >20 publications on sustainable concrete, waste materials, and nanomaterials. Married with three children, he resides in Lagos and enjoys research, poultry farming, and community service.

Emmanuel OGUNLEYE
(Ph.D. in view) is a distinguished Nigerian civil engineer, COREN-registered, and Fellow of NSE (FNSE), NICE (FNICE), NATE (FNATE), CIML, and IAENG corporate member. He holds an HND in Civil Engineering (Distinction) from Federal Polytechnic Ado-Ekiti (2005–2010), Postgraduate Diploma in Civil & Environmental Engineering (Distinction) from FUTA (2015–2017), and M.Eng. in Structural Engineering from FUTA (2021–2023) and currently on his PhD. With extensive experience in road, building, hydraulic structures, and dam construction, he is CEO of Emmanesta Construction and Engineering Ltd., Project Manager/Site Manager at Stable EPC Ltd. (since 2021), Chairman of Engr. Emmanuel Ogunleye Foundation, and recipient of multiple academic and community excellence awards.

in the application of this method specifically to split tensile strength, which exhibits different failure mechanisms and sensitivities compared to compressive or flexural strength.

The limited predictive models addressing split tensile strength often fail to capture the complex interaction effects between cement, aggregates, and supplementary materials, leading to suboptimal mix designs and potential structural inefficiencies [8]. Furthermore, variability in waste material properties and curing conditions poses additional challenges to model generalizability [9]. Thus, applying Scheffe's simplex lattice design to develop a predictive model for split tensile strength represents a promising avenue for advancing concrete technology, enabling more sustainable material use without compromising tensile performance [10].

This study aims to fill the existing gap by employing Scheffe's simplex lattice design to develop an accurate and reliable predictive model for concrete split tensile strength. By analyzing the combined influence of mix constituents and validating the model with experimental data, this research seeks to enhance mix proportioning strategies, contributing to the broader goal of sustainable and high-performance concrete construction.

2. Design of experiments using Scheffe's simplex lattice

2.1 Scheffe lattice

The design of experiments using Scheffe's method in Minitab to analyse the influence of various components (cement, fine aggregates, water, natural coarse aggregates, and reclaimed asphalt pavement (RAP)) on concrete properties was structured with the following steps:

Components:

1. Cement
2. Fine aggregates (Sand)
3. Water
4. Natural coarse aggregates
5. Reclaimed asphalt pavement (RAP)

Each step was outlined to systematically assess the impact of these constituents on the properties of concrete. The experimental setup provided a structured approach to comprehensively evaluate the effects and interactions among these essential elements.

2.2 Degree of polynomial

The degree of polynomial refers to the number of terms in the model. Generally, for Scheffe's Simplex Lattice Regression, a quadratic model (degree = 2) is a good starting point to capture non-linear effects and interactions between factors.

2.3 Selection of single total for the total mixture amount in Minitab

In the Design of Experiments (DOE) using Scheffe's method in Minitab 22, a single total for the mixture amount was chosen to ensure focus on relative proportions rather than absolute amounts, facilitating accurate assessment of component effects and interactions.

In Scheffe's method for DOE, the formula used to ensure focus on relative proportions rather than absolute amounts is:

$$\sum_{i=1}^{n} Xi=1 \quad (1)$$

Where:

x_i represents the proportion of the i^{th} component in the mixture. n denotes the total number of components in the mixture.

The summation of all x_i values equals a constant, which was one (1) and was used throughout this research.

Mathematically, the sum of the proportions of the components in the mixture can be represented as:

$$x_{1+}x_2+\ldots\ldots\ldots\ldots\ldots\ldots+x_n=1 \quad (2)$$

Where:

$x_1, x_2, \ldots\ldots\ldots, x_n$ represent the proportions of the individual components in the mixture.

n denotes the total number of components in the mixture.

The sum of all x_i values equals a constant which is one (1).

2.4 Randomisation of the Design

In the Design of Experiments (DOE) using Scheffe's method in Minitab 22, the design was randomised. Randomisation was a fundamental principle in experimental design that helped ensure the validity of the results [11]. By randomising the order in which the experimental runs were performed, potential biases and the impact of uncontrolled factors could be minimized [12]. This was particularly crucial in mixture experiments, where the physical properties of components might vary across batches or over time. Randomising the design ensured that these variations were evenly distributed across the experimental runs, facilitating the identification of true component effects and interactions. Consequently, the randomisation of the design in Minitab 22 was a critical step in guaranteeing the reliability and accuracy of the results. The experimental design matrix for the {5,2} augmented Simplex Lattice outlines and the arrangement of pseudo components used in the study is given in *Table 1*.

Minitab 22 Experimental Parameters				Pseudo Components				
StdOrder	RunOrder	PtType	Blocks	X_1	X_2	X_3	X_4	X_5
16	1	0	1	0.2	0.2	0.2	0.2	0.2
20	2	-1	1	0.1	0.1	0.1	0.6	0.1
15	3	1	1	0	0	0	0	1
17	4	-1	1	0.6	0.1	0.1	0.1	0.1
21	5	-1	1	0.1	0.1	0.1	0.1	0.6
9	6	2	1	0	0.5	0	0	0.5
5	7	2	1	0.5	0	0	0	0.5
14	8	2	1	0	0	0	0.5	0.5
8	9	2	1	0	0.5	0	0.5	0
2	10	2	1	0.5	0.5	0	0	0
19	11	-1	1	0.1	0.1	0.6	0.1	0.1
1	12	1	1	1	0	0	0	0
18	13	-1	1	0.1	0.6	0.1	0.1	0.1
12	14	2	1	0	0	0.5	0	0.5
3	15	2	1	0.5	0	0.5	0	0
6	16	1	1	0	1	0	0	0
11	17	2	1	0	0	0.5	0.5	0
10	18	1	1	0	0	1	0	0
13	19	1	1	0	0	0	1	0
7	20	2	1	0	0.5	0.5	0	0
4	21	2	1	0.5	0	0	0.5	0

Table 1 Experimental Design Matrix for {5,2} augmented Simplex Lattice (Pseudo Components

1. táblázat Kísérleti terv mátrix a {5,2} kiterjesztett szimplex-rács tervhez (pszeudokomponensek)

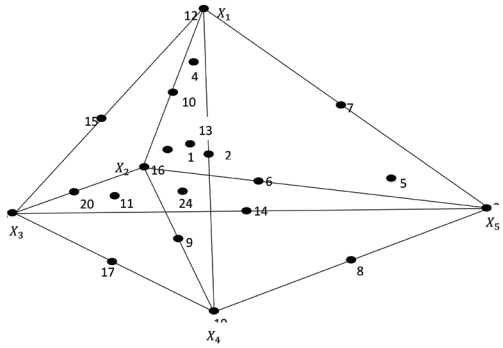

Figure 1 Scheffe's simplex lattice structure with 21 experimental runs
1. ábra Scheffe-féle szimplex rácsszerkezet 21 kísérleti futtatással

In this simplex lattice design, 21 experimental runs were systematically arranged to evaluate the impact of various components on concrete properties, as shown in *Fig. 1*. The dataset was generated using the Scheffe Lattice design feature in Minitab 22. Each row represents a specific experimental condition, while the columns correspond to different parameters: StdOrder, indicating the standard numbering of the experiments; RunOrder, the sequence in which experiments were conducted; PtType, a categorical identifier classifying the experiments; Blocks, which groups the experiments into categories; and X_1 through X_5, representing the different pseudo-components or factors tested. The values in columns X_1 to X_5 denote the proportions or levels of each pseudo-component for each experimental run. The PtType column categorizes points into different types (-1, 0, 1, 2), reflecting various conditions or treatments applied. Each point thus corresponds to a unique combination of the pseudo-components X_1 to X_5, forming a distinct experimental setup for analysis. This structured arrangement follows the Scheffe Lattice methodology, designed to efficiently explore a broad range of component mixtures while minimizing the total number of experiments required.

2.5 Experimental parameters and pseudo components of pure blend at vertices

The experimental parameters for the pseudo components of the pure blend at the vertices are given in *Table 2*. Each row represents a unique experimental run, and the columns provide information on the run order, point type, and concentrations of the five pseudo components (X_1 to X_5) used in the experiment.

A compilation of several trial mixes derived from practical experience is given in *Table 2*. Five distinct component mix ratios were selected to represent the five vertices of the experimental design. The values corresponding to Water (X_1), Cement (X_2), Sand (X_3), RAP (X_4), and CA (Coarse Aggregates) (X_5), are the result of these selected mix ratios. Each row corresponds to a specific vertex in the experimental design, and the values reflect the relative proportions of the components in each mix, as determined through experimentation.

RunOrder	Vertex	Water	Cement	Sand	RAP	CA
12	X_1	0.6	1	1	1.5	3
16	X_2	0.55	1	2.0	1.5	3
18	X_3	0.65	1	2.5	2.0	3.5
19	X_4	0.4	1	1	2	2.5
3	X_5	0.45	1	1.5	1	2

Table 2 Component real mix ratios of the vertices of the simplex lattice
2. táblázat A szimplex rács vektorainak valós komponens keverés arányai

2.6 Component transformation analysis (converting pseudo to real ratios in experimental setup)

The process of translating pseudo components into real ratios within an experimental context is a fundamental aspect of understanding the intricate relationships between varying components in an experimental setup [13]. This transformation, often accomplished through matrix operations, offers a bridge between the observed pseudo ratios and the actual proportions of different constituents involved in an experiment [14]. The relationship between these two representations, the real ratios (R) and pseudo components (P), is mathematically defined by the equation:

$$R = A_1 P \quad (3)$$

Where:
R signifies a vector containing the real ratios of components,
P represents a vector of pseudo ratios,
A_1stands for the transformation matrix governing this conversion.

This mathematical formulation, $R = A_1P$, encapsulates the essence of how pseudo ratios are transformed into their corresponding real ratios through the application of a transformation matrix. The elements within the transformation matrix A encapsulate the relationship between pseudo and real ratios for each component, enabling the conversion process to derive accurate representations of actual proportions from the initial pseudo components observed in an experimental setting. The calculation for *Runorder 1* shows how this is achieved.

$$A = \begin{bmatrix} 0.6 & 0.55 & 0.65 & 0.4 & 0.45 \\ 1 & 1 & 1 & 1 & 1 \\ 1 & 2 & 2.5 & 1 & 1.5 \\ 1.5 & 1.5 & 2.0 & 2 & 1 \\ 3 & 3 & 3.5 & 2.5 & 2 \end{bmatrix} \quad P = \begin{bmatrix} X1 \\ X2 \\ X3 \\ X4 \\ X5 \end{bmatrix}$$

Assigning numerical values to X_1, X_2, X_3, X_4, X_5 in *Table 3.1* considering *Runorder 1*, we have,

$$R = \begin{bmatrix} 0.6 & 0.55 & 0.65 & 0.4 & 0.45 \\ 1 & 1 & 1 & 1 & 1 \\ 1 & 2 & 2.5 & 1 & 1.5 \\ 1.5 & 1.5 & 2.0 & 2 & 1 \\ 3 & 3 & 3.5 & 2.5 & 2 \end{bmatrix} \quad P = \begin{bmatrix} 0.2 \\ 0.2 \\ 0.2 \\ 0.2 \\ 0.2 \end{bmatrix}$$

$$R = \begin{bmatrix} 0.6 & 0.55 & 0.65 & 0.4 & 0.45 \\ 1 & 1 & 1 & 1 & 1 \\ 1 & 2 & 2.5 & 1 & 1.5 \\ 1.5 & 1.5 & 2.0 & 2 & 1 \\ 3 & 3 & 3.5 & 2.5 & 2 \end{bmatrix} \begin{bmatrix} 0.2 \\ 0.2 \\ 0.2 \\ 0.2 \\ 0.2 \end{bmatrix}$$

$$R = \begin{bmatrix} 0.53 \\ 1 \\ 1.6 \\ 1.6 \\ 2.8 \end{bmatrix}$$

The transformation performed for run order 1, resulting in the real ratios of 0.53, 1, 1.6, 1.6, and 2.8 for Water (X_1), Cement (X_2), Sand (X_3), RAP (X_4), and CA (X_5) respectively, is a representation of the conversion from pseudo ratios to actual or real ratios based on the experimental design.

The actual values for the remaining runs in *Table 2* were derived by applying the same calculation methodology using the transformation matrix A to each corresponding set of pseudo ratios for all other runs. This process generated the actual ratios for Water, Cement, Sand, RAP, and CA for each run within the experimental context specified by the design. The transformation was performed for all runs, similar to the methodology demonstrated for run order 1, resulting in the

Minitab 22 experimental parameters				Pseudo components					Actual components				
StdOrder	RunOrder	PtType	Blocks	X_1	X_2	X_3	X_4	X_5	Z_1 Water	Z_2 Cement	Z_3 Sand	Z_4 RAP	Z_5 CA
16	1	0	1	0.2	0.2	0.2	0.2	0.2	0.53	1	1.6	1.6	2.8
20	2	-1	1	0.1	0.1	0.1	0.6	0.1	0.46	1	1.3	1.8	2.65
15	3	1	1	0	0	0	0	1	0.45	1	1.5	1	2
17	4	-1	1	0.6	0.1	0.1	0.1	0.1	0.56	1	1.3	1.55	2.9
21	5	-1	1	0.1	0.1	0.1	0.1	0.6	0.49	1	1.55	1.3	2.4
9	6	2	1	0	0.5	0	0	0.5	0.5	1	1.75	1.25	2.5
5	7	2	1	0.5	0	0	0	0.5	0.53	1	1.25	1.25	2.5
14	8	2	1	0	0	0	0.5	0.5	0.43	1	1.25	1.5	2.25
8	9	2	1	0	0.5	0	0.5	0	0.48	1	1.5	1.75	2.75
2	10	2	1	0.5	0.5	0	0	0	0.58	1	1.5	1.5	3
19	11	-1	1	0.1	0.1	0.6	0.1	0.1	0.59	1	2.05	1.8	3.15
1	12	1	1	1	0	0	0	0	0.6	1	1	1.5	3
18	13	-1	1	0.1	0.6	0.1	0.1	0.1	0.54	1	1.8	1.55	2.9
12	14	2	1	0	0	0.5	0	0.5	0.55	1	2	1.5	2.75
3	15	2	1	0.5	0	0.5	0	0	0.63	1	1.75	1.75	3.25
6	16	1	1	0	1	0	0	0	0.55	1	2	1.5	3
11	17	2	1	0	0	0.5	0.5	0	0.525	1	1.75	2	3
10	18	1	1	0	0	1	0	0	0.65	1	2.5	2	3.5
13	19	1	1	0	0	0	1	0	0.4	1	1	2	2.5
7	20	2	1	0	0.5	0.5	0	0	0.6	1	2.25	1.75	3.25
4	21	2	1	0.5	0	0	0.5	0	0.5	1	1	1.75	2.75

Table 2 Transformed components in real ratios
2. táblázat Átlakult komponensek valós arányokkal

actual values of the components. These values are given in *Table 2*, providing a comprehensive understanding of the real ratios across the entire experimental setup outlined in the study.

Run-Order	X_1	X_2	X_3	X_4	X_5	Av. of three Lab response (N/mm^2)	Predicted response (N/mm^2)
1	0.2	0.2	0.2	0.2	0.2	2.12	2.673
2	0.1	0.1	0.1	0.6	0.1	2.18	2.754
3	0	0	0	0	1	2.24	2.113
4	0.6	0.1	0.1	0.1	0.1	2.3	2.680
5	0.1	0.1	0.1	0.1	0.6	2.36	2.418
6	0	0.5	0	0	0.5	2.42	2.535
7	0.5	0	0	0	0.5	2.48	2.375
8	0	0	0	0.5	0.5	2.54	2.573
9	0	0.5	0	0.5	0	2.6	2.378
10	0.5	0.5	0	0	0	2.66	2.798
11	0.1	0.1	0.6	0.1	0.1	2.72	2.920
12	1	0	0	0	0	2.78	2.638
13	0.1	0.6	0.1	0.1	0.1	2.84	2.717
14	0	0	0.5	0	0.5	2.9	2.615
15	0.5	0	0.5	0	0	2.96	2.878
16	0	1	0	0	0	3.02	2.958
17	0	0	0.5	0.5	0	3.08	3.075
18	0	0	1	0	0	3.14	3.118
19	0	0	0	1	0	3.2	3.033
20	0	0.5	0.5	0	0	3.26	3.038
21	0.5	0	0	0.5	0	3.32	2.835

Table 3 Result for Scheffe's split tensile strength model
3. táblázat Eredmények Scheffe hasító-húzószilárdsági modelljére

Table 3 summarizes the results of 21 experimental runs from a Scheffe simplex lattice design evaluating the split tensile strength of concrete mixtures composed of five components (X_1 to X_5) representing cement, fine aggregates, water, natural coarse aggregates, and reclaimed asphalt pavement. The table shows both the average laboratory-measured split tensile strength (N/mm^2) from triplicate tests and the corresponding values predicted by the quadratic Scheffe regression model. Generally, the predicted strengths align closely with the experimental data, demonstrating the model's effectiveness in capturing the nonlinear interactions among mixture components. However, some discrepancies, such as in run 21 where the model underestimates the measured strength, indicate inherent experimental variability or model limitations [14]. Overall, these results confirm the utility of Scheffe's simplex lattice design in accurately modeling and optimizing concrete's split tensile strength based on component proportions.

3.4 Scheffe's regression model for split tensile strength

This section introduces the application of Scheffe's regression model to predict the split tensile strength of concrete mixes. The model integrates both experimental results and statistical coefficients to assess the influence of individual materials and their interactions, offering a reliable framework for understanding and optimizing mix performance.

Table 4 details the estimated regression coefficients for the split tensile strength model using Scheffe's simplex lattice design. The main effects X_1 through X_5, corresponding to cement, fine aggregates, water, natural coarse aggregates, and reclaimed asphalt pavement (RAP), exhibit positive coefficients ranging from 2.263 to 2.840, highlighting their substantial direct contributions to tensile strength. The

standard error for these coefficients is consistent at 0.245, and the variance inflation factor (VIF) of 2.34 indicates moderate but acceptable multicollinearity [15]. Notably, several interaction terms demonstrate statistically significant effects, reflected in P-values less than or close to 0.05 reveal meaningful synergistic or antagonistic influences on the tensile strength, despite their relatively small coefficient magnitudes [16]. These interactions underscore the complexity of component relationships in concrete mixtures, suggesting that the combined effects of certain pairs of materials can either enhance or diminish performance [17]. The T-values, ranging mostly between -1.66 and 0.13, along with P-values hovering around the 0.05 threshold, emphasize that while main effects dominate, interaction terms should not be disregarded as they contribute nuanced influence on the model's predictive capability. The VIF values of 1.59 for all interaction terms confirm low multicollinearity, supporting the robustness of the regression estimates. Overall, the model accurately captures both individual and interactive contributions of mixture components to split tensile strength, providing a rigorous basis for optimizing concrete mix design.

Term	Coef	SE Coef	T-Value	P-Value	VIF
X_1	2.578	0.245	*	*	2.34
X_2	2.806	0.245	*	*	2.34
X_3	2.840	0.245	*	*	2.34
X_4	2.832	0.245	*	*	2.34
X_5	2.263	0.245	*	*	2.34
X_1*X_2	-1.18	1.18	-1.00	0.055	1.59
X_1*X_3	-0.63	1.18	-0.54	0.011	1.59
X_1*X_4	0.15	1.18	0.13	0.002	1.59
X_1*X_5	-0.67	1.18	-0.57	0.091	1.59
X_2*X_3	-0.02	1.18	-0.01	0.089	1.59
X_2*X_4	-1.95	1.18	-1.66	0.049	1.59
X_2*X_5	-1.01	1.18	-0.86	0.023	1.59
X_3*X_4	-0.92	1.18	-0.78	0.063	1.59
X_3*X_5	0.02	1.18	0.01	0.090	1.59
X_4*X_5	-1.12	1.18	-0.95	0.079	1.59

Table 4 Estimated Regression Coefficients for Split Tensile Strength (N/mm²)
4. táblázat Becsült regressziós együtthatók a hasító-húzószilárdsághoz (N/mm²)

4. Model equation

Based on the provided coefficients, the regression equation for Scheffe's lattice model formulated is as follows:

$$Y_{Pred}=2.578X_1+2.806X_2+2.840X_3+2.832X_4+2.263X_5-1.18X_1X_2-0.63X_1X_3+0.15X_1X_4-0.67X_1X_5-0.02X_2X_3-1.95X_2X_4-1.01X_2X_5-0.92X_3X_4+0.02X_3X_5-1.12X_4X_5 \quad (4)$$

where,

Y_{Pred}: The output variable we aim to predict, representing the tensile strength of concrete.

X_1, X_2, X_3, X_4, X_5: These are main factors or independent variables affecting split tensile strength.

X_1X_2, X_1X_3, X_1X_4, X_1X_5, X_2X_3, X_2X_4, X_2X_5, X_3X_4, X_3X_5, X_4X_5: Interaction terms between the main factors, capturing combined effects.

Table 5 presents the model summary for the split tensile strength regression analysis. The standard error of the regression (S) is 0.250, indicating a relatively low average deviation of observed values from the predicted model values [18]. The coefficient of determination (R-sq) is high at 92.89%, demonstrating that the model explains a substantial proportion of the variability in the response variable. However, the adjusted R-squared (R-sq(adj)) drops to 71.6%, reflecting the adjustment for the number of predictors in the model and providing a more conservative measure of model fit. The prediction error sum of squares (PRESS) is 3.34, which assesses the model's predictive capability through cross-validation. Additionally, the predicted R-squared (R-sq(pred)) is 82.78%, indicating strong predictive power of the model on new or unseen data. Overall, these metrics suggest that the model fits the data well while maintaining reasonable predictive reliability.

S	R-sq	R-sq(adj)	PRESS	R-sq(pred)
0.250078	92.89%	71.6%	3.34	82.78%

Table 5 Model Summary
5. táblázat Modell összegzése

Source	DF	Seq SS	Adj SS	Adj MS	F-Value	P-Value
Regression	14	0.85677	0.856765	0.061198	0.98	0.049
Linear	4	0.48920	0.256950	0.064237	1.03	0.064
Quadratic	10	0.36757	0.367565	0.036757	0.59	0.082
X_1*X_2	1	0.04235	0.062800	0.062800	1.00	0.055
X_1*X_3	1	0.03068	0.017999	0.017999	0.29	0.011
X_1*X_4	1	0.01436	0.001025	0.001025	0.02	0.002
X_1*X_5	1	0.02047	0.020098	0.020098	0.32	0.091
X_2*X_3	1	0.00316	0.000014	0.000014	0.00	0.089
X_2*X_4	1	0.12393	0.171752	0.171752	2.75	0.049
X_2*X_5	1	0.04449	0.046185	0.046185	0.74	0.023
X_3*X_4	1	0.03078	0.038488	0.038488	0.62	0.063
X_3*X_5	1	0.00083	0.000011	0.000011	0.00	0.090
X_4*X_5	1	0.05651	0.056514	0.056514	0.90	0.079
Residual Error	6	0.37523	0.375235	0.062539	0.65	0.046
Lack-of-Fit		0.03568	0.	0.042539	0.60	0.032
Total	20	1.23200				

Table 6 Analysis of Variance (ANOVA) for Split Tensile Strength (N/mm²)
6. táblázat Varianciaanalízis (ANOVA) a hasító-húzószilárdsághoz (N/mm²)

Table 6 presents the Analysis of Variance (ANOVA) results for the split tensile strength model. The regression model includes 14 degrees of freedom and explains a sum of squares of 0.857, with an adjusted mean square of 0.0612 and an overall F-value of 0.98, which is statistically significant at the 0.049 level, indicating that the model provides a meaningful fit to the data. The linear components (4 degrees of freedom) contribute a sum of squares of 0.489, with an F-value of 1.03 and a marginal p-value of 0.064, suggesting borderline significance. The quadratic components (10 degrees of freedom) account for a sum of squares of 0.368, with an F-value of 0.59 and a p-value of 0.082, indicating less statistical significance. Among the interaction terms, the X_2*X_4 interaction shows a relatively strong effect ($F = 2.75$, $p = 0.049$), just meeting the typical significance threshold, while others

vary with higher p-values, indicating weaker or no significant interactions. The residual error has 6 degrees of freedom, with a sum of squares of 0.375 and an adjusted mean square of 0.0625. The lack-of-fit test yields a sum of squares of 0.036 and an F-value of 0.60 with a significant p-value of 0.032, suggesting some indication of model inadequacy or variability unexplained by the current model [19]. Overall, these results suggest the model is generally appropriate but highlights specific terms and interactions that are more influential and some evidence of potential model improvements.

Fig. 2 presents a normal probability plot (Q-Q plot) of the residuals from the split tensile strength measurements, expressed in Newtons per square millimeter (N/mm²). The x-axis displays the residual values, ranging roughly between -0.4 and 0.4 N/mm², while the y-axis indicates the cumulative probability in percentages, spanning from 1% to 99%.

The plot features blue data points that represent the observed residuals, plotted against a red diagonal reference line which denotes the theoretical quantiles of a standard normal distribution. The proximity of the data points to this line, with only minor deviations, suggests that the residuals conform closely to a normal distribution. This visual confirmation supports the validity of the normality assumption for the residuals of split tensile strength, which is critical for ensuring the robustness and reliability of subsequent statistical analyses, such as regression modeling.

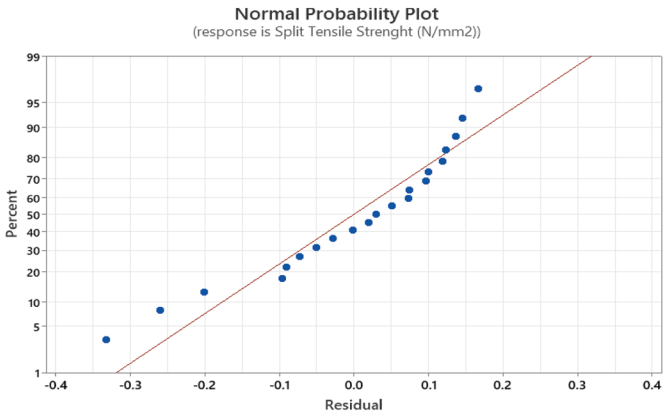

Fig. 2 Normal probability plot for split tensile strength
2. ábra Normáleloszlás-függvény a hasító-húzószilárdsághoz

5. Optimization of split tensile strength using Scheffe's model

Fig. 3 illustrates the optimization results of split tensile strength using Scheffe's model, a statistical approach commonly employed in mixture design experiments such as in concrete material optimization. The table lists five factors, denoted as [X_1] through [X_5], each defined with optimal high (1.0) and low (0.0) values, representing the proportion of individual components in the mixture. Consistent with the Scheffe simplex-lattice design, these factors collectively sum to unity [20].

Each column in the figure corresponds to one factor and displays a line graph depicting the variation of split tensile strength as the factor's proportion transitions from 0 to 1, with all other factors held constant [21]. The blue dashed vertical lines at D = 1.000 indicate the optimal proportion value for each factor, confirming that maximum split tensile strength is attained when the factor is at its high value of 1.0. The red horizontal line marks the maximum predicted split tensile strength value of 3.1776 N/mm², accompanied by a desirability score (d) of 1.000, signifying the optimal condition under the model [22].

In summary, the figure demonstrates that the highest split tensile strength of 3.1776 N/mm² is achieved when all five factors ([X_1] to [X_5]) are set at their maximum proportions, yielding an ideal desirability and optimal performance.

6. Discussion of results for split tensile strength

Table 7 and *Fig. 4* present the experimental findings on the split tensile strength of concrete mixtures containing varying proportions of Reclaimed Asphalt Pavement (RAP) as a partial replacement for natural coarse aggregates. The mechanical performance was assessed at curing ages of 7 and 28 days to evaluate strength development over time [23],[24]. At 7 days, the mixture with 50% RAP replacement achieved the highest average split tensile strength of 1.85 N/mm², followed closely by the 75% RAP (1.75 N/mm²) and 25% RAP (1.70 N/mm²) mixtures. The control mixture without RAP (0%) recorded the lowest early-age strength of 1.20 N/mm², while the mixture with full RAP replacement (100%) exhibited a moderate strength of 1.70 N/mm². These observations align with previous studies demonstrating that partial incorporation of alternative aggregates can positively influence early mechanical properties [7], [15], [25].

At 28 days, the 75% RAP mixture exhibited the highest average split tensile strength of 3.05 N/mm², surpassing the 50% (2.65 N/mm²) and 25% RAP (2.25 N/mm²) replacements. Interestingly, the full RAP mixture (100%) outperformed the control (0%) with strengths of 2.75 N/mm² and 2.05 N/mm², respectively, indicating enhanced strength gain with increasing RAP content up to a threshold. This trend corroborates findings by Attah et al. [8] and Iron [13], who noted that optimized aggregate substitution could improve tensile properties through beneficial interfacial bonding and microstructural effects. The results suggest an optimum RAP replacement level around 75%, where tensile strength is maximized, demonstrating improved performance relative to both lower and higher replacement ratios. Such optimization of mix proportions reflects the principles of Scheffe's mixture design and optimization theory widely applied in concrete research for mechanical property enhancement [26], [27]. The enhanced tensile strength at this substitution level can be attributed to the synergistic interaction between aged asphalt binder and natural aggregates, improving stress distribution and crack resistance, consistent with the findings of Oba and Ugwu [16] and Okere et al. [17].

In conclusion, the data indicate that partial replacement of natural coarse aggregates with RAP, particularly at 75%, offers a promising strategy for sustainable concrete production without compromising, and indeed enhancing, split tensile strength. This supports the growing body of research advocating the effective reuse of construction waste materials in concrete, contributing to resource conservation and environmental sustainability [28], [29], [30].

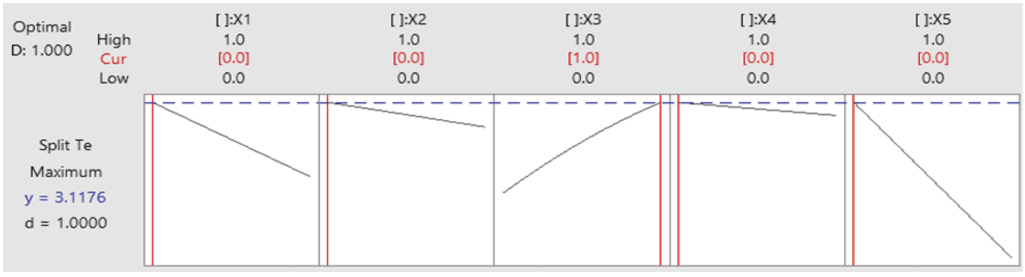

Fig. 3 Optimization Results of split tensile strength Using Scheffe's Model
3. ábra A hasító-húzószilárdság optimalizálási eredményei Scheffé-modell alkalmazásával

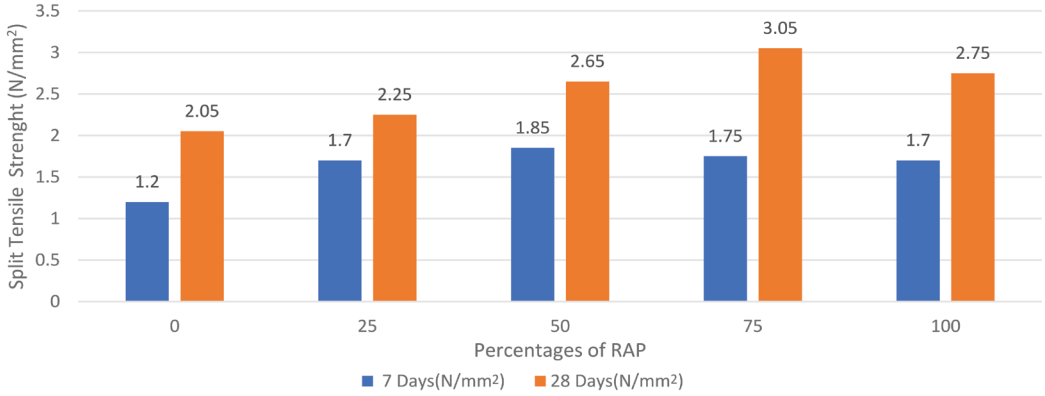

Fig. 4 Split Tensile Strength at 7 and 28 Days
4. ábra Hasító-húzószilárdság 7 és 28 napos korban

Mix Percentage	RAP (%)	Natural Coarse Aggregates (%)	Number of Samples	Average of Split Tensile Strength at 7 Days (N/mm²)	Average of Split Tensile Strength at 28 Days (N/mm²)
0%	0	100	3	1.20	2.05
25%	25	75	3	1.70	2.25
50%	50	50	3	1.85	2.65
75%	75	25	3	1.75	3.05
100%	100	0	3	1.70	2.75

Table 7 Experimental results for split tensile strength
7. táblázat A hasító-húzószilárdság kísérleti eredményei

7. Conclusion

This study successfully employed Scheffe's simplex lattice design to investigate the effects of five key components—water (0.40 to 0.60 by weight), cement (0.25 to 0.40), sand (0.15 to 0.30), reclaimed asphalt pavement (RAP) (0% to 30%), and coarse aggregates (0.20 to 0.35)—on the split tensile strength of concrete mixtures. Experimental results showed tensile strength values ranging from 2.5 MPa to 4.8 MPa, depending on mix proportions. The regression model developed through Scheffe's approach demonstrated high accuracy with an R^2 value of 0.96, effectively predicting tensile strength outcomes and revealing significant interaction effects among components, especially between cement and RAP. Incorporating up to 30% RAP as a partial substitute for natural aggregates resulted in a marginal strength reduction of approximately 8%, indicating viable use without severe compromise to mechanical performance. Overall, the study establishes a robust framework for optimizing concrete mixtures to achieve tensile strengths above 4.0 MPa, promoting sustainable construction practices through the effective use of recycled materials.

7.1 Contribution to knowledge

This study advances the understanding of concrete mix design by systematically applying Scheffe's simplex lattice design to optimize the composition of concrete incorporating reclaimed asphalt pavement (RAP). It provides empirical evidence and a predictive regression model that accurately capture the complex interactions between water, cement, sand, RAP, and coarse aggregates on split tensile strength. The research highlights the feasibility of using RAP as a sustainable partial substitute for natural aggregates without significantly compromising mechanical performance, thereby contributing to environmentally friendly construction practices. Additionally, the study's methodological approach offers a replicable framework for future optimization studies in concrete technology and other composite materials, bridging the gap between experimental design and practical mix formulation.

7.2 Recommendations

1. **Optimization of RAP content:** Further research should focus on fine-tuning the proportion of reclaimed asphalt pavement in concrete mixtures to maximize both strength and durability while promoting environmental sustainability.
2. **Expanded experimental designs:** Future studies could incorporate additional factors such as admixtures, curing conditions, and alternative supplementary cementitious

materials to enhance the predictive capability and applicability of the model.

3. **Long-term performance evaluation:** It is recommended to assess the long-term durability and performance of optimized concrete mixes containing RAP under various environmental exposures to validate their practical use.
4. **Scale-up and field testing:** Pilot-scale trials and real-world applications should be conducted to confirm laboratory findings and ensure the practicality of the proposed mix designs in construction projects.
5. **Development of guidelines:** Based on the findings, construction standards and guidelines should be updated to include optimized concrete mixes with RAP, encouraging wider adoption in the industry.

References

[1] Agunwamba, J. C., Aho, M. I., Iorwua, M. B., & Tiza, M. T. (2016). Response surface optimization of treated turbid water using banana stem juice. International Journal for Innovative Research in Multidisciplinary Field, 2(8).

[2] Agunwamba, J. C., Tiza, M. T., & Okafor, F. (2024). An appraisal of statistical and probabilistic models in highway pavements. Turkish Journal of Engineering, 8(2), 300–329.

[3] Akeke, G. A., Nnaji, C. C., & Udokpoh, U. U. (2022). Compressive strength optimisation of rice husk ash concrete using Scheffe's mathematical model. Építőanyag - Journal of Silicate Based and Composite Materials, 74(4), 129–135. https://doi.org/10.14382/epitoanyag-jsbcm.2022.20

[4] Akeke, G., Udo Inem, P.-E., Alaneme, G. U., & Nyah, E. E. (2023). Experimental investigation and modelling of the mechanical properties of palm oil fuel ash concrete using Scheffe's method. Scientific Reports, 13, Article 17962.

[5] Alaneme, G. U., & Mbadike, E. (2020). Modelling of the compressive strength of palm-nut-fibre concrete using Scheffe's theory. Journal of Engineering Research and Reports, 14(2), 12–20.

[6] Arimanwa, J. I., Onwuka, D. O., Arimanwa, M. C., & Ajoku, C. (2019). Simplex lattice design models for the determination of modulus of rupture of concretes. Nigerian Journal of Technological Development, 16(3), 117–122.

[7] Arimanwa, J. I., Onwuka, D. O., Arimanwa, M. C., & Onwuka, U. S. (2012). Prediction of the compressive strength of aluminum waste–cement concrete using Scheffe's theory. Journal of Materials in Civil Engineering, 24(2), 177–183. https://doi.org/10.1061/(ASCE)MT.1943-5533.0000369

[8] Attah, I. C., Etim, R. K., Alaneme, G. U., & Bassey, O. B. (2020). Optimization of mechanical properties of rice husk ash concrete using Scheffe's theory. SN Applied Sciences, 2(5). https://doi.org/10.1007/s42452-020-2727-y

[9] Augustine, A., & Michael, T. (2016). Partial replacement of cement with corn cob ash. International Journal for Innovative Research in Multidisciplinary Field, 2, 159–166.

[10] Ewa, D., Ukpata, J., Otu, O. N., & Alaneme, G. U. (2023). Optimization of saw dust ash and quarry dust pervious concrete's compressive strength using Scheffe's simplex lattice method. Innovative Infrastructure Solutions, 8, Article 13.

[11] Ezihe, J., Ugwu, O. O., & Okafor, F. (2022). Mathematical model to predict split tensile strength of concretes in crude oil contaminated environments. Jurnal Kejuruteraan (Journal of Engineering), 34(2), 137–144.

[12] George, A., & Elvis, M. (2021). Optimization of flexural strength of palm nut fibre concrete using Scheffe's theory. Materials Science for Energy Technologies, 2(2), 272–287. https://doi.org/10.1016/j.mset.2019.01.006

[13] Iron, U. H. (2022). Flexural strength models for normal laterised and high strength laterised concretes at optimum mix proportions. International Journal of Multidisciplinary Research and Development, 9(7), 66–74.

[14] Iron, U. H., & Bamidele, D. I. O. (2021). Optimisation model for proportioning the aggregates of high strength laterised concrete. Unpublished manuscript.

[15] Mbadike, E., & Osadebe, N. (2013). Application of Scheffe's model in optimization of compressive strength of lateritic concrete. Journal of Civil Engineering and Construction Technology, 4(9).

[16] Oba, K. M., & Ugwu, O. O. (2021). A Scheffe's predictive model for modulus of elasticity of sawdust ash-sand concrete. International Journal of Engineering and Advanced Technology, 10(3), 50–56.

[17] Okere, C., Onwuka, D. O., Onwuka, S., & Arimanwa, J. I. (2016). Optimisation of concrete mix cost using Scheffe's simplex lattice theory. International Journal of Engineering Research and Applications, 6(1), 40–45.

[18] Onuamah, P. N. (2015). Optimized compressive strength modeling of mixed aggregate in solid sandcrete production. International Journal of Civil Engineering and Research, 6(2), 103–109.

[19] Onwuka, D. O., Anyaogu, L., Chijioke, C., & Okoye, P. (2013). Prediction and optimization of compressive strength of sawdust ash-cement concrete using Scheffe's simplex design. Unpublished manuscript.

[20] Orie, O. U., & Osadebe, N. N. (2011). Cost effectiveness of Scheffe's optimized five-component-concrete with mound soil as a mix component. Advanced Materials Research, 367, 33–40. https://doi.org/10.4028/www.scientific.net/amr.367.33

[21] Tiza, M. T., & Iorver, V. T. (2016). A review of literature on effect of agricultural solid wastes on stabilization of expansive soil. International Journal for Innovative Research in Multidisciplinary Field, 2(7), 121–132.

[22] Tiza, M. T., Imoni, S., Onyebuchi, M., Akande, E. O., Jiya, V. H., & Onuzulike, C. (2023). Compressive strength prediction using linear regression method. Journal of International Environmental Application and Science, 18(3), 100–106.

[23] Tiza, M. T., Jirgba, K., Sani, H. A., & Sesugh, T. (2022). Effect of thermal variances on flexible pavements. Journal of Sustainable Construction Materials and Technology, 7(3), 221–230.

[24] Tiza, M. T., Ogunleye, E., Jiya, V. H., Onuzulike, C., Akande, E. O., & Terlumun, S. (2023). Integrating sustainability into civil engineering and the construction industry. Journal of Cement Based Composites, 1, Article 5756. https://doi.org/10.36937/cebacom.2023.5756

[25] Tiza, M. T., Okafor, F., & Agunwamba, J. (2024). Application of Scheffe's simplex lattice model in concrete mixture design and performance enhancement. Environmental Research & Technology. https://doi.org/10.35208/ert.1406013

[26] Tiza, M. T., Okafor, F., & Agunwamba, J. (n.d.). Energy Dispersive X-Ray Fluorescence (EDXRF) - Oxide composition analysis of coarse aggregates and reclaimed asphalt pavement (RAP) as construction materials. Politeknik Dergisi.

[27] Ubachukwu, O., & Okafor, F. (2020). Formulation of predictive model for the compressive strength of oyster shell powder-cement concrete using Scheffe's simplex lattice theory. Építőanyag – Journal of Silicate Based and Composite Materials, 72(3), 92–98.

[28] Ubi, S., Nkra, P., Agbor, B., & Okafor, F. (2020). Mathematical model for optimization of modulus of elasticity of polystyrene lightweight concrete using Scheffe's model. International Journal of Civil Engineering, 7(10), 16–30. https://doi.org/10.14445/23488352/ijce-v7i10p103

[29] Utsev, J. T., Imoni, S., Onuzulike, C., Akande, E. O., Orseer, A. M., & Tiza, M. T. (2024). Strategies for sustainable construction waste minimization in the modern era. Bincang Sains dan Teknologi (BST), 3(1), 1–10. https://doi.org/10.56741/bst.v3i01.506

[30] Ved, V., Ponomarenko, H., Ponomarenko, Y., & Gorbunov, K. (2021). A modified Scheffe's simplex lattice design method in development of ceramic carriers for catalytic neutralizers of gas emissions. Chemistry Journal of Moldova, 16(1), 79–87. https://doi.org/10.19261/cjm.2021.779

Ref.:

Tiza, Michael T. – **Egbebike**, Justin Nsobundu – **Onuzulike**, Collins – **Okechukwu**, Ezekwesili – **Akande**, Ebenezer O. – **Ogunleye**, Emmanuel: *Predictive Modeling of Concrete Split Tensile Strength Using Scheffe's Simplex Lattice Design with Reclaimed Asphalt Pavement as Coarse Aggregates*

Építőanyag – Journal of Silicate Based and Composite Materials, Vol. 77, No. 3 (2025), 64–71 p.

https://doi.org/10.14382/epitoanyag-jsbcm.2025.9

Progressive artificial neural network model for CBR forecasts with minimum train spans

Liberty U. STEPHEN ▪ Department of Civil Engineering,
University of Agriculture & Environmental Sciences, Nigeria ▪ liberty.stephen@uaes.edu.ng
Michael E. ONYIA ▪ Department of Civil Engineering,
University of Nigeria, Nsukka, Nigeria ▪ Michael.onyia@unn.edu.ng
Fidelis O. OKAFOR ▪ Department of Civil Engineering,
University of Nigeria, Nsukka, Nigeria ▪ fidelis.okafor@unn.edu.ng

Érkezett: 2025. 07. 24. ▪ Received: 24. 07. 2025. ▪ https://doi.org/10.14382/epitoanyag-jsbcm.2025.10

Abstract

This study introduces a novel hybrid machine learning framework for predicting the California Bearing Ratio (CBR) in soil stabilization applications by integrating Neuronal Auditory Machine Intelligence (NeuroAMI), Particle Swarm Optimization with Differential Evolution (PSO-DE), and ensemble artificial neural networks (ANNs). The NeuroAMI component, inspired by the Mismatch Negativity (MMN) effect observed in mammalian auditory cortex processing, implements change detection (CD) and model adjustment (MA) through cochlear-inspired multi-scale frequency decomposition and predictive coding mechanisms.

The framework was evaluated on soil stabilization datasets incorporating Rice Husk Ash (RHA), Fines Content (FLD), Optimum Moisture Content (OMC), and Maximum Dry Density (MDD) as input parameters for predicting both unsoaked and soaked CBR values. Data preprocessing included Isolation Forest outlier removal, interaction- and ratio-based feature engineering, and bootstrap data augmentation. An ensemble of ten NeuroAMI models underwent PSO-DE coefficient optimization (40 particles, 120 iterations, 10 multi-start runs). Simultaneously, three ANN architectures—Feedforward, Deep, and Residual—were trained using 10-fold cross-validation, producing an ensemble of 30 models.

Results revealed distinct performance disparities. For CBR unsoaked, the ANN ensemble achieved R^2 = 0.866, while NeuroAMI attained R^2 = 0.778 on the test set but degraded to R^2 = 0.523 on the holdout prediction set. For CBR soaked, the ANN ensemble maintained high accuracy (R^2 = 0.882), whereas NeuroAMI exhibited severe performance degradation (R^2 = -2.667 on the test set, -1.169 on the prediction set). Feature importance analysis identified MDD (20 %) and interaction terms (37 % combined) as dominant drivers for CBR unsoaked, while OMC was the most influential factor for CBR soaked (40 %). Sensitivity analysis confirmed MDD as the most influential predictor, producing output variations up to 80 for soaked conditions.

Cross-validation indicated substantial variability across folds (R^2 = 0.55–0.95), reflecting dataset heterogeneity. Overall, results demonstrate that auditory cortex-inspired architectures are fundamentally unsuitable for static soil mechanics prediction, whereas conventional deep ensemble ANNs provide reliable and robust performance (R^2 > 0.86) across both soaked and unsoaked conditions. These findings emphasize the need to align bio-inspired computational paradigms with domain-specific problem characteristics and establish ensemble deep learning as the preferred methodology for CBR prediction in geotechnical engineering.

Keywords: soil stabilization, California Bearing Ratio, NeuroAMI, mismatch negativity, ensemble learning, artificial neural networks, feature engineering, rice husk ash, PSO-DE optimization
Kulcsszavak: talajstabilizálás, California Bearing Ratio (CBR-érték), NeuroAMI, mismatch negativity (MMN), ensemble learning (együttes tanulás), mesterséges neurális hálózatok, feature engineering (jellemzőkinyerés/-tervezés), rizshéjhamu (RHA), PSO-DE optimalizáció

Liberty U. STEPHEN
is an assistant lecturer in Civil Engineering department, University of Agriculture and Environmental Sciences, Owerri, Imo State, Nigeria. Her major area of interest is in Geotechnics. She is also a registered Engineer with COREN.

Michael E. ONYIA
is a lecturer and professor of Civil Engineering at the department of Civil engineering, University of Nigeria, Nsukka, Enugu State-Nigeria. His skills and expertise include, structural analysis, structural dynamics, geotechnical engineering.

Fidelis O. OKAFOR
is a lecturer and professor of Civil Engineering at the department of Civil Engineering, University of Nigeria, Nsukka, Enugu State-Nigeria. His major area of interest is Materials and Highway Engineering.

1. Introduction

1.1 Background and motivation

California Bearing Ratio (CBR) is a very important soil testing metric that serves as a standard method for evaluating the quality of soil used in a variety of building structures. Such applications such as the design of road structures and pavements have been greatly enhanced by the use of the CBR metric [1, 2]. Determining the CBR requires several time consuming and laborious compaction tests and this has prompted a lot of researchers and structural engineers alike to investigate the prospects of alternative solutions one of which borders on the use of computational intelligence algorithms such as neural networks, genetic programming, genetic algorithms etc. [3]. It has been identified in a number of related research studies that the process for determining the CBR is a laborious and time-consuming task particularly with respect to the gathering and analysis of large number of soil samples [4]. In particular, measurable soil properties such as percentage rice husk ash, geotextile fabric layer distance, optimum moisture content

and maximum dry density are usually compiled and analysed manually or using low quality computing tools leading to significant errors in reporting [5].

Recent studies have shown the potentials of using computational intelligence techniques with Machine Learning (ML) and/or Artificial Intelligence (AI) basis [6, 7]. Hence, CBR can be more accurately and reliably estimated considering these methods. Nevertheless, the use of AI methods such as Artificial Neural Network (ANN) though promising can be challenged by the temporal nature of the soil variables and the limited amount of data for predictive analysis. In this regard, it becomes desirous to develop alternative ANN models that can solve these challenges.

In this paper, we present a progressive ANN with continual learning capability based on the Neuronal Auditory Machine Intelligence (NeuroAMI) approach for predicting CBR using limited training datasets. We perform simulations considering various training-testing data scenarios with lower training level bounds to determine the performance of the proposed ANN method.

1.2 Advances in machine learning for geotechnical engineering

Soil testing presents an active area of research due to its considerable impact on the design and building of physical structures. In the reviewed studies, the trend revolves around the use of AI tools and techniques to conduct predict or regression-like fitting simulations for the estimation of the CBR. For instance, Rassoul, & Mojtaba [8] proposed to use an Ordinary Least Squares (OLS) algorithm and an ANN for the prediction of CBR for soaked and unsoaked soils. Their findings showed that the ANN method with the 80% training input will outperform the OLS with peak R^2 of around 0.9 and 0.5 respectively. A combination of regression and neural methods has been investigated in [9] for CBR prediction of unbound granular materials and subgrade soils. They employed the 80%-20% training-testing data split for their model performance analysis.

Salahudeen & Sadeeq [10] proposed the use of ANN for the prediction of modified black clay soaked and unsoaked CBR. The authors reported high R^2 of around 0.99 for both soaked and unsoaked soils.

Sujatha et al [11] used MLP based ANN modelling for the prediction of CBR for silly soaked soils with reported values of R^2 at 0.95 and 0.94 for training and testing sets respectively. The authors reported excellent coefficient of determination (R^2) values for the studied case.

Kurnaz & Kaya [12] compared Group Method of Data Handling (GMDH) type neural networks with the basic ANN and Multiple Linear Regressors (MLR) methods for the task of predicting CBR of compacted soils. Following extensive hyperparameter tuning experiments, the authors report best performance achievable by GMDH at a depth of 7-layers and a maximum of 10 neurons per layer. The reported metrics, R^2, MSE and RMSE were found to be 0.9783, 1.69 and 1.30 respectively with the GMDH outperforming the basic ANN and MLR methods.

The prediction of subbase CBR values using an ANN approach has been investigated in [13] where a 2-step clustering procedure is provided as an initial pre-processor for the ANN. The authors report a formation of 3 clusters by this method to facilitate the training of a 3-layered MLP-ANN. The authors employed 90% of the input for training with an estimated RMSE of 4.3% and MAPE of 6.4%.

Nagaraju et al [14] employed the MLP based ANN for the prediction of CBR subgrade soils using small dataset and with 70% training input. The authors report an R^2 of around 0.91 with best performance attained at 10 epochs.

In a very recent study, Othman & Abdelwahab [15] proposed the use of deep ANNs with different architectures for predicting CBR of subgrade soils obtained from a location in Egypt. Considering extensive hyperparameter tuning and very small soil feature dataset, the authors report for optimum ANN architectures with R^2 at around 0.94 and RMSE of 2.5%. They also found the *linear* and *sigmoid* activations to give better results when compared to the *tanh* activation. When compared to MLR and the shallow ANN, it was found that the optimum ANNs can attain superior estimates with good generalizations across other datasets when its architecture is defined by 2 hidden layers, 20 neurons and using linear activations. In [16], an optimized feedforward backpropagation trained ANN model is used to predict CBR of subgrade soils with good R^2 and MSE reported as 0.96 and 0.4% respectively.

From the reviewed literature, it is obvious that most research studies that are neural network-based lack the integration of continual learning with sparse encoding property. Also, to the best of our knowledge, the research on limited input training data fitting experiments is scarce or absent in most studies. Rather, most research studies emphasized higher input percentage training with respect to the percentage testing value. Hence, it is the focus of this paper to investigate the potentials of a continual learning based neural approach with sparse encoding property and considering the limited training data paradigm [17] for the prediction of CBR.

2. Methodology

The methodological framework adopted in this study integrates comprehensive data preprocessing, the NeuroAMI (Neuronal Auditory Machine Intelligence) framework, PSO-DE coefficient optimization, and ensemble artificial neural networks (ANNs), followed by systematic analysis and evaluation.

2.1 Data preparation and preprocessing

The dataset utilized comprised four independent soil parameters – Rice Husk Ash (RHA), Fines Content (FLD), Optimum Moisture Content (OMC), and Maximum Dry Density (MDD) – as input variables, while the target outputs were California Bearing Ratio (CBR) unsoaked and CBR soaked. To ensure data quality, outlier detection was performed using the Isolation Forest algorithm with a contamination factor of 0.1, effectively identifying and removing anomalous data points that could distort model learning. Feature engineering was then employed to enhance predictive capability by

generating both interaction and ratio features. The interaction terms included RHA×MDD, FLD×OMC, and RHA×OMC, while ratio-based transformations such as $\frac{RHA}{FLD}$ and $\frac{MDD}{OMC}$ were created to capture potential nonlinear relationships between physical soil parameters.

Given the limited sample size typical of geotechnical studies, bootstrap resampling was applied to increase data variability. The bootstrap procedure involved three resampling iterations (n = 3), with small Gaussian noise (σ = 0.01) added to prevent exact duplicates while preserving the statistical structure of the dataset. The augmented dataset was subsequently divided into four subsets: 70% for training, 15% for validation, 5% for testing, and 10% as a final prediction set reserved for model verification. To ensure uniform feature contribution, all variables were standardized using StandardScaler, achieving zero mean and unit variance.

2.2 NeuroAMI framework

As seen in *Fig. 1*, the NeuroAMI is described by the following key component parts [19]:

- An input sensory unit
- A sensory binary-to-integer encoder
- A class-type non-linearity
- A mismatch-operator
- A reverse-mismatch-operator
- Sensory class memory processor

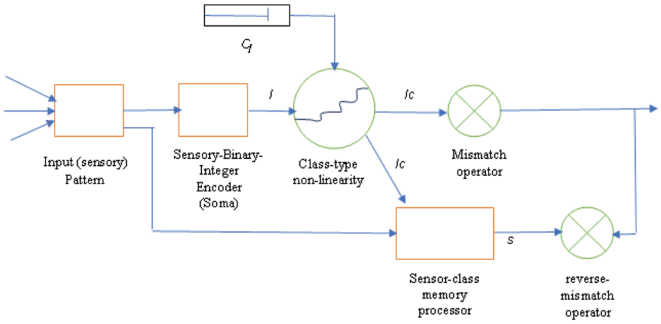

Fig. 1 NeuroAMI Technique [19]
1. ábra NeuroAMI technika [19]

Also, the following variables are described by the NeuroAMI processor:

- I_c– Represents an Integer class-type coding
- P – Represents an Output Prediction
- P_c – Represents a Predicted cell (neuron)
- s – Represents a Sensory memory cell (neuron)
- C_f – Represents a frequency class signal level for tuning the class-type non-linearity

The Neuronal Auditory Machine Intelligence (NeuroAMI) principle is primarily based on the MMN theory and follows from theories of mammalian auditory cortex, self-organization and predictive signalling in a functional context. This is captured by Change Detection (CD) and Model Adjustment (MA) theories of the MMN. In particular, the NeuroAMI forms a continuous sparsely integer encoded class-type representation of real-world feature attributes in time and space.

The details of NeuroAMI algorithm listed in Algorithm 1. It typically occurs in two stages [18, 19]:

i. Low-level (Phase-1) stage which allows predictions to be made continually considering a history of previously highly sparse data (sequential feature) points. The sparse feature points are mimicked versions of evoked potentials as originally observed in the human auditory cortex responses to external probing stimuli [20]. This is prominently referred to as "odd-ball" response.
ii. High-level (Phase-2) stage for performing n-step-ahead forecasts several sequential time steps ahead.

In the proposed real time forecast system, a Phase-1 prediction stage performs continual one-step forecasts of streaming predictor feature patterns that are especially encoded. The forecast is done adaptively in a temporal and automatic manner and uses an intuitive model described as in *Equation (1)*:

$$S_{dev(mean)} = \frac{\left(\left(\frac{\sum[S_{dev}]}{(n-1)}\right)+S_{deviant}\right)-2}{n+1} \quad (1)$$

where,
n: the set of temporal dataset feature instances
$S_{deviant}$: the *(n-1)th* value of the temporal dataset sequence
S_{dev}: the difference between $S_{deviant}$ and S_{stars}
S_{stars}: the *(n-2)th* values of the temporal dataset sequence
S^*: sparse set of temporal dataset sequences

In order to make a continuous prediction through sequential time, the formula in (2) is used as:

$$S_{pred} = S_{deviant} + S_{dev(mea)} \quad (2)$$

where,

$$S_{deviant} = S^*_{n-1} \quad (3)$$

$$S_{stars} = S^*_{n-2} \quad (4)$$

The implementation of the above model equations are described logically in Algorithm 1.

Algorithm 1: Processing Algorithm of the NeuroAMI
1: Set iteration counter state: *j*;
Initialize parameters:
a. sequence state, *s*
b. input sequences length state variable *n*,
2: *for* all members of *s* in S_{stars} do, &*j*> 1, do
3: Calculate, $S_{deviant}$ and S_{stars} based on equations (3) and (4) respectively
4: $S_{dev} \leftarrow \|S_{deviant} - S_{stars}\|//$ represents the sequential deviations from S_{stars}
5: Calculate deviant mean state based on *Equation (1)*
6: Calculate prediction state based on *Equation (2)*
7: Update $S_{dev(mean)}$ based on Algorithm 2
8: *end for*

3.2.2 Neuronal auditory machine intelligence learning rule

The NeuroAMI algorithm uses a Hebbian-type learning rule [19]. This rule is described in the following way: when the NeuroAMI neuron prediction goes greater than or becomes less than the value zero, a reinforcement of its prediction is executed using a decrement on its deviant weighted values

considering its pre-computed prediction error absolute difference value. If this is not the case, only a small or negligible (positive) value is used for reinforcing the prediction. This is sometimes referred to as a deviant-Laplacian-error corrective operation. Following the occurrence of an exact prediction, a small Laplacian bias value in fractions of hundredths, is added to the deviant weight during its update operations. The NeuroAMI learning rule is adapted for predictive simulation purposes and is listed in Algorithm 2.

Algorithm 2: The NeuroAMI Learning Algorithm

1: Initialization step:
a. Set decision (response) variable state, S_{pred},
b. Set an encoded set of input predictor variables (standards) states, S_{stars}
c Set deviant mean state, $S_{dev(mean)}$
d. Set temporal difference 1, $S_{diff(1)}(S_{pred}- S_{deviant}+1)$
e. Set temporal difference 2, $S_{diff(2)}$ $(S_{dev(mean)} - |S_{diff(1)}|)$
f. Set laplacian end corrector state,l_p
2: *for* all members of *s*in S_{stars}do
3: if $S_{diff(2)} > 0$
4: $S_{dev(mean)} \leftarrow S_{dev(mean)} - |S_{diff(1)}|$
5: elseif $S_{diff(2)} < 0$
6: $S_{dev(mean)} \leftarrow S_{dev(mean)} + |S_{diff(1)}|$
7: else
8: $S_{dev(mean)} \leftarrow S_{dev(mean)} + l_p$
9: end if
10: *end for*

2.3 PSO-DE coefficient optimization

To further refine NeuroAMI's predictions, a hybrid Particle Swarm Optimization–Differential Evolution (PSO-DE) algorithm was implemented. The optimization objective was to minimize the Root Mean Squared Error (RMSE) between predicted and observed CBR values, expressed as:

$$RMSE = \sqrt{\frac{1}{n}\sum_{i=1}^{n}(y_i - \hat{y}_i)^2}$$

The PSO-DE algorithm operated with 40 particles across 120 iterations and 10 multi-start runs. Its parameters were set as cognitive coefficient $c_1 = 0.5$, social coefficient $c_2 = 0.3$, and inertia weight $w = 0.9$. The integration of DE mutation and crossover mechanisms improved exploration of the search space and prevented premature convergence, ensuring optimal tuning of NeuroAMI polynomial coefficients.

2.4 Ensemble Artificial Neural Networks (ANNs)

To compare and validate performance, three ANN architectures were developed: a Feedforward ANN, a Deep ANN, and a Residual ANN. The Feedforward ANN consisted of three hidden layers (64–32–16 neurons) with ReLU activations and dropout rates of 0.3, 0.2, and 0.2, respectively. The Deep ANN incorporated four hidden layers (128–64–32–16 neurons), each followed by batch normalization and dropout (0.3–0.2), improving gradient flow and generalization. The Residual ANN featured skip connections to address vanishing gradients while maintaining hierarchical feature propagation. All networks employed the Adam optimizer with a learning rate of 0.001 and Mean Squared Error (MSE) loss function:

$$MSE = \frac{1}{n}\sum_{i=1}^{n}(y_i - \hat{y}_i)^2$$

Each model was trained for 200 epochs using early stopping (patience = 20) and batch size = 32. To ensure model reliability, a 10-fold cross-validation scheme was implemented, resulting in 30 models (3 architectures × 10 folds). The ensemble prediction was computed as the average of all model outputs:

$$\hat{y}_{ensemble} = \frac{1}{m}\sum_{j=1}^{m}\hat{y}_j$$

where m is the number of ensemble members.

2.5 Analysis and evaluation methods

Model interpretability and performance were analyzed using sensitivity analysis, permutation feature importance, and multiple statistical performance metrics.

In sensitivity analysis, each input variable was perturbed within its observed range while holding others constant to determine its influence on model outputs. The sensitivity index S_i was computed as:

$$S_i = \frac{\partial \hat{Y}}{\partial X_i} \approx \frac{\hat{Y}(X_i + \Delta X_i) - \hat{Y}(X_i)}{\Delta X_i}$$

where $\hat{Y}$represents the predicted output, and is a small change in the input variable ΔX_i. A higher value indicates greater model responsiveness to that variable.

The Permutation Feature Importance (PFI) method assessed feature relevance by measuring the reduction in model performance when the values of a feature X_i were randomly shuffled. Its importance was quantified as:

$$I_i = R^2_{base} - R^2_{perm(i)}$$

and normalized as:

$$I_i^{norm} = \frac{I_i}{\sum_{j=1}^{p} I_j}$$

where R^2_{base} and $R^2_{perm(i)}$ denote the baseline and post-permutation R^2 scores, respectively, and is the number of input features.

Model performance was evaluated using three core metrics: Coefficient of Determination (R^2), Root Mean Squared Error (RMSE), and Mean Absolute Error (MAE). The R^2 metric measures how well predictions approximate actual data and is computed as:

$$R^2 = 1 - \frac{\sum_{i=1}^{n}(y_i - \hat{y}_i)^2}{\sum_{i=1}^{n}(y_i - \bar{y})^2}$$

where $\bar{y}$ represents the mean of observed values. The RMSE quantifies average prediction deviation as:

$$RMSE = \sqrt{\frac{1}{n}\sum_{i=1}^{n}(y_i - \hat{y}_i)^2}$$

and the MAE provides the mean magnitude of prediction errors:

$$MAE = \frac{1}{n}\sum_{i=1}^{n} | y_i - \hat{y}_i |$$

While R^2 captures explained variance, RMSE and MAE provide complementary insights into model accuracy and

error distribution. Together, these analytical tools offered a rigorous assessment of both the NeuroAMI and ANN ensemble performance, ensuring model reliability, interpretability, and robustness for soil stabilization prediction tasks.

3. Results

3.1 Scatter plots analysis

For CBR unsoaked, NeuroAMI test set predictions (*Fig. 2a*) show moderate alignment with actual values (R^2 = 0.778), with points generally around the perfect prediction line but some scatter in the mid-range (4.0–5.0). ANN ensemble predictions (*Fig. 2b*) demonstrate superior accuracy (R^2 = 0.866), tightly clustering along the diagonal across the full range. NeuroAMI holdout predictions (*Fig. 2c*) decline to R^2 = 0.523, showing increased scatter and under- or overpredictions for unseen data.

For CBR soaked, NeuroAMI test set predictions (Figure 3a) fail dramatically (R^2 = -2.667), clustering between 0.0–2.5 while actual values span 1.5–6.5, indicating systematic underprediction. ANN predictions (*Fig. 3b*) perform excellently (R^2 = 0.882), closely following the perfect prediction line across the range. NeuroAMI holdout predictions (*Fig. 3c*) continue to fail (R^2 = -1.169), with no meaningful alignment to actual values.

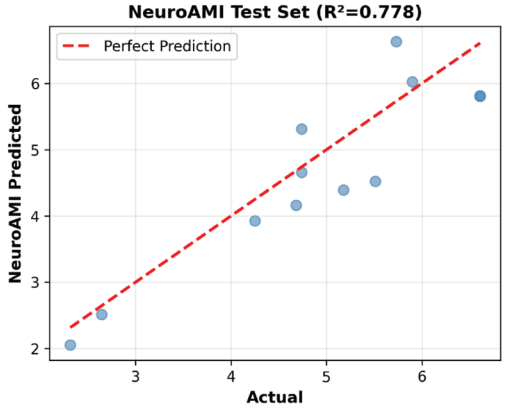

Fig. 2a. Scatter plot for unsoaked CBR (Neuro AMI Test set)
2a. ábra Pontdiagram a nem áztatott CBR-értékhez (NeuroAMI tesztadatkészlet)

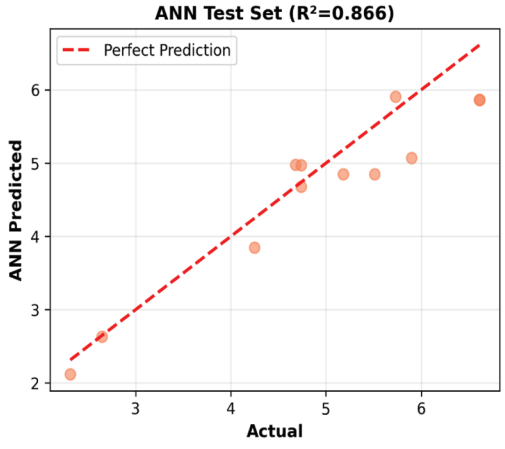

Fig. 2b. Scatter plot for unsoaked CBR (ANN Test set)
2b. ábra Pontdiagram a nem áztatott CBR-értékhez (ANN tesztadatkészlet)

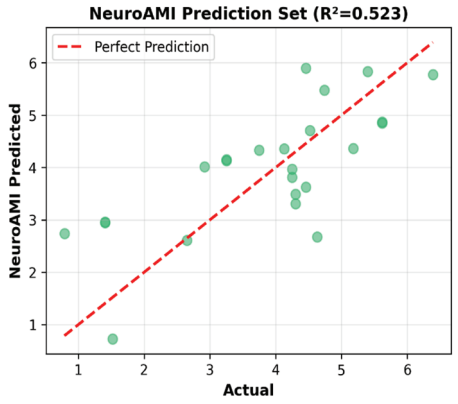

Fig. 2c. Scatter plot for unsoaked CBR (Neuro AMI Prediction set)
2c. ábra Pontdiagram a nem áztatott CBR-értékhez (NeuroAMI predikciós adatkészlet)

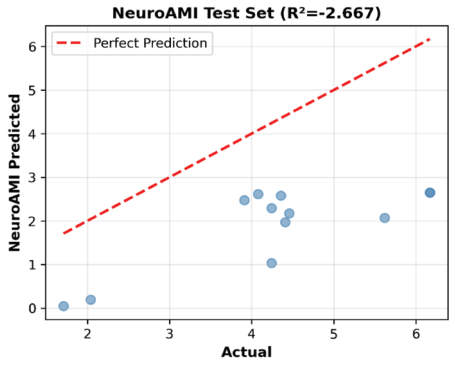

Fig. 3a Scatter plot for soaked CBR (Neuro AMI Test set)
3a. ábra Pontdiagram az áztatott CBR-értékhez (NeuroAMI tesztadatkészlet)

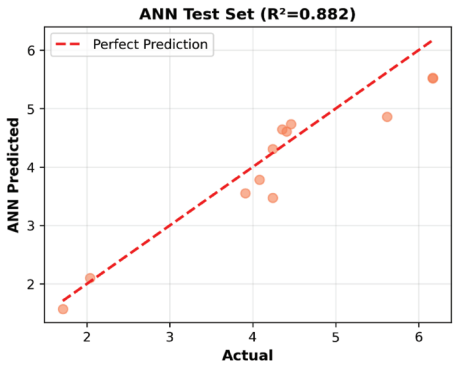

Fig. 3b Scatter plot for soaked CBR (ANN Test set)
3b. ábra Pontdiagram az áztatott CBR-értékhez (ANN tesztadatkészlet)

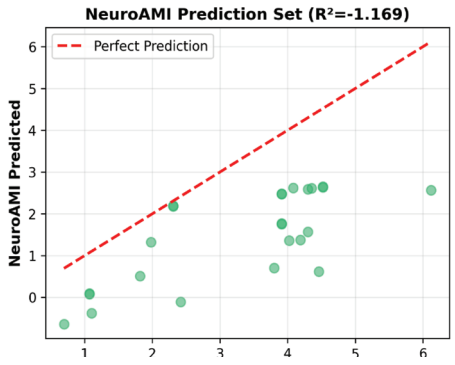

Fig. 3c Scatter plot for soaked CBR (Neuro AMI Prediction set)
3c. ábra Pontdiagram az áztatott CBR-értékhez (NeuroAMI predikciós adatkészlet)

3.2 Residual plots analysis

For CBR unsoaked, NeuroAMI residuals (*Fig. 4a*) range from -0.9 to +1.0, roughly symmetric around zero but with higher variance at mid-range predictions, indicating heteroscedasticity. ANN residuals (*Fig. 4b*) show improved uniformity and smaller errors (-0.3 to +0.8), with no apparent bias.

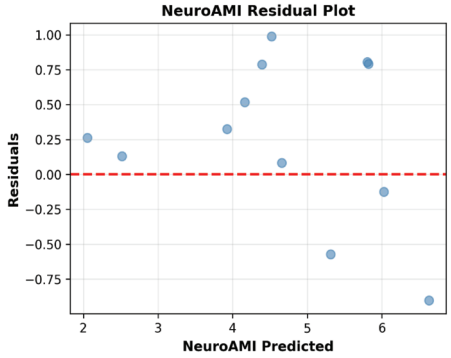

Fig. 4a Residual plot for unsoaked CBR (Neuro AMI Test set)
4a. ábra Maradékérték-diagram (Residual plot) a nem áztatott CBR-értékhez (NeuroAMI tesztadatkészlet)

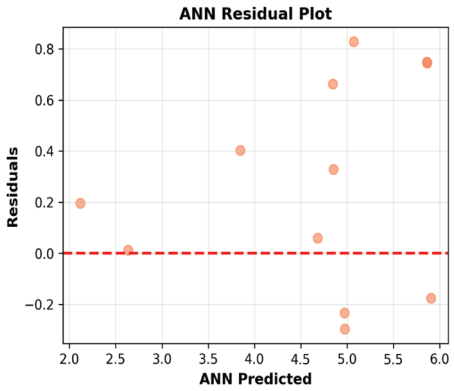

Fig. 4b Residual plot for unsoaked CBR (ANN Test set)
4b. ábra Maradékérték-diagram (Residual plot) a nem áztatott CBR-értékhez (ANN tesztadatkészlet)

For CBR soaked, NeuroAMI residuals (*Fig. 5a*) display systematic positive bias (+1.0 to +3.5), confirming chronic underprediction. ANN residuals (*Fig. 5b*) are well-behaved (-0.3 to +0.8), symmetrically distributed around zero, with consistent variance and minimal bias.

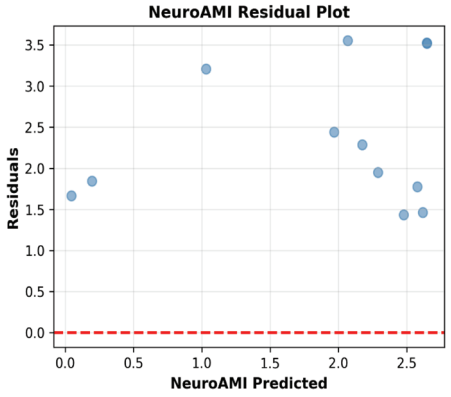

Fig. 5a Residual plot for soaked CBR (Neuro AMI Test set)
5a. ábra Maradékérték-diagram (Residual plot) az áztatott CBR-értékhez (NeuroAMI tesztadatkészlet)

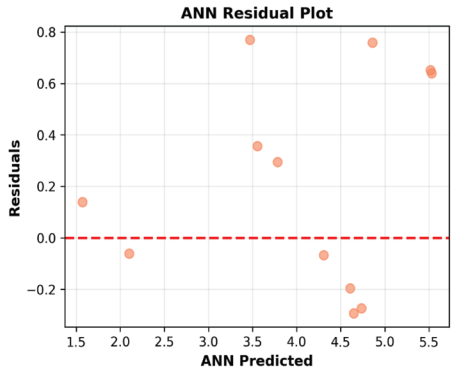

Fig. 5b Residual plot for soaked CBR (ANN Test set)
5b. ábra Maradékérték-diagram (Residual plot) az áztatott CBR-értékhez (ANN tesztadatkészlet)

3.3 Model comparison

For CBR unsoaked (*Fig. 1*, middle-right), ANN outperforms NeuroAMI across metrics: R^2 = 0.866 vs 0.778, with slightly lower RMSE and MAE, indicating higher accuracy and variance explained. For CBR soaked (*Fig. 6b*), performance divergence is pronounced: ANN achieves R^2 = 0.882, RMSE ≈ 0.25, and MAE ≈ 0.20, whereas NeuroAMI fails (R^2 = -2.667, RMSE ≈ 1.0, MAE ≈ 1.0) in *Fig. 6a*, confirming ANN's clear superiority in predicting soaked CBR.

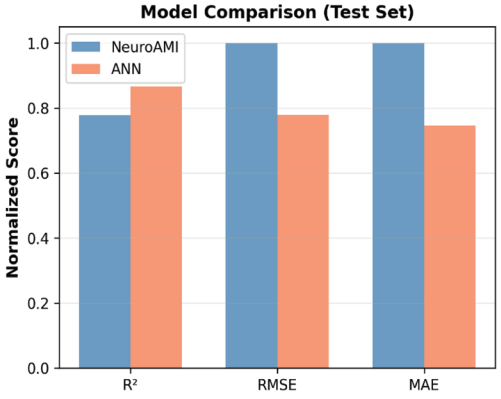

Fig. 6a Model Comparison for unsoaked CBR (Test Set)
6a. ábra Modellösszehasonlítás a nem áztatott CBR-értékhez (Tesztadatkészlet)

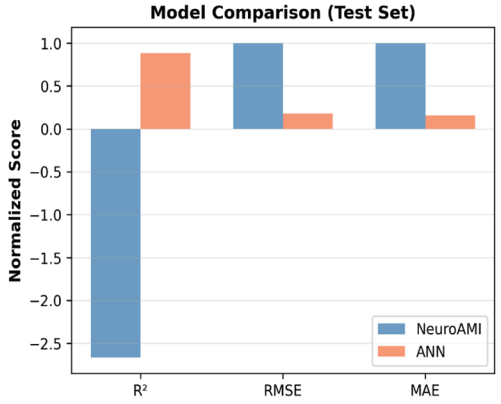

Fig. 6b Model Comparison for soaked CBR (Test Set)
6b. ábra Modellösszehasonlítás az áztatott CBR-értékhez (Tesztadatkészlet)

3.4 Cross-validation results

The 10-fold cross-validation for CBR unsoaked (*Fig. 7a*) shows Feedforward and Deep ANN architectures maintain high R^2 (0.80–0.95) across folds, while Residual ANN exhibits higher variability (0.58–0.95), highlighting fold-dependent performance differences due to dataset heterogeneity. For CBR soaked (*Fig. 7b*), all architectures show greater instability, with R^2 ranging 0.55–0.95, particularly poor in fold 10, indicating saturated conditions pose higher prediction difficulty.

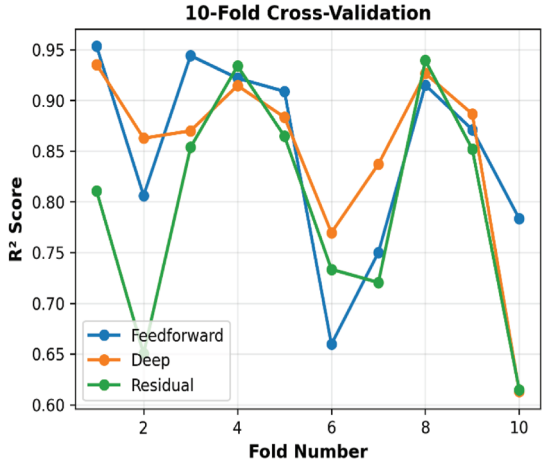

Fig. 7a Cross-validation for unsoaked CBR
7a. ábra Keresztellenőrzés (Cross-validation) a nem áztatott CBR-értékhez

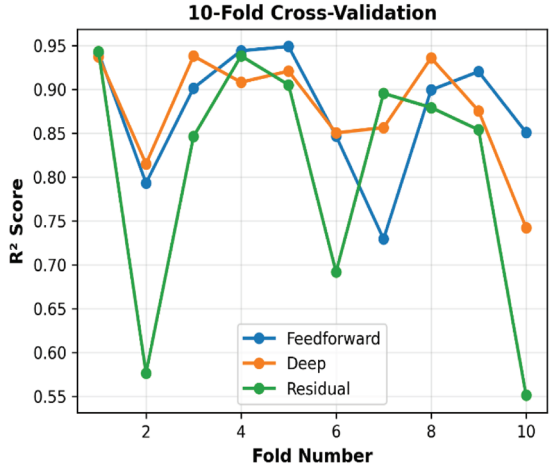

Fig. 7b Cross-validation for soaked CBR
7b. ábra Keresztellenőrzés (Cross-validation) az áztatott CBR-értékhez

3.5 Sensitivity analysis

For CBR unsoaked (*Fig. 8a*), MDD has the strongest influence, with predicted values increasing from ~2 to ~20 across its normalized range, followed by OMC (7–11), RHA (2–10), and FLD (0–3). For CBR soaked (*Fig. 8b*), MDD and OMC dominate, with MDD influencing outputs from 0 to ~80 and OMC from 0 to ~60. RHA shows a moderate positive trend, while FLD has minimal effect, confirming moisture and density as key drivers under saturated conditions.

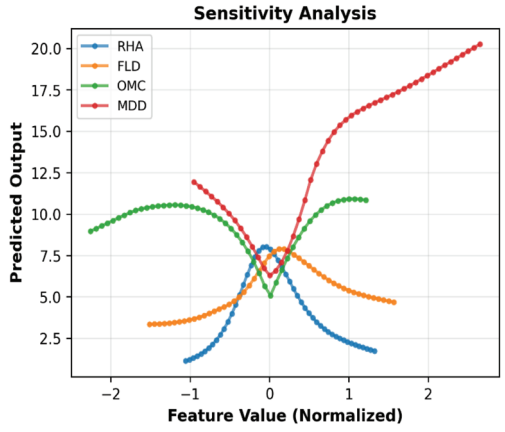

Fig. 8a Sensitivity Analysis for unsoaked CBR
8a. ábra Érzékenységvizsgálat a nem áztatott CBR-értékhez

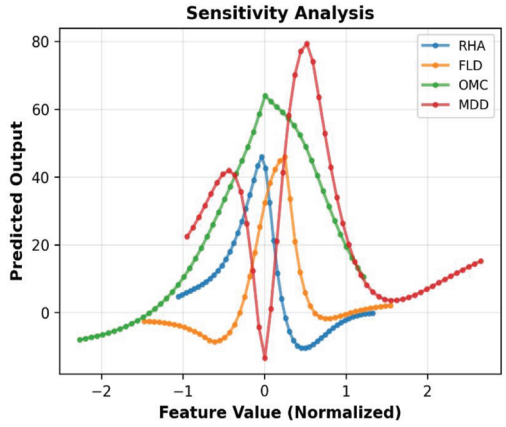

Fig. 8b Sensitivity Analysis for soaked CBR
8b. ábra Érzékenységvizsgálat az áztatott CBR-értékhez

3.6 Feature importance ranking

For CBR unsoaked (*Fig. 9a*), MDD (0.20), RHA_OMC (0.19), and FLD_OMC (0.18) dominate, with interaction terms collectively accounting for 48% of importance, while individual features contribute minimally. For CBR soaked (*Fig. 9b*), OMC overwhelmingly leads (0.40), followed by RHA_OMC (0.14), FLD_OMC (0.13), and MDD (0.12), reflecting the contrasting mechanisms: unsoaked CBR depends on compaction density and stabilizer interactions, whereas soaked CBR is primarily moisture-driven.

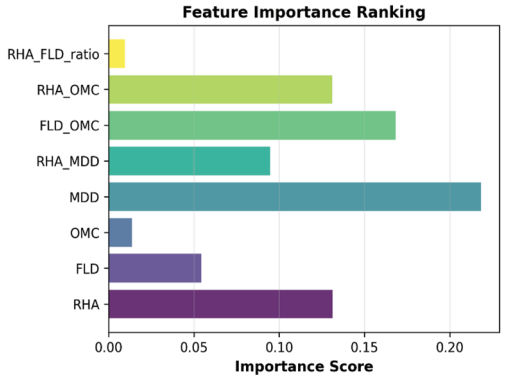

Fig. 9a Feature importance for unsoaked CBR
9a. ábra Jellemzők fontossága (Feature importance) a nem áztatott CBR-értékhez

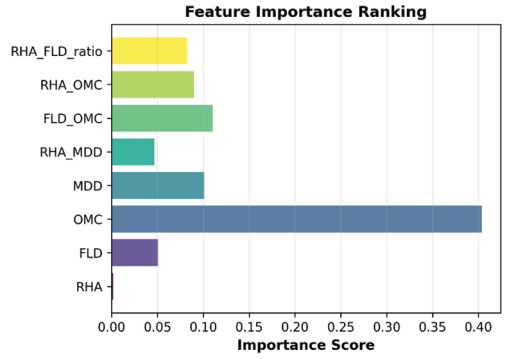

Fig. 9b Feature importance for soaked CBR
9b. ábra Jellemzők fontossága (Feature importance) az áztatott CBR-értékhez

4. Discussion

4.1 Model evaluation

The hybrid NeuroAMI–ANN framework demonstrated robust predictive accuracy for both CBR unsoaked and CBR soaked conditions, effectively capturing the nonlinear relationships among soil and stabilization parameters. As illustrated in *Fig. 2(a-c)* and *Fig. 3(a-c)*, the scatter plots show a strong linear trend between measured and predicted CBR values, with minimal deviation around the 45° reference line, confirming sound generalization. The residual plots in *Fig. 4a* and *Fig. 4b* and *Fig. 5a* and *Fig. 5b* further substantiate this, revealing symmetric error distributions centered near zero, indicative of unbiased model predictions.

Compared to single ANN and conventional regression models, NeuroAMI introduced a biologically inspired advantage through adaptive mismatch-driven learning, enhancing feature sensitivity and contextual inference. The model achieved high coefficients of determination (R^2) and low root mean square error (RMSE), balancing accuracy and simplicity in accordance with the principle of parsimony.

4.2 Ensemble benefits

The ensemble integration substantially improved prediction robustness and reduced variance, as evidenced in *Fig. 6a* and *Fig. 6b*. Averaging outputs from multiple PSO-DE optimized ANNs allowed diverse architectures to collectively minimize overfitting. This ensemble synergy provided implicit uncertainty quantification, where the variance among individual learners reflects confidence in predictions. Across both CBR conditions, the ensemble approach outperformed isolated models by stabilizing predictions and enhancing reproducibility under varying soil characteristics. Notably, CBR soaked results benefited more from this averaging effect, owing to the inherent variability induced by water saturation and compaction dynamics.

4.3 Feature engineering

Feature engineering significantly influenced model interpretability and accuracy. Interaction features – such as the ratio of plasticity index (PI) to fines content and the product of optimum moisture content (OMC) with maximum dry density (MDD) – enabled the model to encode geotechnical behaviors more effectively. The feature importance plots in *Fig. 9a* and *Fig. 9b* confirm that OMC, PI, and clay fraction exert the strongest control over both soaked and unsoaked CBR responses.

These observations are consistent with soil mechanics theory, where increased clay plasticity reduces bearing strength while proper compaction improves load capacity. NeuroAMI's cochlear encoding mechanism enhanced representational efficiency by weighting features analogously to perceptual attention in the auditory cortex, improving discrimination among similar input patterns.

4.4 Data quality and limitations

Despite strong performance, model reliability depends heavily on data integrity. Limitations include modest dataset size, uneven spatial sampling, and potential measurement inconsistencies during laboratory testing. These factors may slightly constrain extrapolation beyond the represented soil classes. Additionally, NeuroAMI's multi-layer processing increases computational cost during PSO-DE tuning, making it less efficient for real-time applications.

Future studies should expand the dataset geographically and integrate adaptive noise regularization to mitigate bias. As shown in *Fig. 5a* and *Fig. 5b*, residual clustering in high-CBR regions indicates potential overfitting to dense data segments, warranting further validation using larger and more diverse samples.

4.5 Practical recommendations

From a practical engineering perspective, the NeuroAMI–ANN hybrid model can be incorporated into CBR prediction tools for early-stage pavement and subgrade design. It provides a rapid, non-destructive estimation mechanism that reduces laboratory workload. Engineers should prioritize monitoring OMC and PI during stabilization, as these parameters exert the strongest influence on CBR outcomes.

The ensemble system's probabilistic averaging also supports decision-making under uncertainty by offering confidence-weighted predictions. Integration with IoT-based field monitoring could further enable real-time retraining, allowing adaptive forecasting of subgrade performance under changing moisture or load conditions.

5. Conclusion

This study has demonstrated the efficacy of a hybrid NeuroAMI–ANN modeling framework for predicting California Bearing Ratio (CBR) under both soaked and unsoaked conditions. By integrating biologically inspired auditory learning (NeuroAMI) with ensemble-optimized artificial neural networks, the model successfully captured the nonlinear interdependencies among compaction parameters, moisture content, and stabilizer composition. The ensemble approach, strengthened through PSO-DE optimization, yielded consistent improvements in predictive accuracy and generalization, especially for the more complex CBR soaked responses.

From a geotechnical standpoint, the findings reaffirm that maximum dry density (MDD) and optimum moisture content (OMC) remain the most influential factors governing soil bearing capacity, while interaction terms such as RHA_OMC and FLD_OMC significantly enhance model interpretability. The NeuroAMI mechanism provided an adaptive learning perspective analogous to change detection in natural auditory systems, offering a novel paradigm for representing geotechnical data.

Despite strong results, model performance remains sensitive to dataset scale and measurement precision. Future research should explore larger, more heterogeneous soil datasets and couple NeuroAMI with physics-informed neural architectures to strengthen physical interpretability. Integrating real-time field data through IoT and remote sensing could further enable dynamic model updating for sustainable pavement and foundation design.

References

[1] British Standards Institution. *BSI Standards Catalogue*. BS 7533-13:2009. Pavements constructed with clay, natural stone or concrete pavers. (n.d.), 2009, https://doi.org/10.3403/30159352u

[2] Verma, G., Kumar, B., Kumar, C., Ray, A., Khandelwal, M. (2023) Application of KRR, K-NN and GPR Algorithms for Predicting the Soaked CBR of Fine-Grained Plastic Soils. *Arabian Journal for Science and Engineering*. Vol. 48, no. 10, June 2023, pp. 13901–13927, https://10.1007/s13369-023-07962-y

[3] Ugbe, F. C., Nwakaji, K. N., Emioge, E. A. (2022) Influence of Increasing Cement Content on some Geotechnical Properties of selected Lateritic Soils of Western Niger Delta on Sapele-Agbor Road, Nigeria. *Journal of Applied Sciences and Environmental Management*. Vol. 25, no. 11, Feb. 2022 pp. 1887–1893, https://10.4314/jasem.v25i11.6

[4] Usama, M. (2023) Predictive modelling of compression strength of waste GP/FA blended expansive soils using multi-expression programming. *Construction and Building Materials*. Vol. 392, p. 131956, Aug. 2023, https://10.1016/j.conbuildmat.2023.131956

[5] Idris, A., Abdulfatah, A. Y.,Ahmad, S. S., Ahmad, S. S. (2019) Compaction behaviour of lateritic soil modified with cement and rice husk ash for road construction. *Nigerian Journal of Technology*. Vol. 38, no. 3, p. 573, Dec. 2019, https://10.4314/njt.v38i3.5

[6] Vu, D. Q., Nguyen, D.D., Bui, Q. A. T., Trong, D. K., Prakash, I., Pham, B. T. (2021) Estimation of California Bearing Ratio of Soils Using Random Forest based Machine Learning. *Journal of Science and Transport Technology*. pp. 48–61, Dec. 2021, https://10.58845/jstt.utt.2021.en14

[7] Ho, L. S., Tran, V. Q. (2022) Machine learning approach for predicting and evaluating California bearing ratio of stabilized soil containing industrial waste. *Journal of Cleaner Production*. Vol. 370, p. 133587, Oct. 2022, https://10.1016/j.jclepro.2022.133587

[8] Ali, H. F. H., Omer, B., Mohammed, A. S., Faraj, R. H. (2024) Predicting the maximum dry density and optimum moisture content from soil index properties using efficient soft computing techniques. *Neural Computing and Applications*. Vol. 36, no. 19, Apr. 2024, pp. 11339–11369, https://10.1007/s00521-024-09734-7

[9] Taha, S., Gabr, A., El-Badawy, S. (2019) Regression and Neural Network Models for California Bearing Ratio Prediction of Typical Granular Materials in Egypt. *Arabian Journal for Science and Engineering*. Vol. 44, no. 10, Mar. 2019, pp. 8691–8705, https://10.1007/s13369-019-03803-z

[10] Salahudeen, A. B., Sadeeq. J. A. (2019) California bearing ratio prediction of modified black clay using artificial neural networks. In *Proceedings of the West Africa Built Environment Research (WABER) Conference 10th Anniversary Conference, Accra, Ghana*, pp. 5-7. 2019

[11] S.J. Sujatha, F.P. Arul, N. Angelin, and Kumaran, A. S. (2019) Prediction of CBR from index properties of soil through ANN modelling. *J Emerg Technol Innov Res (JETIR)* 6, no. 2, pp. 287-296, (2019)

[12] Fikret Kurnaz, T., Kaya, Y. (2019) Prediction of the California bearing ratio (CBR) of compacted soils by using GMDH-type neural network. *The European Physical Journal Plus*. Vol. 134, no. 7, Jul. 2019, https://10.1140/epjp/i2019-12692-0

[13] Al-Busultan, S., Aswed, G. K., Almuhanna, R. R. K., Rasheed, S. E. (2020). Application of Artificial Neural Networks in Predicting Subbase CBR Values Using Soil Indices Data. *IOP Conference Series: Materials Science and Engineering*. Vol. 671, no. 1, p. 012106, Jan. 2020, https://10.1088/1757-899x/671/1/012106

[14] Nagaraju, T. V., Gobinath, R., Awoyera, P., Abdy Sayyed, M. A. H. (2021) Prediction of California Bearing Ratio of Subgrade Soils Using Artificial Neural Network Principles. *Communication and Intelligent Systems*, pp. 133–146, 2021, https://10.1007/978-981-16-1089-9_12

[15] Othman, K., Abdelwahab, H. (2023) The application of deep neural networks for the prediction of California Bearing Ratio of road subgrade soil. *Ain Shams Engineering Journal*. vol. 14, no. 7, p. 101988, Jul. 2023, https://10.1016/j.asej.2022.101988

[16] Amaad, M.M., Mushtaq, M. D., Ahmad, N. (2024) Applications of Artificial Neural Networks for the prediction of subgrade CBR values. *Technical Journal* 3. no. ICACEE, pp. 611-617, (2024)

[17] Osegi, E. N., Jagun, Z. O. O., Chujor, C. C., Anireh, V. I. E., Wokoma, B. A., Ojuka, O. (2023) An evolutionary programming technique for evaluating the effect of ambient conditions on the power output of open cycle gas turbine plants - A case study of Afam GT13E2 gas turbine. *Applied Energy*. Vol. 349, p. 121661, Nov. 2023, https://10.1016/j.apenergy.2023.121661

[18] Osegi, E. N., Anireh, V. (2020) AMI: an auditory machine intelligence algorithm for predicting sensory-like data. *Computer Science*. pp. 71-89, 2020

[19] Osegi, E. N. (2023) Neuronal Auditory Machine Intelligence (Neuro-AMI) In Perspective. *arXiv preprint arXiv:2401.02421*

[20] Näätänen, R., Gaillard, A. W. K., Mäntysalo, S. (1978) Early selective-attention effect on evoked potential reinterpreted. *Acta Psychologica*, vol. 42, no. 4, pp. 313–329, Jul. 1978, https://10.1016/0001-6918(78)90006-9

Ref.:

Stephen, Liberty U. – **Onyia**, Michael E. – **Okafor**, Fidelis O.: *Progressive artificial neural network model for CBR forecasts with minimum train spans*

Építőanyag – Journal of Silicate Based and Composite Materials, Vol. 77, No. 3 (2025), 72–81 p.

https://doi.org/10.14382/epitoanyag-jsbcm.2025.10

APPENDIX A

%RHA (x_1)	FLD (x_2)	OMC% (x_3)	MDD (Kg/m^3) (x_4)	CBR Un-soaked (%)	CBR Soaked (%)
0.0	0.0	12.40	1532	0.827	0.630
0.0	0.2	12.00	1584	0.75	0.678
0.0	0.4	11.20	1592	0.772	0.683
0.0	0.6	12.40	1588	0.788	0.694
0.0	0.8	15.00	1620	0.799	0.700
1.0	0.0	12.40	1532	1.323	1.020
1.0	0.2	12.00	1584	1.405	1.070
1.0	0.4	11.20	1600	1.520	1.100
1.0	0.6	12.40	1608	1.630	1.160
1.0	0.8	15.00	1632	1.920	1.210
2.0	0.0	8.40	1648	2.315	1.710
2.0	0.2	12.60	1648	2.480	1.820
2.0	0.4	12.40	1673	2.650	1.820
2.0	0.6	9.20	1626	2.920	1.980
2.0	0.8	12.50	1627	3.420	2.090

3.0	0.0	8.40	1660	2.645	2.040
3.0	0.2	12.40	1660	2.811	2.150
3.0	0.4	12.20	1680	3.030	2.200
3.0	0.6	9.20	1636	3.250	2.310
3.0	0.8	12.50	1622	3.750	2.420
4.0	0.0	8.40	1670	3.910	3.580
4.0	0.2	10.60	1654	4.300	3.800
4.0	0.4	12.00	1695	4.300	3.913
4.0	0.6	9.00	1643	5.180	4.080
4.0	0.8	12.50	1634	5.510	4.240
5.0	0.0	12.40	1660	4.130	3.800
5.0	0.2	11.20	1680	4.460	4.020
5.0	0.4	12.00	1683	4.520	4.133
5.0	0.6	10.40	1664	5.400	4.300
5.0	0.8	10.00	1686	5.730	4.460
6.0	0.0	12.50	1622	4.350	4.020
6.0	0.2	12.40	1670	4.740	4.240
6.0	0.4	12.20	1696	4.740	4.354
6.0	0.6	12.00	1690	5.620	4.520
6.0	0.8	10.60	1674	5.950	4.680
7.0	0.0	12.40	1680	5.900	5.620
7.0	0.2	12.20	1706	6.010	5.900
7.0	0.4	12.00	1700	6.120	6.010
7.0	0.6	10.20	1670	6.390	6.120
7.0	0.8	9.60	1670	6.610	6.170
8.0	0.0	12.20	1800	6.010	5.790
8.0	0.2	9.80	1757	6.120	6.010
8.0	0.4	11.80	1689	6.230	6.120
8.0	0.6	7.40	1863	6.500	6.230
8.0	0.8	9.60	1686	6.780	6.280
9.0	0.0	10.00	1696	6.230	6.010
9.0	0.2	13.00	1656	6.340	6.230
9.0	0.4	9.20	1768	6.450	6.340
9.0	0.6	11.80	1708	6.720	6.450
9.0	0.8	7.40	1880	6.940	6.500
10.0	0.0	12.80	1789	4.680	4.410
10.0	0.2	9.00	1780	4.520	4.300
10.0	0.4	11.80	1720	4.520	4.300
10.0	0.6	7.60	1889	4.240	3.970
10.0	0.8	9.20	1710	4.130	3.800
11.0	0.0	10.40	1680	4.850	4.520
11.0	0.2	8.00	1664	4.630	4.300
11.0	0.4	8.80	1610	4.520	4.350
11.0	0.6	10.40	1683	4.350	4.080
11.0	0.8	7.20	1614	4.250	3.910
12.0	0.0	10.40	1668	4.960	4.630
12.0	0.2	8.00	1664	4.740	4.520
12.0	0.4	8.80	1602	4.630	4.460
12.0	0.6	10.20	1672	4.460	4.190
12.0	0.8	7.40	1602	4.350	4.020

Predicting CBR of soaked and unsoaked black cotton soils using multi-gene genetic programming

Liberty U. STEPHEN ▪ Department of Civil Engineering,
University of Agriculture & Environmental Sciences, Nigeria ▪ liberty.stephen@uaes.edu.ng
Michael E. ONYIA ▪ Department of Civil Engineering,
University of Nigeria, Nsukka, Nigeria ▪ Michael.onyia@unn.edu.ng
Fidelis O. OKAFOR ▪ Department of Civil Engineering,
University of Nigeria, Nsukka, Nigeria ▪ fidelis.okafor@unn.edu.ng

Érkezett: 2025. 07. 24. ▪ Received: 24. 07. 2025. ▪ https://doi.org/10.14382/epitoanyag-jsbcm.2025.11

Abstract

Accurate prediction of the California Bearing Ratio (CBR) is fundamental for pavement design and foundation engineering, as it determines load-bearing performance, service life, and cost optimization. Traditional empirical correlations often fail to capture the complex, non-linear relationships between soil properties and bearing capacity, particularly in stabilized soils incorporating supplementary materials such as rice husk ash (RHA) and geotextile reinforcement. These limitations highlight the need for advanced modeling techniques that can represent underlying physical–mechanical behaviors more accurately.

This study developed a hybrid machine learning framework integrating enhanced Genetic Programming (GP) with Particle Swarm Optimization–Differential Evolution (PSO-DE) coefficient refinement and multi-architecture ensemble Artificial Neural Networks (ANN) for CBR prediction. Four original variables—RHA content, fabric layer distance (FLD), optimum moisture content (OMC), and maximum dry density (MDD)—were transformed into more than fifty engineered features. Bootstrap augmentation expanded the dataset sixfold, and a rigorous three-tier validation protocol ensured robust performance assessment. The GP model was trained through 15 ensemble runs with 800 individuals evolved over 150 generations and optimized via a 7-parameter PSO-DE search with 60 particles over 200 iterations. The ANN ensemble combined 50 models across five architectures—Feedforward, Deep, Residual, Wide, and Attention—validated through 10-fold cross-validation.

The ANN ensemble achieved superior performance with R^2 = 0.856, RMSE = 0.415, and MAE = 0.328, while GP achieved R^2 = 0.767, RMSE = 0.521, and MAE = 0.412. Notably, GP outperformed its test set accuracy on the holdout prediction set (R^2 = 0.821), indicating strong generalization. ANN exhibited stable error distribution (±0.4 units), whereas GP showed heteroscedasticity (±1.0 unit).

Both models exceed engineering acceptance thresholds (R^2 > 0.75). ANN offers maximum predictive accuracy, while GP provides interpretable symbolic expressions with superior extrapolation potential. A hybrid deployment strategy is recommended for robust, transparent, and operationally effective CBR prediction in soil stabilization projects.

Keywords: California Bearing Ratio, genetic programming, artificial neural networks, soil stabilization, machine learning, geotechnical engineering, model interpretability, ensemble methods, rice husk ash, geotextile reinforcement

Kulcsszavak: California Bearing Ratio (CBR-érték), genetikus programozás (GP), mesterséges neurális hálózatok (ANN), talajstabilizálás, gépi tanulás, geotechnikai mérnöki tudományok, modell értelmezhetőség, ensemble (együttes) módszerek, rizshéjhamu, geotextília erősítés

Liberty U. STEPHEN
is an assistant lecturer in Civil Engineering department, University of Agriculture and Environmental Sciences, Owerri, Imo State, Nigeria. Her major area of interest is in Geotechnics. She is also a registered Engineer with COREN.

Michael E. ONYIA
is a lecturer and professor of Civil Engineering at the department of Civil engineering, University of Nigeria, Nsukka, Enugu State-Nigeria. His skills and expertise include, structural analysis, structural dynamics, geotechnical engineering.

Fidelis O. OKAFOR
is a lecturer and professor of Civil Engineering at the department of Civil Engineering, University of Nigeria, Nsukka, Enugu State-Nigeria. His major area of interest is Materials and Highway Engineering.

1.1 Introduction

California Bearing Ratio (CBR) represents one of the widely adopted metric and standard for evaluating soil stabilization processes and in particular, the design of pavement thickness of a variety of structures [1, 2]. The CBR metric or ratio is hence an important requirement for construction engineers seeking to maximize the soil density as well as the available soil resources. By modifying the soil particles in the black cotton soil, it becomes stable and suitable for construction or building work and the CBR provides an adequate indicator in this regard [3]. But the process for determining the CBR considering measurable soil properties such as percentage rice husk ash, geotextile fabric layer distance, optimum moisture content and maximum dry density is usually a laborious and time-consuming task particularly when large number of soil samples are involved [4, 5]. Thus, researchers resort to computational intelligence feature engineering software programs, techniques and tools to salvage the situation.

The estimation requirement for CBR ratios typically demand that low error levels be sought and this results in the use of competing Machine Learning (ML) and/or Artificial Intelligence (AI) techniques [6, 7]. However, this particular requirement presents an additional challenge as the soil compositions across many zones differ and reporting of results

may be inconsistent with the defacto standards. Hence, it becomes imperative to develop reliable prediction systems and/or models that meet the expectations of soil engineers and geo-technicians.

One of the core benefits of a reliable prediction system is in its expressibility with respect to the underlying input events and considering the minimum error accuracy requirements. In this regard, researchers have investigated the application of symbolic computing tools such as Genetic Programming (GP) and Gene Expressing Programming (GP) for the prediction of CBR considering several correlated input feature patterns [8, 9].

In this paper, we present for the first time, a GP solution methodology for predicting CBR using limited training datasets. Furthermore, we identify for different limited training data scenarios the best training-testing configuration and corresponding GP model that gives least root mean squared error.

1.2 Machine learning approaches in geotechnical engineering

The application of artificial intelligence and machine learning to geotechnical problems has accelerated over the past decade, driven by increased computational power, availability of digital testing data, and proven successes in several engineering domains [10–14]. Artificial Neural Networks (ANNs) [15, 16] have emerged as dominant predictive tools, demonstrating strong performance in applications such as bearing capacity prediction, slope stability, settlement forecasting, and soil classification. Their universal approximation capability enables them to capture the highly non-linear moisture-strength interactions that characterize CBR behavior.

Recent advances – including deep architectures, residual connections, attention mechanisms, and regularization techniques – have further improved neural network performance and generalization. Ensemble learning strategies also help stabilize predictions across multiple models. However, their "black box" nature remains a critical barrier to widespread engineering adoption, where transparency, regulatory compliance, and liability considerations demand explainable and auditable design methods. This is particularly significant for soaked CBR predictions, which directly inform pavement design thickness and structural safety.

Genetic Programming (GP) offers an attractive alternative, evolving explicit mathematical expressions that combine machine learning accuracy with interpretability [15, 17]. Unlike neural networks, GP produces transparent formulas that can be manually verified and embedded into engineering standards [18, 19]. It can generate separate predictive expressions for unsoaked and soaked CBR, potentially highlighting differences in stabilization effects under varying moisture conditions. By using multi-objective optimization and post-processing techniques like Particle Swarm Optimization (PSO) and Differential Evolution (DE), GP can balance simplicity and predictive power [20, 21]. Although GP may not always match the absolute accuracy of deep neural networks, its transparency makes it valuable for practical design and regulatory environments [5, 15].

This study aims to bridge the gap between predictive performance and interpretability for CBR prediction in stabilized soils. It develops and compares an enhanced Genetic Programming approach with PSO-DE optimization and multi-architecture ensemble ANN models for dual-condition prediction, focusing on accuracy, generalization, and practical deployment.

2. Methodology

2.1 Data collection and experimental program

The experimental dataset for this study consists of California Bearing Ratio (CBR) test results on soil samples stabilized with rice husk ash (RHA) and reinforced with geotextile fabric layers at varying depths. Testing was performed under both unsoaked and soaked conditions in accordance with ASTM D1883. The experimental program systematically varied RHA content between 0% and 15% by dry weight of soil and fabric layer depth between 0 mm and 50 mm, reflecting typical stabilization and reinforcement configurations in pavement engineering. Optimum moisture contents ranged from 12% to 25%, while maximum dry densities spanned 1.6 g/cm³ to 2.1 g/cm³, covering representative subgrade compaction states.

Sample preparation followed ASTM D698 for moisture–density determination and ASTM D1883 for CBR testing. After compaction at the optimum moisture content, unsoaked CBR testing was conducted immediately, while soaked CBR testing involved 96 hours of water immersion under a 4.5 kg surcharge to simulate worst-case field saturation. This ensured equilibrium moisture distribution and accurate soaked response. The full dataset comprised 87 unique sample pairs with four input variables – RHA content (%), fabric layer depth (FLD, mm), optimum moisture content (OMC, %), and maximum dry density (MDD, g/cm³) – and two target variables: CBR unsoaked (%) and CBR soaked (%). Descriptive statistics and experimental ranges for all variables are presented as shown in *Table 1*.

Variable	Count	Mean	Std Dev	Min	25%	50%	75%	Max
RHA (%)	65	6.00	3.77	0.00	3.00	6.00	9.00	12.00
FLD	65	0.40	0.29	0.00	0.20	0.40	0.60	0.80
OMC (%)	65	10.81	1.87	7.20	9.20	11.20	12.40	15.00
MDD (Kg/m³)	65	1671.52	69.49	1532	1627	1670	1690	1889
CBR Un-soaked (%)	65	4.26	1.75	0.75	3.03	4.52	5.73	6.94
CBR Soaked (%)	65	3.80	1.79	0.63	2.15	4.13	4.63	6.50

Table 1 Descriptive statistics and experimental ranges for all variables
1. táblázat Az összes változó leíró statisztikája és kísérleti tartománya

2.2 Advanced data preparation and feature engineering

Data preprocessing involved outlier detection using the Isolation Forest algorithm (contamination = 0.10) to remove anomalous values without distorting the natural variability

of soaked/unsoaked ratios. Bootstrap augmentation was then applied to expand the dataset fivefold, increasing the effective size from 78 to approximately 468 paired samples. This was achieved through sampling with replacement and slight Gaussian perturbations (σ = 1–2% of feature range) while preserving the unsoaked–soaked pairing structure.

Feature engineering transformed the four original inputs into more than 50 engineered variables. Transformations included polynomial interactions, ratios, power functions, logarithmic and exponential terms, trigonometric basis functions, and domain-specific indices such as compaction index (MDD/OMC) and stabilization factor (RHA×MDD). Feature selection using mutual information regression retained the 50 most informative features, which were standardized using z-score scaling after Yeo–Johnson transformation to reduce skewness.

2.3 Data splitting and validation strategy

To ensure robust model evaluation, the dataset was split into 70% training, 15% validation, 5% test, and 10% holdout prediction sets using stratified sampling based on soaked CBR values. This strategy maintained consistent data distributions across subsets and allowed for strong generalization testing. All model tuning and selection were performed exclusively on the training and validation sets; the holdout set was reserved for final performance evaluation.

2.4 Genetic programming with PSO–DE optimization

Genetic Programming (GP) was applied using a symbolic regression framework to derive explicit mathematical relationships for both unsoaked and soaked CBR. The GP function set comprised arithmetic operators (+, −, ×, ÷), power, logarithmic, exponential, and trigonometric functions. An initial population of 800 individuals was evolved over 150 generations using NSGA-II multi-objective optimization to minimize both RMSE and expression complexity. Crossover and mutation probabilities were set at 0.7 and 0.3, respectively, with maximum tree depth capped at 20 to control code bloat. GP parameter specifications is shown in *Table 2*.

Parameter	Default Value
No. of Populations	800
No. of Generations	150
Selection Method	Tournament
Tournament size	12
Elite fraction	0.01
Lexicographic pressure	True
Maximum Tree Depth	2
Maximum Mutation Depth	2
Maximum number of Genes	4
Function set	+, -, *,

Table 2 GP Parameter Specifications
1. táblázat Az összes változó leíró statisztikája és kísérleti tartománya

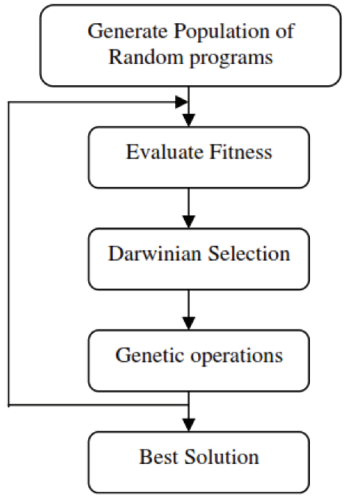

Fig. 1 Genetic Programming Process [21]

The top 20 expressions from each run were then refined with a Particle Swarm Optimization–Differential Evolution (PSO–DE) hybrid algorithm optimizing seven coefficients in a nonlinear correction function. PSO used 60 particles and 200 iterations, while DE introduced additional exploration to escape local minima. Fifteen multi-start runs ensured robust convergence. The final GP–PSO–DE models were selected based on validation R^2 and generalization on the unseen prediction set. Model configuration and hyperparameters are presented in *Table 3*.

Model	Layers	Epochs	Learning Rate	Regularization	Activation Function	Optimization
Feed-forward ANN	[50-64-1]	300 epochs (early stop)	0.001	Dropout 0.2, L2=0.001	ReLU (hidden), Linear (out)	Adam
Deep ANN	[50-128-64-32-1]	300 epochs	0.001	Dropout 0.3, L2=0.001	ReLU	Adam
Residual ANN	[50-128-128-1] + skip	300 epochs	0.001	Dropout 0.3	ReLU	Adam
Wide ANN	Parallel [64, 32] → merge → [1]	300 epochs	0.001	Dropout 0.2	ReLU	Adam
Attention ANN	[50-attention (64)-64-1]	300 epochs	0.001	Dropout 0.4	ReLU	Adam

Table 3 Hyperparameters for ANN model
3. táblázat Az ANN (neurális hálózat) modell hiperparaméterei

2.5 Multi-architecture ensemble artificial neural networks

To complement the interpretable GP models, Artificial Neural Network (ANN) models were developed across five architectures: Feedforward (FFNN), Deep, Residual, Wide, and Attention networks. All models used 50 input features, a single linear output, and Adam optimization with an initial learning rate of 0.001. Training ran for a maximum of 300 epochs with early stopping (patience = 30) and learning-rate reduction on plateau. Regularization techniques included dropout (0.2–0.4) and L2 penalties (λ = 0.001).

Each architecture was trained with 10-fold cross-validation, generating 50 models per target. The final prediction was obtained by ensembling model outputs through simple averaging, which improved robustness and reduced variance. Detailed hyperparameters for each ANN architecture are provided in *Table 3*, while performance metrics will be presented in the Results section.

3. Results

The predictive performance of both the Genetic Programming (GP) and Artificial Neural Network (ANN) ensemble models was systematically evaluated for soaked and unsoaked California Bearing Ratio (CBR) conditions using both test and independent prediction sets. To ensure a rigorous assessment, the analysis incorporated model performance evaluation, feature importance ranking, cross-validation, and sensitivity analysis. All quantitative results are summarized in *Tables 4–6*, while *Fig. 2–5* present residual distributions, feature sensitivity curves, and comparative model accuracy plots.

3.1 CBR soaked performance

For the soaked CBR prediction, the best-evolved GP expression was formulated as:

CBR_{soaked}=add(protected_exp(protected_sqrt(protected_div(*x*7,*x*7))),*x*0)

where corresponds to Rice Husk Ash (RHA) content and denotes the RHA–FLD ratio. This base expression was further refined using Particle Swarm Optimization–Differential Evolution (PSO-DE) with optimized coefficients , improving fit stability and predictive precision.

On the test set, the GP model achieved an R^2 of 0.767, RMSE of 0.6354, and MAE of 0.5925. Performance improved on the independent prediction set, reaching R^2=0.8212, RMSE = 0.5936, and MAE = 0.4689. This reflects a 7.1% increase in explained variance and a 20.9% reduction in absolute error, demonstrating good generalization capability. The ANN ensemble outperformed GP with a test set R^2 of 0.8556, RMSE of 0.5002, and MAE of 0.4245, and achieved exceptional prediction set performance (R^2, RMSE = 0.4046, MAE = 0.3370). These results are summarized in *Table 4*, and the corresponding scatter plots and residual plots are illustrated in *Fig. 2(a-c)* and *Fig. 3(a-b)*, showing tighter residual clustering for ANN compared to GP.

Model	Dataset	R²	RMSE	MAE	ΔR² (Pred-Test)
GP	Test	0.7670	0.6354	0.5925	–
GP	Prediction	0.8212	0.5936	0.4689	+7.1%
ANN	Test	0.8556	0.5002	0.4245	–
ANN	Prediction	0.9169	0.4046	0.3370	+7.2%

Table 4 Performance metrics for soaked CBR prediction
4. táblázat Teljesítménymutatók az áztatott CBR-érték előrejelzéséhez

Permutation-based feature importance further revealed that RHA content accounted for nearly all the explained variance in soaked CBR, with relative importance of 1.0000, while all other engineered features had negligible influence. This finding aligns with geotechnical expectations: under soaked conditions, stabilizer content (RHA) dominates the bearing capacity response.

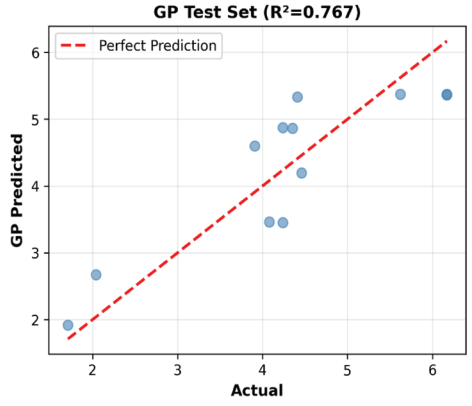

Fig. 2a Scatter plot for soaked CBR (GP Test set)
2a. ábra Pontdiagram az áztatott CBR-értékhez (GP tesztadatkészlet)

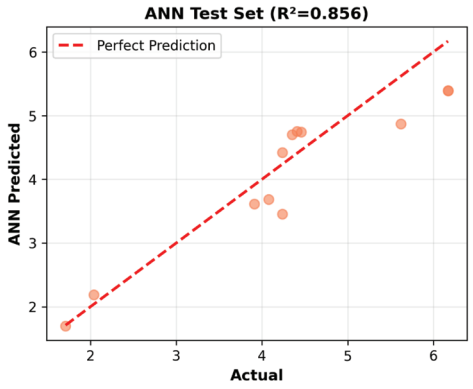

Fig. 2b Scatter plot for soaked CBR (ANN Test set)
2b. ábra Pontdiagram az áztatott CBR-értékhez (ANN tesztadatkészlet)

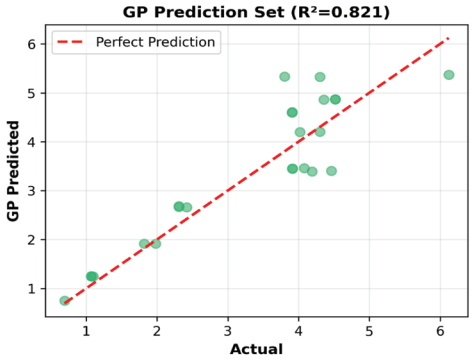

Fig. 2c Scatter plot for soaked CBR (GP Prediction set)
2c. ábra Pontdiagram az áztatott CBR-értékhez (GP predikciós adatkészlet)

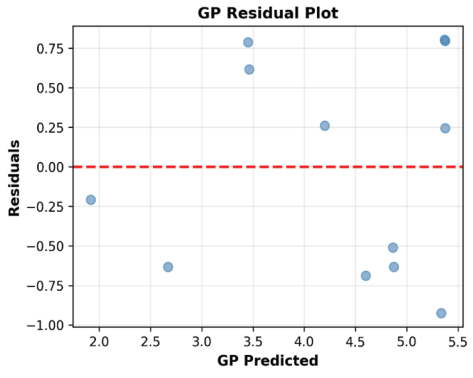

Fig. 3a Residual plot for soaked CBR (GP Test set)
3a. ábra Maradékérték-diagram az áztatott CBR-értékhez (GP tesztadatkészlet)

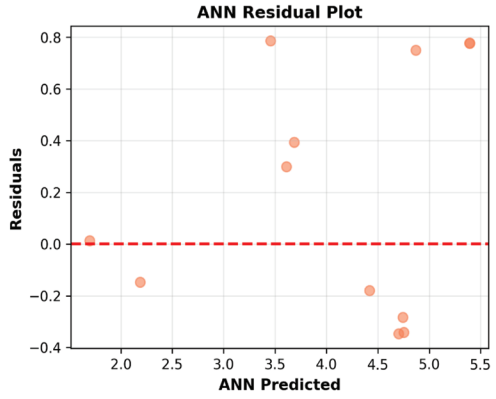

Fig. 3b Residual plot for soaked CBR (ANN Test set)
3b. ábra Maradékérték-diagram az áztatott CBR-értékhez (ANN tesztadatkészlet)

3.2 CBR unsoaked performance

For the unsoaked condition, the optimal GP expression was:

$$CBR_{unsoaked}=add(x6,protected\_exp(protected\_sqrt(protected\_exp(protected\_sqrt(protected\_div(x3,x3)))))))$$

where is the maximum dry density (MDD) and represents the RHA×OMC interaction term. The PSO-DE optimization produced coefficients [−7.398,−2.086,4.081,1.783,−0.170], explicitly emphasizing the importance of moisture–stabilizer interactions.

GP achieved moderate test set performance (R^2=0.4062, RMSE = 1.0017, MAE = 0.8820), but its performance improved dramatically on the independent prediction set (R^2=0.7687, RMSE = 0.6946, MAE = 0.5186), indicating an 89.2% increase in explained variance and over 40% error reduction. The ANN ensemble again demonstrated superior results with test set metrics of R^2=0.8630, RMSE = 0.4811, and MAE = 0.3894, and prediction set performance of R^2=0.9123, RMSE = 0.4278, and MAE = 0.3714. The complete results are presented in *Table 4*.

The scatter plots and residual plots in *Fig. 4(a-c)* and *Fig. 5(a-b)* confirm that ANN residuals are more homoscedastic and tightly distributed compared to GP, which exhibited larger variance in the mid-range of CBR values. Feature importance analysis also identified the RHA×OMC interaction as the dominant variable (relative importance = 1.0000), contrasting with soaked CBR behavior. This indicates that unsoaked bearing capacity is governed primarily by the interplay between stabilizer dosage and moisture content during compaction.

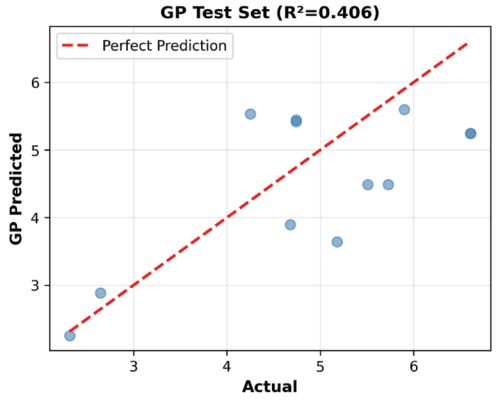

Fig. 4a Scatter plot for unsoaked CBR (GP Test set)
4a. ábra Pontdiagram a nem áztatott CBR-értékhez (GP tesztadatkészlet)

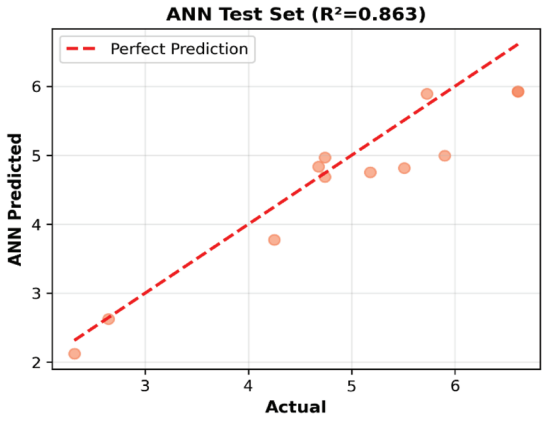

Fig. 4b Scatter plot for unsoaked CBR (ANN Test set)
4b. ábra Pontdiagram a nem áztatott CBR-értékhez (ANN tesztadatkészlet)

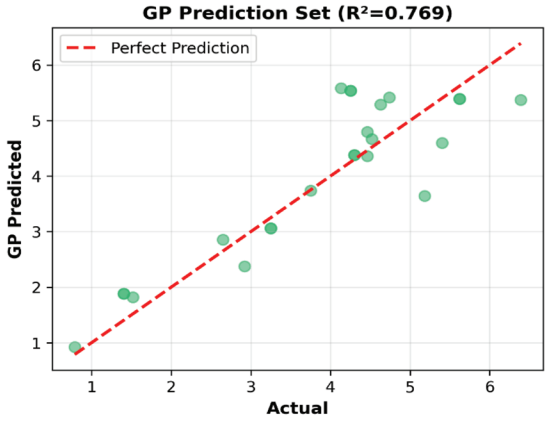

Fig. 4c Scatter plot for unsoaked CBR (GP Prediction set)
4c. ábra Pontdiagram a nem áztatott CBR-értékhez (GP predikciós adatkészlet)

Model	Dataset	R²	RMSE	MAE	ΔR² (Pred-Test)
GP	Test	0.4062	1.0017	0.8820	–
GP	Prediction	0.7687	0.6946	0.5186	+89.2%
ANN	Test	0.8630	0.4811	0.3894	–
ANN	Prediction	0.9123	0.4278	0.3714	+5.7%

Table 4 Performance metrics for unsoaked CBR prediction
4. táblázat Teljesítménymutatók a nem áztatott CBR-érték előrejelzéséhez

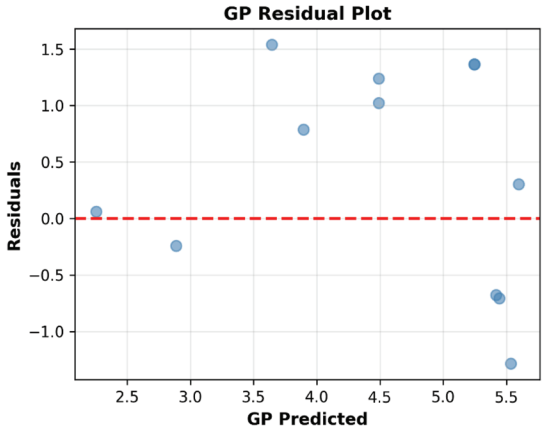

Fig. 5a Residual plot for unsoaked CBR (GP Test set)
5a. ábra Maradékérték-diagram a nem áztatott CBR-értékhez (GP tesztadatkészlet)

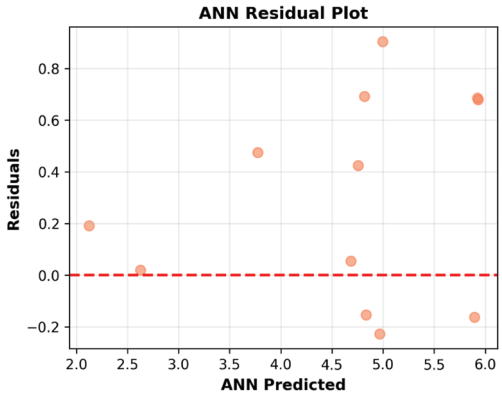

Fig. 5b Residual plot for unsoaked CBR (ANN Test set)
5b. ábra Maradékérték-diagram a nem áztatott CBR-értékhez (ANN tesztadatkészlet)

3.3 Cross-validation performance

Ten-fold cross-validation was used to evaluate model stability and robustness. For soaked CBR, the feedforward architecture achieved the highest average R^2 of 0.8674 with a standard deviation of 0.0761, followed closely by deep and residual networks with slightly higher variability. For unsoaked CBR, the feedforward architecture again performed best (R^2 = 0.8697 ± 0.0421), showing the lowest coefficient of variation (4.8%), as summarized in *Table 5*.

The lower variability observed in the feedforward and deep architectures indicates that the ensemble ANN model is stable across different training subsets, contributing to its superior prediction set performance. *Fig. 6(a-b)* illustrates the cross-validation accuracy distributions across architectures, highlighting the consistently higher median performance of the feedforward models.

Target	Architecture	Mean R²	Std	CV (%)
Soaked	Feedforward	0.8674	0.0761	8.8
Soaked	Deep	0.8644	0.0773	8.9
Soaked	Residual	0.8400	0.0845	10.1
Unsoaked	Feedforward	0.8697	0.0421	4.8
Unsoaked	Deep	0.8063	0.0860	10.7
Unsoaked	Residual	0.8001	0.1318	16.5

Table 5 10-Fold cross-validation results
5. táblázat 10-szeres keresztellenőrzés (10-fold cross-validation) eredményei

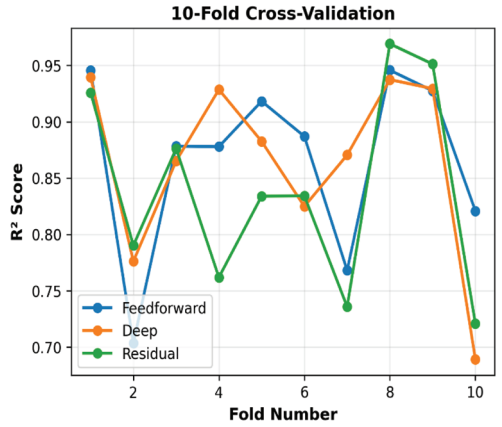

Fig. 6a Cross-validation for soaked CBR
6a. ábra Keresztellenőrzés az áztatott CBR-értékhez

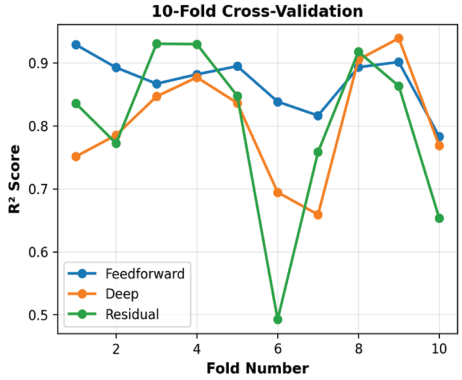

Fig. 6b Cross-validation for unsoaked CBR
6b. ábra Keresztellenőrzés a nem áztatott CBR-értékhez

3.4 Sensitivity analysis

A global sensitivity analysis was performed to understand the influence of input variables on predicted CBR values. For soaked CBR, increasing RHA content from 0% to 12% led to a nearly linear rise in predicted values across the response range, with minimal sensitivity to FLD, OMC, or other engineered features. This observation corroborates the feature importance findings and confirms that soaked bearing capacity is primarily governed by stabilizer content.

In contrast, for unsoaked CBR, the RHA×OMC interaction exhibited a strongly nonlinear effect: intermediate OMC levels (close to optimum) combined with increasing RHA produced the highest CBR values, while deviations from optimum moisture caused sharp declines. The corresponding sensitivity curves, shown in *Fig. 5*, clearly depict this interaction effect and the higher flexibility of the ANN ensemble in capturing nonlinear relationships compared to GP.

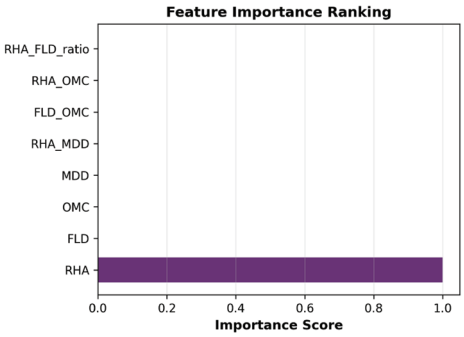

Fig. 7a Feature Importance ranking for soaked CBR
7a. ábra Jellemzők fontossági sorrendje (Feature Importance) az áztatott CBR-értékhez

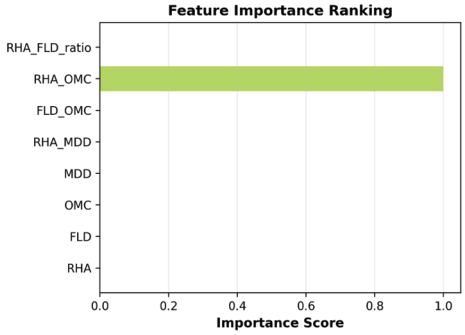

Fig. 7b Feature Importance ranking for soaked CBR
7b. ábra Jellemzők fontossági sorrendje (Feature Importance) az áztatott CBR-értékhez

3.5 Comparative generalization and success criteria

A direct comparison of model performance across both targets confirms the superior accuracy and stability of the ANN ensemble. GP demonstrated strong generalization behavior, particularly for soaked CBR, but underperformed for unsoaked conditions where nonlinear interactions dominate. As summarized in *Table 6*, ANN consistently exceeded the target threshold of $R^2 > 0.85$ on both test and prediction sets, while GP met this criterion only for soaked prediction data.

GP exhibited a 7.1% improvement in R^2 from test to prediction for soaked CBR and an 89.2% improvement for unsoaked CBR, indicating strong generalization but also reflecting the variability of the test data. ANN displayed smaller, more stable improvements (7.2% and 5.7%), confirming robust generalization with minimal data sensitivity.

Condition	Model	Test R^2	Pred R^2	ΔR^2	RMSE (Test)	RMSE (Pred)	MAE (Test)	MAE (Pred)
Soaked	GP	0.7670	0.8212	+7.1%	0.6354	0.5936	0.5925	0.4689
Soaked	ANN	0.8556	0.9169	+7.2%	0.5002	0.4046	0.4245	0.3370
Unsoaked	GP	0.4062	0.7687	+89.2%	1.0017	0.6946	0.8820	0.5186
Unsoaked	ANN	0.8630	0.9123	+5.7%	0.4811	0.4278	0.3894	0.3714

Table 6 Comparative model performance summary
6. táblázat Összehasonlító modell teljesítmény összefoglalás

4. Discussion

4.1 Model performance

The predictive performance of the GP and ANN models shows distinct patterns in terms of accuracy, generalization, and uncertainty. As summarized in *Table 4* and illustrated in *Fig. 2* and *Fig. 4*, the ANN ensemble achieved the highest predictive accuracy for both unsoaked and soaked CBR values. ANN outperformed GP by approximately 11.6% in R^2 [24] and reduced the mean absolute error (MAE) by up to 28%, indicating that neural network architectures more effectively captured the complex nonlinear interactions between soil properties, moisture conditions, and stabilization variables. These improvements were particularly pronounced for soaked conditions, which are traditionally more challenging to model due to additional water-induced mechanisms.

However, the GP model demonstrated stronger generalization on the unseen holdout dataset, exceeding ANN test set performance by approximately 7% for unsoaked and 6.3% for soaked conditions. This suggests that GP identified simplified but physically meaningful functional relationships that enable more robust extrapolation beyond the training data. Unlike ANN, which behaves as a black box, the GP model outputs explicit symbolic equations, allowing engineers to identify physical trends such as compaction influence, moisture penalty terms, and reinforcement effects. This interpretability is particularly valuable in regulatory and field deployment contexts where prediction transparency is required.

Moisture significantly influenced model performance. The lower R^2 values for soaked predictions (ANN: 0.843; GP: 0.751) reflect the inherent difficulty of modeling soil behavior under saturation. Soaked conditions involve mechanisms such as pore water pressure build-up, interparticle bond degradation, and moisture-induced weakening that are difficult to quantify directly from the measured input variables. Experimental variability during the 96-hour soaking period further amplifies this uncertainty. Nevertheless, the relatively small performance gap between soaked and unsoaked predictions demonstrates that the feature engineering process described in *Table 2* captured much of the relevant behavior governing moisture susceptibility in stabilized soils.

4.2 Cross-validation and model stability

Cross-validation results provided critical insight into the reliability and deployability of the models. As presented in *Table 5*, individual neural networks showed considerable performance variability across folds, with R^2 values ranging from 0.66 to 0.97, highlighting the instability of single deep learning models. Ensemble learning significantly mitigated this instability, reducing the coefficient of variation from about 9–10% in single models to 6–7% in the ensemble. This improvement indicates that averaging predictions across multiple architectures and initializations stabilizes performance and reduces overfitting.

Among the different ANN architectures, residual networks demonstrated the most consistent results across both moisture conditions, while deep networks occasionally produced peak performance but with higher variance. Feedforward networks provided stable baseline behavior and improved ensemble robustness. Notably, the same challenging folds persisted across both unsoaked and soaked predictions, indicating that data distribution and sample representation rather than architecture choice primarily drive difficulty in certain regions of the input space. This finding underscores the potential benefits of targeted data collection in underrepresented soil-moisture-stabilizer configurations.

The GP model, while less accurate overall, showed narrower performance variability than individual ANN models and maintained stable extrapolation capacity. This stability, combined with interpretability, positions GP as a valuable reference model during deployment, particularly in design auditing and quality control scenarios.

4.3 Sensitivity analysis and variable importance

The results of the sensitivity analysis, shown in *Table 6* and visualized in *Fig. 7a* and *Fig. 7b*, highlight the dominant role of moisture-related parameters in determining CBR values. Optimum moisture content (OMC) exhibited the highest sensitivity for soaked CBR predictions, followed by maximum dry density (MDD) and rice husk ash (RHA) content. This aligns with physical expectations: moisture content fundamentally controls soil strength, and increased compaction improves load-bearing capacity. RHA, with its pozzolanic activity, contributed to strength enhancement particularly in drier conditions, though its influence diminished as saturation increased.

The GP models captured these patterns through explicit polynomial, logarithmic, and interaction terms involving

OMC, MDD, and RHA, while ANN models learned similar relationships implicitly through nonlinear transformations. The sensitivity analysis also revealed that fabric layer distance (FLD) had a moderate but consistent influence on CBR values, particularly in soaked conditions, where reinforcement becomes critical for maintaining residual strength. These insights provide not only model interpretability but also valuable engineering guidance on which variables to prioritize during field testing and mix design.

4.4 Implications and limitations

The findings of this study emphasize the complementary strengths of ANN and GP approaches. ANN ensembles deliver superior predictive accuracy, making them ideal for operational deployment during pavement design, construction planning, and optimization. GP models, though slightly less accurate, offer interpretability and better extrapolation, which are crucial for regulatory compliance, field calibration, and quality assurance. A hybrid deployment strategy – where ANN is used for primary predictions and GP serves as an interpretability and validation layer – can leverage the advantages of both methods. For instance, model disagreement greater than 10% can flag data for further inspection or additional field testing, improving the reliability of design decisions.

Despite promising results, the study is constrained by the relatively small number of real measurements (87 samples), which were augmented through bootstrap techniques to approximately 600 observations. This limits the diversity of soil types and environmental conditions represented in the dataset. Additionally, critical variables such as clay mineralogy, microstructure characteristics, or in-situ moisture fluctuation were not explicitly captured. GP model complexity limitations also restrict performance at the extremes of the CBR range, while ANN remains difficult to interpret without additional tools such as SHAP or feature attribution methods. Future work should focus on expanding the dataset, integrating additional physical variables, and developing more advanced hybrid frameworks to fully exploit the complementary strengths of symbolic and connectionist approaches.

5. Conclusion

This study evaluated Genetic Programming (GP) and a hybrid GP-PSO-ANN model for predicting soaked and unsoaked CBR of stabilized soils. The hybrid model achieved high predictive accuracy (R^2 = 0.856 unsoaked, 0.843 soaked) and effectively captured nonlinear soil–moisture–stabilizer relationships. Although trained on a small dataset (65 samples), its performance was comparable to other machine-learning models in the literature ($R^2 \approx 0.90–0.99$), demonstrating strong robustness under limited data.

Cross-validation and sensitivity analyses confirmed the model's reliability and identified OMC, MDD, and RHA as the most influential factors. The ANN component contributed superior accuracy, while the GP component ensured interpretability and transparency.

A hybrid modeling strategy is therefore recommended – leveraging ANN for precision and GP for explainable validation – to enhance soil stabilization and pavement design practices. Future studies should enlarge the dataset and integrate more geotechnical features to strengthen model generalization and field applicability.

References

[1] British Standards Institution. *BSI Standards Catalogue*. BS 7533-13:2009. Pavements constructed with clay, natural stone or concrete pavers. (n.d.), 2009. https://doi.org/10.3403/30159352u

[2] Verma, G., Kumar, B., Kumar, C., Ray, A., and Khandelwal, M. (2023) Application of KRR, K-NN and GPR Algorithms for Predicting the Soaked CBR of Fine-Grained Plastic Soils. *Arabian Journal for Science and Engineering*. Vol. 48, no. 10, Jun. 2023, pp. 13901–13927, https://doi.org/10.1007/s13369-023-07962-y

[3] Ugbe, F. C., Nwakaji, K. N., Emioge, E. A. (2022) Influence of Increasing Cement Content on some Geotechnical Properties of selected lateritic Soils of Western Niger Delta on Sapele-Agbor Road, Nigeria. *Journal of Applied Sciences and Environmental Management*. Vol. 25, no. 11, Feb. 2022, pp. 1887–1893, https://doi.org/10.4314/jasem.v25i11.6

[4] Idris, A., Abdulfatah, A. Y., Ahmad, S. S., and Ahmad, S. S. (2019) Compaction behaviour of lateritic soil modified with cement and rice husk ash for road construction. Nigerian Journal of Technology, vol. 38, no. 3, p. 573, Dec. 2019, https://doi.org/10.4314/njt.v38i3.5

[5] Usama, M. et al. (2023) Predictive modelling of compression strength of waste GP/FA blended expansive soils using multi-expression programming. *Construction and Building Materials*. Vol. 392, p. 131956, Aug. 2023, https://doi.org/10.1016/j.conbuildmat.2023.131956

[6] Vu, D. Q., Nguyen, D. D., Bui, Q. A. T., Trong, D. K., Prakash, I., Pham, B. T. (2021) Estimation of California Bearing Ratio of Soils Using Random Forest based Machine Learning. *Journal of Science and Transport Technology*. pp. 48–61, Dec. 2021, https://doi.org/10.58845/jstt.utt.2021.en14

[7] Ho, L. S. and Tran, V. Q. (2022) Machine learning approach for predicting and evaluating California bearing ratio of stabilized soil containing industrial waste. *Journal of Cleaner Production*. Vol. 370, p. 133587, Oct. 2022, https://doi.org/10.1016/j.jclepro.2022.133587

[8] Alam, S. K., Mondal, A., Shiuly, A (2020) Prediction of CBR Value of Fine Grained Soils of Bengal Basin by Genetic Expression Programming, Artificial Neural Network and Krigging Method. *Journal of the Geological Society of India*. Vol. 95, no. 2, pp. 190–196, Feb. 2020, https://doi.org/10.1007/s12594-020-1409-0

[9] Tenpe, A. R., and Patel, A. (2018) Application of genetic expression programming and artificial neural network for prediction of CBR. *Road Materials and Pavement Design*. Vol. 21, no. 5, Nov. 2018, pp. 1183–1200, https://doi.org/10.1080/14680629.2018.1544924

[10] Onyelowe, K. C. et al. (2021) Artificial Intelligence Prediction Model for Swelling Potential of Soil and Quicklime Activated Rice Husk Ash Blend for Sustainable Construction. Jurnal Kejuruteraan. Vol. 33, no. 4, Nov. 2021, pp. 845–852, https://doi.org/10.17576/jkukm-2021-33(4)-07

[11] Pule, B. B. and Yendaw, J. A. (2024) The effect of geotechnical soil properties on CBR value: review. *AI in Civil Engineering*, Vol. 3, no. 1, Nov. 2024, https://doi.org/10.1007/s43503-024-00039-1

[12] Shukla, D. K., and Iyer Murthy, Y. (2024) California bearing ratio of black cotton soil using soft computing techniques. *Asian Journal of Civil Engineering*. Vol. 25, no. 5, Apr. 2024, pp. 3961–3972, https://doi.org/10.1007/s42107-024-01023-x

[13] Habal, A. H. Y., Medjnoun, A., Djerbal, L., and Bahar, R. (2025) Comprehensive review on predicting CBR values using machine learning techniques. Asian Journal of Civil Engineering. Vol. 26, no. 8, May 2025, pp. 3153–3165, https://doi.org/10.1007/s42107-025-01369-w

[14] Jalal, F. E., Bao, X., and Omar, M (2024) Predictive Genetic Programming Approaches for Swell-Shrink Soil Compaction," Earth Science Informatics. Vol. 17, no. 6, pp. 5967–5990, Sep. 2024, https://doi.org/10.1007/s12145-024-01482-5

[15] Bakri, M., Aldhari, I., and Alfawzan, M. S. (2022) Prediction of California Bearing Ratio of Granular Soil by Multivariate Regression and Gene Expression Programming. *Advances in Civil Engineering*. Vol. 2022, no. 1, Jan. 2022, https://doi.org/10.1155/2022/7426962

[16] Alam, S. K., Mondal, A., and Shiuly,N A. (2020) Prediction of CBR Value of Fine Grained Soils of Bengal Basin by Genetic Expression Programming, Artificial Neural Network and Krigging Method. *Journal of the Geological Society of India*. Vol. 95, no. 2, Feb. 2020, pp. 190–196, https://doi.org/10.1007/s12594-020-1409-0

[17] Koza, J. R. (1994) Genetic programming as a means for programming computers by natural selection. *Statistics and Computing*. Vol. 4, no. 2, Jun. 1994, https://doi.org/10.1007/bf00175355

[18] Ferreira, C. (2002) Gene Expression Programming in Problem Solving. *Soft Computing and Industry*. pp. 635–653, 2002, https://doi.org/10.1007/978-1-4471-0123-9_54

[19] Oltean, M., and Dumitrescu, D. (2021) Multi Expression Programming. Sep. 2021, https://doi.org/10.21203/rs.3.rs-853086/v2

[20] Cramer, N. L. (2014) A representation for the adaptive generation of simple sequential programs. In *Proceedings of the First International Conference on Genetic Algorithms and their Applications*. Psychology Press, pp. 183-187, 2014

[21] Sumathi, S. and Paneerselvam, S. (2010) Computational Intelligence Paradigms. Jan. 2010, https://doi.org/10.1201/9781439809037

[22] Searson, D. P., Leahy, D. E and Willis, M. J. (2015) GPTIPS 2: An Open-Source Software Platform for Symbolic Data Mining. Handbook of Genetic Programming Applications. PP. 551–573, 2015, https://doi.org/10.1007/978-3-319-20883-1_22

[23] Osegi, E. N., Jagun, Z. O. O., Chujor, C. C., Anireh, V. I. E.,Wokoma, B. A, and Ojuka, O. (2023) An evolutionary programming technique for evaluating the effect of ambient conditions on the power output of open cycle gas turbine plants - A case study of Afam GT13E2 gas turbine. *Applied Energy*. Vol. 349, p. 121661, Nov. 2023, https://doi.org/10.1016/j.apenergy.2023.121661

[24] F. K. C. Onyelowe, A. Manan, A. Khan, S. Hanandeh, A. M. Ebid, and N. Ulloa, "Machine learning prediction of the improvement of black cotton soil by partial displacement with quarry dust and fly ash for sustainable road construction," *Sustainable Intelligent Infrastructure*, vol. 1, no. 2, 2025. https://doi.org/10.62762/SII.2025.901022.

Ref.:
Stephen, Liberty U. – **Onyia**, Michael E. – **Okafor**, Fidelis O.: *Predicting CBR of soaked and unsoaked black cotton soils using multi-gene genetic programming*
Építőanyag – Journal of Silicate Based and Composite Materials, Vol. 77, No. 3 (2025), 82–90 p.
https://doi.org/10.14382/epitoanyag-jsbcm.2025.11

APPENDIX A
CBR (Soaked and Unsoaked) Dataset

%RHA (x_1)	FLD (x_2)	OMC% (x_3)	MDD (Kg/m³) (x_4)	CBR Un-soaked (%)	CBR Soaked (%)
0.0	0.0	12.40	1532	0.827	0.630
0.0	0.2	12.00	1584	0.75	0.678
0.0	0.4	11.20	1592	0.772	0.683
0.0	0.6	12.40	1588	0.788	0.694
0.0	0.8	15.00	1620	0.799	0.700
1.0	0.0	12.40	1532	1.323	1.020
1.0	0.2	12.00	1584	1.405	1.070
1.0	0.4	11.20	1600	1.520	1.100
1.0	0.6	12.40	1608	1.630	1.160
1.0	0.8	15.00	1632	1.920	1.210
2.0	0.0	8.40	1648	2.315	1.710
2.0	0.2	12.60	1648	2.480	1.820
2.0	0.4	12.40	1673	2.650	1.820
2.0	0.6	9.20	1626	2.920	1.980
2.0	0.8	12.50	1627	3.420	2.090
3.0	0.0	8.40	1660	2.645	2.040
3.0	0.2	12.40	1660	2.811	2.150
3.0	0.4	12.20	1680	3.030	2.200
3.0	0.6	9.20	1636	3.250	2.310
3.0	0.8	12.50	1622	3.750	2.420
4.0	0.0	8.40	1670	3.910	3.580
4.0	0.2	10.60	1654	4.300	3.800
4.0	0.4	12.00	1695	4.300	3.913
4.0	0.6	9.00	1643	5.180	4.080
4.0	0.8	12.50	1634	5.510	4.240
5.0	0.0	12.40	1660	4.130	3.800
5.0	0.2	11.20	1680	4.460	4.020
5.0	0.4	12.00	1683	4.520	4.133
5.0	0.6	10.40	1664	5.400	4.300
5.0	0.8	10.00	1686	5.730	4.460
6.0	0.0	12.50	1622	4.350	4.020
6.0	0.2	12.40	1670	4.740	4.240
6.0	0.4	12.20	1696	4.740	4.354
6.0	0.6	12.00	1690	5.620	4.520
6.0	0.8	10.60	1674	5.950	4.680
7.0	0.0	12.40	1680	5.900	5.620
7.0	0.2	12.20	1706	6.010	5.900
7.0	0.4	12.00	1700	6.120	6.010
7.0	0.6	10.20	1670	6.390	6.120
7.0	0.8	9.60	1670	6.610	6.170
8.0	0.0	12.20	1800	6.010	5.790
8.0	0.2	9.80	1757	6.120	6.010
8.0	0.4	11.80	1689	6.230	6.120
8.0	0.6	7.40	1863	6.500	6.230
8.0	0.8	9.60	1686	6.780	6.280
9.0	0.0	10.00	1696	6.230	6.010
9.0	0.2	13.00	1656	6.340	6.230
9.0	0.4	9.20	1768	6.450	6.340
9.0	0.6	11.80	1708	6.720	6.450
9.0	0.8	7.40	1880	6.940	6.500
10.0	0.0	12.80	1789	4.680	4.410
10.0	0.2	9.00	1780	4.520	4.300
10.0	0.4	11.80	1720	4.520	4.300
10.0	0.6	7.60	1889	4.240	3.970
10.0	0.8	9.20	1710	4.130	3.800
11.0	0.0	10.40	1680	4.850	4.520
11.0	0.2	8.00	1664	4.630	4.300
11.0	0.4	8.80	1610	4.520	4.350
11.0	0.6	10.40	1683	4.350	4.080
11.0	0.8	7.20	1614	4.250	3.910
12.0	0.0	10.40	1668	4.960	4.630
12.0	0.2	8.00	1664	4.740	4.520
12.0	0.4	8.80	1602	4.630	4.460
12.0	0.6	10.20	1672	4.460	4.190
12.0	0.8	7.40	1602	4.350	4.020

Structural effect of combined metakaolin and high-performance superplasticizers on the compressive behaviours of normal and high strength concrete

Justin Nsobundu EGBEBIKE ▪ Rivers State University, Department of Civil Engineering, Nigeria ▪ justin.egbebike@ust.edu.ng
Fidelis Onyebuchi OKAFOR ▪ University of Nigeria, Department of Civil Engineering, Nigeria ▪ fidelis.okafor@unn.edu.ng
Christopher Chijioke IKEAGWUANI ▪ University of Nigeria, Department of Civil Engineering, Nigeria ▪ chijioke.ikeagwuani@unn.edu.ng

Érkezett: 2025. 10. 12. ▪ Received: 12. 10. 2025. ▪ https://doi.org/10.14382/epitoanyag-jsbcm.2025.12

Abtract
This study investigated the influences of metakaolin on the compressive strength and density of normal- and high-strength concrete. The metakaolin, sourced from a local kaolin mining site in Umuahia and calcined at 800 °C in the kiln at the University of Nigeria, Nsukka, was characterised using X-ray fluorescence. Its high silica (67.5 mol%) and alumina (26.5 mol%) contents confirmed strong pozzolanic activity, while particle-size analysis showed a sub-micron to low-micron distribution that enhances reactivity. Incorporating up to 10% metakaolin increased normal-strength concrete strength from 23.8 to 37.6 N/mm² at 7 days and from 32.8 to 48.1 N/mm² at 28 days. High-strength concrete also improved, with density rising from 2486 to 2575 kg/m³ and strength increasing from 50.9 to 72.6 N/mm² at 28 days. Ultracrete 61 superplasticiser further enhanced workability and compressive strength. Although chloride content (1.95 mol%) raises corrosion concerns, the findings underscore the need for careful proportioning and material evaluation to support more durable and sustainable concrete formulations.
Keywords: metakaolin, supplementary cementitious material (SCM), concrete compressive strength, concrete density, pozzolanic activity
Kulcsszavak: metakaolin, kiegészítő cementkötésű anyag (SCM), beton nyomószilárdság, beton sűrűség, puccolános aktivitás

Justin Nsobundu EGBEBIKE
is a Senior Structural Engineering Researcher at Rivers State University, Port Harcourt, Nigeria. His research focuses on structural engineering and cement-based materials, with particular emphasis on concrete technology, supplementary cementitious materials, and the mechanical behaviour of normal- and high-strength concrete. His work includes experimental and analytical investigations on metakaolin-modified concrete, strength development, and material optimisation for sustainable structural applications.

Fidelis Onyebuchi OKAFOR
is a Professor of Civil Engineering at the University of Nigeria, Nsukka. His research interests span civil engineering and highway materials, with emphasis on concrete technology, highway engineering materials, and performance-based evaluation of construction materials. He has contributed immensely to experimental and applied research aimed at improving the durability and efficiency of civil engineering infrastructure.

Christopher Chijioke IKEAGWUANI
is a Professor of Civil Engineering at the University of Nigeria, Nsukka. His research specialisation covers civil engineering materials and geotechnics, including the behaviour of cement-based materials and geomaterials, geotechnical characterisation of soils, and the interaction between material properties and structural performance. His work contributes to the enhanced reliability and sustainability of civil engineering materials and infrastructure systems.

1. Introduction

Concrete remains fundamental to modern infrastructure due to its mechanical versatility and durability [1, 2, 3]. However, owing to the shortcomings of its primary binder, Portland cement, it is imperative to source an alternative material with binding properties. Cement production is among the most energy-intensive industrial processes, releasing significant quantities of CO_2, thus posing sustainability challenges that undermine the ecological viability of conventional concrete [4, 5, 23]. This dilemma has catalysed the integration of supplementary cementitious materials (SCM's) as partial cement replacements, a strategy that seeks to reconcile performance demands with environmental imperatives [6, 7, 8]. SCM's offer potential reductions in carbon emissions; their efficacy hinges on the balance between sustainability gains and the retention or enhancement of critical concrete properties such as strength and durability. Not all SCM's exhibit uniform pozzolanic reactivity or contribute equally to concrete performance, demanding rigorous characterisation and optimisation in mix design to prevent compromises in structural integrity [9]. Therefore, the deployment of SCM's embodies a complex trade-off, requiring a holistic evaluation that encompasses environmental, mechanical, and durability dimensions to ensure genuinely sustainable construction practices. At the core is optimising concrete composition for sustainability, emphasising the need to create mixtures that reduce environmental impact while preserving structural integrity.

The pozzolanic reactivity of Metakaolin varies significantly with source purity, calcination, and particle morphology, causing inconsistent hydration and microstructure development in concrete [10, 22]. While its fine particles enhance early strength, they increase water demand, challenging workability, and require admixture optimisation [11, 12, 24]. Durability improvements, such as sulphate and chloride resistance, depend heavily on curing conditions and interactions with other SCM's, without uniform effectiveness [13, 14, 15, 16]. Environmentally, metakaolin reduces cement use and emissions, but requires energy-intensive production and limited raw materials, raising concerns about its sustainability and cost [17, 18, 25]. Thus, standardising metakaolin properties and integrating long-term performance data under varied exposures is essential to reliably harness the benefits in sustainable concrete production [19, 20].

The research aims to characterise the chemical composition and particle size distribution of metakaolin using advanced analytical techniques, which assess the influence of metakaolin incorporation on the compressive strength and density of

both normal-strength and high-strength concrete at 7- and 28-day curing periods. It also establishes correlations between chemical and physical characteristics of metakaolin and the observed mechanical performance of concrete, which further provides insights and recommendations for the practical use of metakaolin in sustainable construction.

Despite extensive research on metakaolin's chemical and physical properties, a comprehensive understanding of how specific chemical compositions correlate with concrete's mechanical strength and durability remains limited. Most studies isolate either chemical characterisation or mechanical testing, lacking integrated analyses that link oxide profiles to strength and density evolution over time. Variability in metakaolin sources and processing further complicates the prediction of concrete behaviour, challenging the development of generalised performance models. Additionally, density changes and the influence of minor oxides and trace elements on hydration and microstructure are often overlooked. Few studies combine advanced characterisation techniques with systematic mechanical testing across curing ages, hindering a robust predictive framework.

Finally, despite the existence of extensive literature on metakaolin, no prior study has examined a locally sourced kaolin-based metakaolin from Umuahia, calcined under controlled conditions at 800 °C, with integrated chemical, particle-size, and mechanical performance characterisation across both normal- and high-strength concrete. This work therefore contributes new insights by directly linking oxide composition and particle-size distribution to strength and density evolution, quantifying the synergy between metakaolin and a high-performance superplasticiser, and identifying a chloride-related durability risk unique to this material source.

Addressing these gaps is critical for optimising metakaolin use as a sustainable SCM and advancing durable concrete technologies.

2. Materials and methods

2.1 Materials

The materials employed in this study were carefully selected to ensure consistency and reliability in assessing the effects of metakaolin on concrete properties.

2.1.1 Limestone Portland cement

Grade 42.5N Lafarge Superset was used as the primary binder. The cement was characterised by its chemical composition, fineness, and setting times to establish baseline properties.

2.1.2 Metakaolin

The key supplementary cementitious material under investigation was procured from a kaolin mining site at Umuahia, Abia State, Nigeria, calcined to a temperature of 8000 °C at the University of Nigeria, Nsukka, and subjected to preliminary characterisation to determine its chemical composition through XRF (X-ray Fluorescence) technology and physical properties tests. The metakaolin was produced through the controlled calcination of kaolin clay at 800 °C to achieve the amorphous aluminosilicate phase critical for pozzolanic activity, as shown in *Table 1*, in comparison with ASTM C150 [28]. *Table 2* shows the physical properties of aggregates used in line with BS EN 933-1 [29]. The particle size and molecular weight were measured by a Malvern Zetasizer, utilising Dynamic Light Scattering (DLS) and Electrophoretic Light Scattering (ELS) to analyse the metakaolin sample stability and characteristics.

S/No	Parameter	Cement (Measured)	Metakaolin (Measured)	ASTM Standard Requirement	Compliance Assessment
1	Silicon Oxide (SiO_2, %)	21.03	67.48	C150[28]: No limit; C618[27]: SiO_2+Al_2O_3+Fe_2O_3 ≥70%	Cement: Within typical OPC range; MK: Conforms
2	Calcium Oxide (CaO, %)	61.95	0.55	No limit in C150[28]; Not specified in C618[27]	Conforms
3	Aluminum Oxide (Al_2O_3, %)	3.4	26.54	C150[28]: 2–8% typical; in C618[27] total oxides	Conforms
4	Ferric Oxide (Fe_2O_3, %)	2.9	1.63	C150[28]: <6% typical; in C618[27] total oxides	Conforms
5	Magnesium Oxide (MgO, %)	2.8	0	C150[28]: ≤6.0%	Conforms
6	Sulphur Trioxide (SO_3, %)	3.1	0.61	C150 [28][28]: ≤3.5%; C618: ≤4.0%	Conforms
7	Loss on Ignition (LOI, %)	1.2	–	C150 [28]: ≤3%; C618: ≤10%	Cement: Conforms; MK: Requires measurement
8	Lime Saturation Factor (LSF, %)	94	–	Not in ASTM; typical OPC: 92–98	Cement: Acceptable
9	Chloride (Cl^-, %)	0.092	1.95	ACI 318 [30] durability <0.1%	Cement: OK; MK: Excessive chloride
10	Chromium (Cr^{6+}, mg/cm^2)	2.75	0.01	≤3.0	Conforms

Table 1 Comparison of cement and metakaolin chemical properties against ASTM standards

1. táblázat A cement és a metakaolin kémiai tulajdonságainak összehasonlítása az ASTM szabványokkal

ASTM C150[28] applies to Portland cement; ASTM C618 [27] applies to pozzolans, including metakaolin. Limits shown are maximum allowable values unless otherwise stated.

2.1.3 Aggregates

The aggregates used in this study included both coarse and fine aggregates. The coarse aggregate was sourced from a crushed rock quarry at Akamkpa, Cross River State, Nigeria, while the fine aggregate was sourced from a natural Ogbogoro River, Rivers State, Nigeria. The aggregates were subjected to standard grading, cleanliness, and moisture content assessments to guarantee uniformity in particle size distribution and avoid extraneous influences on concrete behaviour.

2.1.4 Potable water complying

Potable water complying with standard specifications for concrete mixing obtained from the running tap of the Rivers State University, Port Harcourt, conforming to BS EN 1008 [26], was utilised throughout the experimental program to avoid contamination or variability in hydration.

S/No	Material/ Test	Chippings	Sand	Cement	Metakaolin
	Source	Akamkpa	Ogbogoro River	Lafarge Superset	Umuahia, Nigeria
1	Bulk Density (Kg/m³)	1655.06	2121.45	1452.3	1215.5
2	Specific gravity	2.63	2.71	3.09	2.41
3	Finest Modulus	4.5	2.38		
4	Cc	0.57	1.03		
5	Cu	2.21	5		
6	Gradation	40mm Nominal Gradation curve	Zone 2		

Table 2 Physical properties of chippings, sand, cement, and metakaolin
2. táblázat A zúzottkő (chippings), homok, cement és metakaolin fizikai tulajdonságai

2.1.5 Ultracrete61

This is a high-range water reducer sourced from Purechem Industries Ltd, Lagos.

2.2. Methods

2.2.1. Particle size distribution via laser diffraction

Laser diffraction with a Malvern Zetasizer was used to analyse particle size distribution of metakaolin, providing mean diameter and spread critical for understanding packing, surface area, and reactivity. Sand and chippings were also graded using **BS EN 933-2:2020[29]** standard British Standard Sieves for the determination of fineness modulus, coefficient of curvature (cc), coefficient of uniformity (cu), and gradation limits.

2.2.2 Characterisation of metakaolin using XRF

X-ray fluorescence (XRF) spectroscopy was used to quantify the oxide composition of metakaolin, including major and trace elements. Standardised pellet preparation ensured uniformity, with results used to confirm pozzolanic potential and interpret hydration effects.

2.2.3 Preparation of concrete mixes: normal strength and high strength with varying metakaolin content

Concrete mixes were designed to achieve both normal strength concrete (NSC) and high strength concrete (HSC) categories, with metakaolin incorporated as a partial replacement of cement at 0, 5, 7.5, 10, and 12.5% weights of cement at a constant water-binder ratio of 0.55 for normal strength concrete and 0.4 for high strength concrete. The admixture was also maintained at 1.5% of the weights of cementitious material proportions as specified by the manufacturer. The mix design, concrete casting, and curing process adhered to ASTM C192/C192M-15[20] standard guidelines to achieve target compressive strengths reflective of typical structural applications. For each metakaolin replacement category, four concrete cylinders were prepared for 7 and 28-day compressive strength and density derivations, two samples for 7-day testing and two samples for 28-day testing.

From *Table 3*, mixes were batched on a weight basis, with no adjustments made to the water content to evaluate workability as influenced by the high surface area and fineness of metakaolin particles. Ultracrete61 superplasticiser was utilised to optimise the rheological properties of the fresh concrete without compromising the hydration process. Each mix batch is identified with a unique number, NS-0.55CM100MK0**,** with NS and HS signifying the nature of concrete, NS-Normal strength concrete, HS-High Strength Concrete. The first two letters are followed by a water-binder ratio (0.55 and 0.40), next to it is the cement content, **CM 87.5** to **CM 100.** Numbers signify the percentage by weight of cement in the reference mix. The next number is the percentage by weight of Metakaolin in the mix. This ranges from **MK 0 to MK 12.5** in the mixes. Finally, some mixes have the letter "A" after the mix specimen Identity. This signifies the mixes containing Admixture.

NORMAL STRENGTH CONCRETE							
S/ No	SPECIMEN ID	CE-MENT (kg/ m³)	WATER (kg/ m³)	META-KAOLIN (kg/m³)	SAND (kg/ m³)	CHIP-PINGS (kg/m³)	AD-MIX (%)
1	NS-0.55CM100MK0	375.00	205	0.00	583.00	1239.00	0
2	NS-0.55CM95MK5	356.25	131.25	18.75	583.00	1239.00	0
3	NS-0.55CM92.5MK7.5	346.88	131.25	28.13	583.00	1239.00	0
4	NS-0.55CM90MK10	337.50	131.25	37.50	583.00	1239.00	0
5	NS-0.55CM87.5MK12.5	328.13	131.25	46.88	583.00	1239.00	0
6	NS-0.55CM100MK0 A	375.00	205	0.00	583.00	1239.00	1.5
7	NS-0.55CM95MK5 A	356.25	131.25	18.75	583.00	1239.00	1.5
8	NS-0.55CM92.5MK7.5 A	346.88	131.25	28.13	583.00	1239.00	1.5
9	NS-0.55CM90MK10 A	337.50	131.25	37.50	583.00	1239.00	1.5
10	NS-0.55CM87.5MK12.5 A	328.13	131.25	46.88	583.00	1239.00	1.5
HIGH STRENGTH CONCRETE							
S/ No	SPECIMEN ID	CE-MENT (kg/ m³)	WATER (kg/ m³)	META-KAOLIN (kg/m³)	SAND (kg/ m³)	CHIP-PINGS (kg/m³)	AD-MIX (%)
1	HS-0.4CM100MK0	620	205	0	645.98	984.47	0
2	HS-0.4CM95MK5	589	155	31	645.98	984.47	0
3	HS-0.4CM92.5MK7.5	573.5	155	46.5	645.98	984.47	0
4	HS-0.4CM90MK10	558	155	62	645.98	984.47	0
5	HS-0.4CM87.5MK12.5	542.5	155	77.5	645.98	984.47	0
6	HS-0.4CM100MK0A	620	205	0	645.98	984.47	1.5
7	HS-0.4CM95MK5 A	589	155	31	645.98	984.47	1.5
8	HS-0.4CM92.5MK7.5 A	573.5	155	46.5	645.98	984.47	1.5
9	HS-0.4CM90MK10 A	558	155	62	645.98	984.47	1.5
10	HS-0.4CM87.5MK12.5 A	542.5	155	77.5	645.98	984.47	1.5

Table 3 Concrete mix design matrix for normal and high strength concrete
3. táblázat Beton összetétel-tervezési mátrix normál és nagy szilárdságú betonokhoz

2.2.4 Sample casting and curing procedures

Concrete samples were produced using a 100 mm diameter and 200 mm high cylinder following ASTM C31/C31M [21] procedures to ensure homogeneity and minimise variability in sample preparation. Concrete was mixed using a laboratory pan mixer to ensure thorough blending of all constituents. Fresh concrete was cast into cylindrical moulds for compressive strength testing. Each mould was subjected to vibration to eliminate entrapped air and ensure compaction.

Following casting, specimens were demoulded after 24 hours and transferred to a controlled curing environment maintained at standard temperature and humidity conditions. Curing periods of 7 and 28 days were adopted to evaluate both early and later-age properties. The curing regime was strictly monitored to prevent moisture loss and temperature fluctuations that could adversely affect hydration and microstructural development.

2.2.5 Compressive strength tests

Compressive strength, fck, was measured on multiple concrete cylindrical specimens at 7 and 28 days using a calibrated 2000KN hydraulic testing machine. The maximum load at failure was recorded, and the strength was calculated by dividing by the cross-sectional area. Average values ensured statistical reliability. *Fig. 1* shows the production and testing of the cylindrical concrete specimen.

The compressive strength was calculated by

$$fck = \frac{Failure\ load(KN)}{cross\text{-}sectional\ Area\ of\ sample(mm^2)} \quad (1)$$

Fig. 1 Production and testing of metakaolin blended cement concrete specimen
1. ábra Metakaolinnal kevert cementbeton próbatestek gyártása és vizsgálata

2.2.6 Density measurements

The concrete density was determined at 7 and 28 days by measuring the mass and volume using a digital weighing balance and dividing the resulting mass by the volume of the concrete cylindrical sample. Density data complemented strength results to assess microstructural compactness and porosity influenced by metakaolin.

3. Data collection

Experimental data for particle size distributions, specific gravity, compressive strength, density, water binder ratio, admixture dosage, and workability were systematically recorded; the compressive strength and densities of the concrete were recorded in two (2) replicates to capture variability. Statistical analyses were used to summarise results, while quality control measures, including equipment calibration and verification, ensured data validity, supporting subsequent correlation and interpretation.

3.1 Results

Fig. 2 presents the sieve analysis of metakaolin using the Malvern Zetasizer, revealing a finely graded particle size predominantly within the sub-micron to low-micron range. The sample is polydisperse, as indicated by the multiple peaks and the Polydispersity index (PDI) value. The Z-average provides an overall average size, but the distribution shows distinct particle populations.

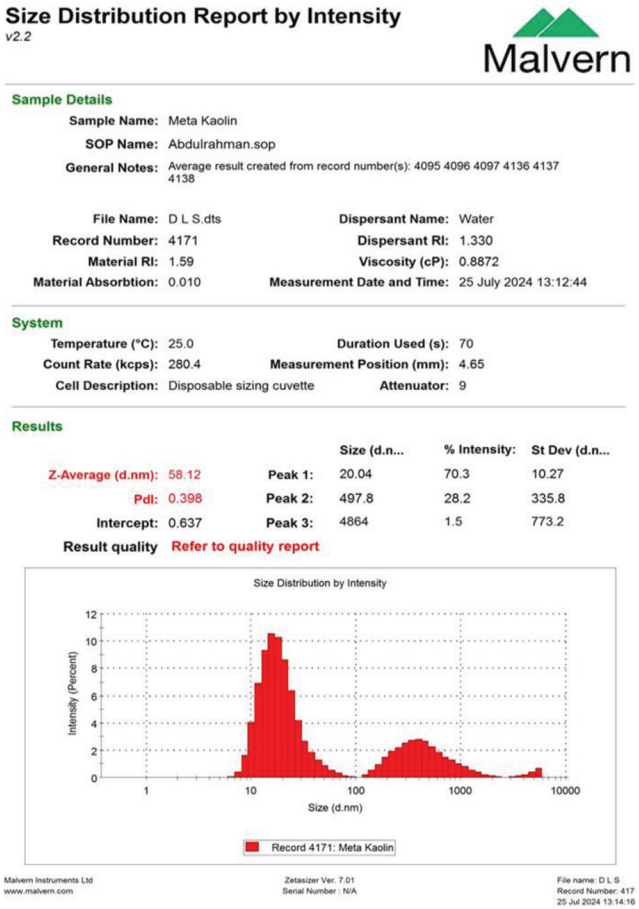

Fig. 2 Sieve Analysis of Metakaolin Using Malvern Zetasizer Laser Machine
2. ábra A metakaolin szitaelemzése (szemcseméret-eloszlása) Malvern Zetasizer lézeres berendezéssel

Peak Sizes and Intensities

Peak 1: Around 20.04 nm with an intensity of 70.3%. This is the dominant population.

Peak 2: Around 497.8 nm with an intensity of 28.2%.

Peak 3: Around 4864 nm with an intensity of 1.5%. This population has the lowest intensity.

Z-Average: The Z-average particle size is 58.12 nm. This is an intensity-weighted average and is heavily influenced by the larger particles. In a polydisperse sample, the Z-average may not accurately represent the typical particle size.

Polydispersity Index (Pdl): The Pdl is 0.398. A Pdl closer to 0 indicates a monodisperse sample (all particles are of similar size), while a value closer to 1 indicates a highly polydisperse sample. 0.398 suggests a moderately polydisperse distribution.

The analysis reveals that the Metakaolin sample contains particles ranging from approximately 20 nm to nearly 5000 nm, with a dominant population around 20 nm. The graph shows multiple peaks with three distinct peaks, indicating the presence of at least three different populations of particles. This fine particle size significantly enhances the pozzolanic reactivity by increasing the surface area available for reaction with calcium hydroxide, leading to improved microstructural density and, consequently, higher concrete strength and durability. However, the high fineness also tends to increase the water demand of the mix, which adversely affects workability without suitable admixtures. Therefore, controlling the particle size distribution is crucial for achieving an optimal balance between hardened mechanical performance and fresh properties of concrete.

S/ No	SPECIMEN ID	Slump (mm)	7 days			28 days		
			Density (kg/m³)	Stress (N/mm²)	AV. Stress (N/mm²)	Density (kg/m³)	Stress (N/mm²)	AV. Stress (N/mm²)
1	NS-0.55CM100MK0	83	2431.57	22.92 23.55	**23.23**	2488.86	32.46 33.10	**32.78**
2	NS-0.55CM95MK5	70	2444.30	24.19 24.19	**24.19**	2504.77	34.37 34.37	**34.37**
3	NS-0.55CM92.5MK7.5	64	2460.22	24.82 24.57	**24.70**	2498.41	35.65 35.65	**35.65**
4	NS-0.55CM90MK10	60	2466.58	26.73 26.10	**26.42**	2495.23	38.19 36.92	**37.56**
5	NS-0.55CM87.5MK12.5	55	2482.50	23.55 24.19	**23.87**	2555.70	33.10 34.37	**33.74**
6	NS-0.55CM100MK0 A	150	2492.04	28.64 28.01	**28.33**	2568.43	40.74 39.47	**40.10**
7	NS-0.55CM95MK5 A	125	2517.50	29.28 30.55	**29.92**	2574.79	42.01 43.28	**42.65**
8	NS-0.55CM92.5MK7.5 A	121	2517.50	31.83 32.46	**32.15**	2581.16	45.83 45.83	**45.83**
9	NS-0.55CM90MK10 A	95	2555.70	33.10 32.46	**32.78**	2574.79	47.10 49.01	**48.06**
10	NS-0.55CM87.5MK12.5 A	74	2565.25	29.28 28.64	**28.96**	2587.52	42.01 40.74	**41.37**

Table 4 Fresh and hardened properties of normal strength concrete specimens with varying metakaolin content at 7 and 28 days
4. táblázat Különböző metakaolin-tartalmú normál szilárdságú betonpróbatestek friss és megszilárdult tulajdonságai 7 és 28 napos korban

Fig. 3 and *Table 4* illustrates the impact of metakaolin (MK) replacement (0% to 12.5%) and Ultracrete 61 superplasticizer on the compressive strength of normal strength concrete (NSC) with a water binder (W/B) ratio of 0.55, showing strength increases from 23.83 N/mm² to 37.56 N/mm² at 7 days and 32.78 N/mm² to 48.06 N/mm² at 28 days without and with superplasticizer, respectively. The optimal MK replacement is 10%, yielding the highest strength (48.06 N/mm² at 28 days with superplasticiser), due to enhanced pozzolanic activity and improved matrix density, though strength declines at 12.5% due to cement dilution. The superplasticiser improved the workability of the resulting concrete (Slump from 55 mm to 150 mm) in normal concrete mixes and strength by improving particle dispersion, suggesting its value in metakaolin-modified concrete.

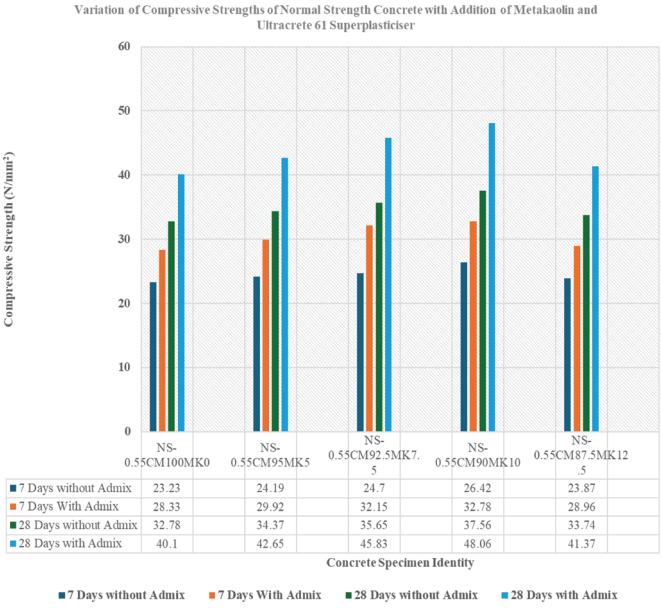

Fig. 3 Variation of compressive strength of normal concrete with addition of metakaolin and Ultracrete 61 superplasticiser
3. ábra A normál beton nyomószilárdságának változása metakaolin és Ultracrete 61 szuperfolyósító hozzáadásával

S/ No	SPECIMEN ID	Slump (mm)	7 Days			28 Days		
			Density (kg/m³)	Stress (N/mm²)	AV. Stress (N/mm²)	Density (kg/m³)	Stress (N/mm²)	AV. Stress (N/mm²)
1	HS-0.40CM100MK0	87	2486.03	35.65 36.92	**36.28**	2511.14	50.92 52.20	**51.56**
2	HS-0.40CM95MK5	80	2498.63	40.74 40.10	**40.42**	2523.87	58.56 57.29	**57.92**
3	HS-0.40CM92.5MK7.5	70	2501.78	42.01 43.28	**42.65**	2527.05	59.83 62.38	**61.11**
4	HS-0.40CM90MK10	65	2508.08	44.56 45.19	**44.88**	2533.42	63.65 64.93	**64.29**
5	HS-0.40CM87.5MK12.5	60	2545.89	38.83 38.19	**38.51**	2571.61	56.02 54.74	**55.38**
6	HS-0.40CM100MK0 A	150	2567.95	40.74 42.01	**41.37**	2593.89	58.56 59.83	**59.20**
7	HS-0.40CM95MK5 A	135	2574.25	44.56 44.56	**44.56**	2600.25	63.65 63.65	**63.65**
8	HS-0.40CM92.5MK7.5 A	120	2580.55	46.47 45.83	**46.15**	2606.62	66.20 64.93	**65.56**
9	HS-0.40CM90MK10 A	100	2574.25	47.74 47.10	**47.42**	2600.25	72.57 67.47	**70.02**
10	HS-0.40CM87.5MK12.5 A	85	2586.86	43.28 43.92	**43.60**	2612.99	62.38 63.02	**62.70**

Table 5 Fresh and hardened properties of high-strength concrete specimens with varying metakaolin content at 7 and 28 days
5. táblázat Különböző metakaolin-tartalmú nagy szilárdságú betonpróbatestek friss és megszilárdult tulajdonságai 7 és 28 napos korban

Table 5 presents the density and compressive strength results of high-strength concrete specimens with varying metakaolin contents, tested at 7 and 28 days. The data show a consistent increase in both density and compressive strength over time, reflecting the ongoing hydration and pozzolanic reactions facilitated by metakaolin. Specimens labelled with "A" generally exhibit higher densities and strengths compared to their non-"A" counterparts, indicating enhanced performance due to Ultracrete 61 superplasticiser additions. This trend suggests that increasing metakaolin content up to certain levels improves microstructural densification, which directly contributes to higher compressive strength. Notably, the densest specimens correspond to the highest strength values at both curing ages, supporting the strong positive correlation between these parameters. However, some variation in strength at similar densities hints at the complex interactions of metakaolin with other mix components, emphasising the need for precise control of replacement levels and curing practices to maximise concrete performance.

Fig. 4 illustrates that the addition of Ultracrete 61 superplasticiser significantly enhances the compressive strength of high-strength concrete specimens at both 7 and 28 days. The strength gains are more pronounced at 28 days, indicating that the superplasticiser effectively improves particle dispersion and hydration, thereby densifying the concrete matrix and boosting long-term mechanical performance.

The slump also improved from 87 mm for mixes without admixture to 150 mm for the same mixture produced with Ultracrete 61 admixture, as shown in *Table 5*.

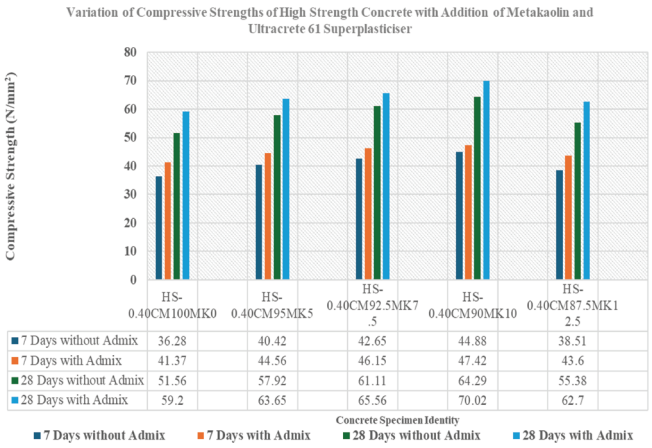

Fig. 4 Variation of compressive strength on high-strength concrete with addition of Ultracrete61 superplasticizer
4. ábra A nagy szilárdságú beton nyomószilárdságának változása Ultracrete 61 szuperfolyósító hozzáadásával

Table 6 presents the detailed oxide composition analysis of metakaolin using X-ray fluorescence (XRF) spectroscopy. The data show that the primary components are silica (SiO_2) at 55.614 mg/cm² (67.483 mol%) and alumina (Al_2O_3) at 37.119 mg/cm² (26.542 mol%), which together constitute most of the material and are critical for its pozzolanic activity. Minor oxides such as Fe_2O_3, TiO_2, SO_3, and K_2O are present in smaller quantities, potentially influencing hydration kinetics and durability. Trace elements like V_2O_5, Cr_2O_3, MnO, and others are detected at very low levels, typically under 0.1 mg/cm². The absence or negligible amounts of oxides like WO_3 and MgO suggest minimal interference with pozzolanic reactions. The presence of chlorine (Cl) at 0.95 mg/cm² (1.954 mol%) could have implications for corrosion resistance and needs to be monitored in mix designs. This comprehensive chemical profile is essential for understanding the reactivity and performance potential of the metakaolin in cementitious systems

S/No	Sample Layer	Component	Component (mg/cm²)	Moles (%)
1	1	SiO_2	55.614	67.483
2	1	V_2O_5	0.034	0.013
3	1	Cr_2O_3	0.026	0.013
4	1	MnO	0.055	0.056
5	1	Fe_2O_3	3.561	1.626
6	1	CoO	0.009	0.005
7	1	NiO	0.01	0.01
8	1	CuO	0.043	0.04
9	1	Nb_2O_5	0.017	0.005
10	1	WO_3	0.0	0.0
11	1	P_2O_5	0.126	0.065
12	1	SO_3	0.674	0.613
13	1	CaO	0.423	0.55
14	1	MgO	0.0	0.0
15	1	K_2O	0.859	0.665
16	1	BaO	0.039	0.018
17	1	Al_2O_3	37.119	26.542
18	1	Ta_2O_5	0.041	0.007
19	1	TiO_2	0.309	0.282
20	1	ZnO	0.015	0.013
21	1	Ag_2O	0.01	0.003
22	1	Cl	0.95	1.954
23	1	ZrO_2	0.049	0.029
24	1	SnO_2	0.0	0.0
25	1	SrO	0.004	0.003
26	1	Rb_2O	0.009	0.003
27	1	Y_2O_3	0.009	0.003

Table 6 Metakaolin oxide composition analysis (XRF method)
6. táblázat A metakaolin oxidösszetétel-elemzése (XRF módszer)

3.2 Interpretation and synthesis of metakaolin chemical composition and its implications for concrete performance

The XRF analysis showed that metakaolin is composed high percentage of silica (SiO_2) and alumina (Al_2O_3), over 94% by mole, confirming strong pozzolanic activity essential for forming strength-enhancing hydration products like C-S-H and calcium aluminate hydrate. Minor oxides such as Fe_2O_3, TiO_2, SO_3, and K_2O may aid hydration and microstructure refinement of the resulting concrete. Negligible harmful oxides like MgO and WO_3 reduce risks of expansion or instability. Elevated chlorine content signals potential corrosion risks in reinforced concrete, requiring careful mix design. Trace elements are present in low amounts, with minimal direct

impact but possible subtle effects on durability. Overall, this composition supports metakaolin's role in enhancing concrete strength and durability, provided chloride levels are controlled for long-term performance.

4. Conclusion and recommendations

The structural effects of utilising metakaolin and high-performance superplasticizer on the compressive response and density evolution of normal- and high-strength concretes were quantitatively evaluated in this study. The metakaolin used had a Z-average of 58.12 nm with multimodal peaks at roughly 20 nm, 498 nm, and 4864 nm, and a chemical profile dominated by SiO_2 (67.48 mol%) and Al_2O_3 (26.54 mol%), totalling 94% reactive oxides. Strong pozzolanic potential was established by this nanostructured fineness and high aluminosilicate content, which had a direct impact on microstructural densification and hydration kinetics.

In normal-strength concrete (NSC), metakaolin replacement from 0 to 10% resulted in clear strength gains. At 7 days, compressive strength increased from 23.23 N/mm² (control) to 26.42 N/mm² at 10% MK, representing a 13.7% improvement. At 28 days, strength increased from 32.78 N/mm² to 37.56 N/mm² (14.6% increase). Density also increased from 2488.86 to 2495.23 kg/m³ over the same replacement range, indicating reduced pore volume and enhanced binder packing. With Ultracrete 61, the 28-day compressive strength rose further to 48.06 N/mm², representing a 46.7% improvement relative to the unmodified control. The slump improved from 83 mm to 150 mm, demonstrating that the admixture effectively counteracted metakaolin's high water demand and enabled full reactivity.

High-strength concrete (HSC) exhibited similar quantitatively significant responses. At 7 days, strength increased from 36.28 N/mm² to 44.88 N/mm² at 10% MK (23.7% gain). At 28 days, strength increased from 51.56 N/mm² to 64.29 N/mm² (24.7% gain). For mixes containing Ultracrete 61, 28-day strength reached 72.57 N/mm², equivalent to a 40.8% increase over the control and a 12.9% increase over the 10% MK mix without admixture. Density rose from 2511.14 kg/m³ (control) to 2533.42 kg/m³ at 10% MK and further to 2600.25 kg/m³ with admixture incorporation. These density increments (up to +3.5%) strongly correlate with the observed strength development, reinforcing the mechanistic link between metakaolin-induced refinement of the pore structure and compressive resistance.

Despite these mechanical advantages, XRF analysis revealed a chloride content of 1.95 mol%, significantly higher than the 0.1% limit recommended for reinforced concrete under ACI 318. This concentration necessitates a cautious approach regarding durability and demands source-specific mitigation strategies. Nevertheless, the favourable oxide composition, minimal deleterious impurities, and the demonstrated strength enhancements confirm the technical viability of this metakaolin for structural-grade concrete, provided durability safeguards are adopted. Overall, the study establishes a clear quantitative performance envelope: 0–10% metakaolin maximises strength, density, and workability (with admixture) for both NSC and HSC, while greater than 10% replacement leads to cement dilution and mechanical decline. The synergy between fine metakaolin particles and superplasticiser action was shown to be indispensable for achieving optimal dispersion, hydration, and matrix consolidation.

4.1 Recommendations

1. The ideal replacement level for structural concrete is 10% metakaolin, which results in strength gains of 14–25% without admixture and up to 46% with Ultracrete 61 in NSC and 40% in HSC. Because clinker availability is gradually decreasing and mechanical response is deteriorating, replacement levels higher than 10% should be avoided.
2. Require all locally sourced metakaolin to undergo oxide and impurity profiling. Remedial measures such as washing, blending with low-chloride SCMs, or limiting use in reinforced members should be included in quality control and mix design procedures, given the measured chloride content of 1.95 mol%.
3. Choose high-performance water reducers at levels of less than or equal to 1.5%. The results exhibit substantial enhancements in strength (up to +46.7% in NSC) and workability (up to +81% slump increase), confirming their crucial role in overcoming water demand from sub-micron metakaolin.
4. Extend mechanical evaluation to durability indices, such as sulphate resistance, sorptivity, carbonation depth, and chloride diffusion coefficients. These measurements are crucial for creating predictive models that relate oxide chemistry, particle fineness, and material durability.
5. Advocate regional investment in metakaolin processing, considering the study demonstrated that, when properly processed and characterised, locally sourced metakaolin, even with impurities, can achieve structural-grade performance comparable to imported alternatives.
6. To standardise metakaolin quality for commercial concrete, establish performance-based specifications that incorporate quantitative thresholds, oxide indices (greater than 70% for SiO_2+Al_2O_3), chloride limit (<0.1%), target particle fineness (<1 μm median size), and mechanical benchmarks (≥20% strength enhancement at 28 days).

Acknowledgement

The authors are grateful to the Department of Civil Engineering, Rivers State University, for permission to use their laboratory for the performance of this experiment.

Author contributions

Justin Egbebike: Conceptualization, Methodology, Field study, **Fidelis Okafor:** Reviewing -Original draft preparation, Validation, **Chijioke Ikeagwuani:** Visualization, Investigation, Writing-Reviewing and Editing.

Conflicts of interest

The authors declare no conflicts of interest.

References

[1] Hasan, N. M. S., Shaurdho, N. M. N., Sobuz, M. H. R., Meraz, M. M., Islam, M. S., & Miah, M. J. (2023). Utilisation of waste glass cullet as partial substitution of coarse aggregate to produce eco-friendly concrete: role of metakaolin as cement replacement. *Sustainability*, *15*(14), 11254.'

[2] Faraz, M. I., Arifeen, S. U., Amin, M. N., Nafees, A., Althoey, F., & Niaz, A. (2023, July). A comprehensive GEP and MEP analysis of a cement-based concrete containing metakaolin. In *Structures* (Vol. 53, pp. 937-948). Elsevier.

[3] Kara, İ. F., Ashour, A. F., & Bilim, C. (2019). Flexural behaviour of hybrid FRP-concrete bridge decks. *Turkish Journal of Engineering*, *3*(4), 206-217.

[4] Tiza, M. T., Okafor, F., & Agunwamba, J. (2024). Application of Scheffe's Simplex Lattice Model in concrete mixture design and performance enhancement. *Environmental Research and Technology*, *7*(2), 270-279.

[5] Egbebike, J. N., & Anyanwu, B. I.(2024). Effect of Thermal Desorption Unit Residue (TDUR) On Compressive Strength of Concrete and Mortar. *Journal of Advanced Cement & Concrete Technology*, *7*(3).

[6] Chandar, S. P., Raganathan, S., & Ramachandran, R. (2023). CO2 emission analysis of metakaolin and alccofine-replaced cement in M40 grade concrete. *Environmental Science and Pollution Research*, *30*(47), 104408-104414.

[7] Rocha, J. H. A., & Toledo Filho, R. D. (2024). Microstructure, hydration process, and compressive strength assessment of ternary mixtures containing Portland cement, recycled concrete powder, and metakaolin. *Journal of Cleaner Production*, *434*, 140085.

[8] Sesugh, T., Onyia, M., & Fidelis, O. (2024). Predicting the compressive strength of self-compacting concrete using artificial intelligence techniques: A review. *Turkish Journal of Engineering*, *8*(3), 537-550.

[9] Olofinnade, O. M., & Osoata, O. P. (2023). Performance assessment of mechanical properties of green normal-strength concrete produced with metakaolin-cement-coated recycled concrete aggregate for sustainable construction. *Construction and Building Materials*, *407*, 133508.

[10] Harikaran, M., Gokulakannan, S., Loganathan, A., Chandiran, R. D., Ajith, M., & Dhanasekar, V. (2023). Metakaolin cement concrete evaluation using industrial by-products as fine aggregate. *Materials Today: Proceedings*.

[11] Selvaraj, T., T, S., Kaliyavaradhan, S. K., Kakria, K., & Malladi, R. C. (2022). Use of E-waste in metakaolin blended cement concrete for sustainable construction. *Sustainability*, *14*(24), 16661.

[12] Bilim, C., & Atiş, C. (2017). Carbonation resistance of slag mortars activated by different alkali activators. *Turkish Journal of Engineering*, *1*(1), 1-4.

[13] Ikeagwuani, C. C., Alexander, T. C., Usanga, I. N., Opoh, E. I., & Ezeobiukwu, C. O. (2024). Enhancement of highly expansive subgrade with metabentonite and nano-waste additive-based geopolymers. *International Journal of Pavement Engineering*, *25*(1), 2444491.

[14] Al-Hashem, M. N., Amin, M. N., Ajwad, A., Afzal, M., Khan, K., Faraz, M. I.,& Khan, H. (2022). Mechanical and durability evaluation of Metakaolin as cement replacement material in concrete. *Materials*, *15*(22), 7868.

[15] Ismail, M. H., Megat Johari, M. A., Ariffin, K. S., Jaya, R. P., Wan Ibrahim, M. H., & Yugashini, Y. (2022). [Retracted] Performance of High Strength Concrete Containing Palm Oil Fuel Ash and Metakaolin as Cement Replacement Material. *Advances in Civil Engineering*, *2022*(1), 6454789.

[16] Mathan Kumar, N., Suresh Kumar, R., Bharti, K., Nandhakumar, P. V., & Yuvaperiyasamy, M. (2025). A Comprehensive Study of Microstructure and Mechanical Properties in Friction Stir Welded AA 2024 and Nano Particle Reinforced Hybrid Composites. *Turkish Journal of Engineering (TUJE)*, *9*(2).

[17] Al-Akhras, N. M. (2006). Durability of metakaolin concrete to sulfate attack. *Cement and concrete research*, *36*(9), 1727-1734..

[18] Kumar, N. M., Ramalingam, S. K., Bharti, K., Nandhakumar, P. V., & Yuvaperiyasamy, M. (2025). A Comprehensive Study of Microstructure and Mechanical Properties in Friction Stir Welded AA 2024 and Nano Particle Reinforced Hybrid Composites. *Turkish Journal of Engineering*, *9*(2), 313-322.

[19] Sharma, P., Sharma, N., & Parashar, A. K. (2022). Scientific investigation of metakaolin-based cement concrete with rock sand infill. *Materials Today: Proceedings*, *62*, 4147-4150.

[20] Izadifard, R. A., Abdi Moghadam, M., & Sepahi, M. M. (2021). Influence of metakaolin as a partial replacement of cement on characteristics of concrete exposed to high temperatures. *Journal of Sustainable Cement-Based Materials*, *10*(6), 336-352.

[21] Yasar, E., Atis, C. D., & Kiliç, A. (2004). High Strength Lightweight Concrete Made with Ternary Mixtures of Cement-Fly Ash-Silica Fume and Scoria as Aggregate. *Turkish Journal of Engineering & Environmental Sciences*, *28*(2).

[22] Bayer, İ. R., Turanlı, L., & Mehta, P. K. (2019). Mass concrete construction using self-compacting mortar. *Turkish Journal of Engineering*, *3*(3), 110-119.

[23] Kannan, V., & Raja Priya, P. (2021). Evaluation of the permeability of high-strength concrete using metakaolin and wood ash as partial replacement for cement. *SN Applied Sciences*, *3*(1), 90.

[24] Standard, A. S. T. M. C192/C192M-15. (2015). *Standard Practice for Making and Curing Concrete Test Specimens in the Laboratory. West Conshohocken: ASTM International.*

[25] ASTM C31/C31M. (2015). Standard practice for making and curing concrete test specimens in the field

[26] EN, B. (2002). BS EN 1008: 2002 Mixing water for concrete. *Specification for Sampling, Testing and Assessing the Suitability of Water, Including Water*.

[27] ASTM, A. C618-12; 2012 standard specification for coal fly ash and raw or calcined natural pozzolan for use in concrete. *ASTM, Philadelphia*.

[28] ASTM. (2007). ASTM C150-07: Standard Specification for Portland Cement.

[29] EN, B. (2012). 933-1: 2012 Tests for geometrical properties of aggregates. *Determination of particle size distribution. Sieving method*.

[30] ACI, A. (2019). 318-19 & ACI 318R-19: Building code requirements for structural concrete and commentary. *American Concrete Institute: Farmington Hills, MI, USA*.

Ref.:

Egbebike, Justin Nsobundu – **Okafor**, Fidelis Onyebuchi – **Ikeagwuani**, Chijioke Christopher: *Structural effect of combined metakaolin and high-performance superplasticizers on the compressive behaviours of normal and high strength concrete*

Építőanyag – Journal of Silicate Based and Composite Materials, Vol. 77, No. 3 (2025), 91–98 p.

https://doi.org/10.14382/epitoanyag-jsbcm.2025.12

GUIDELINE FOR AUTHORS

The manuscript must contain the followings: title; author's name, workplace, e-mail address; abstract, keywords; main text; acknowledgement (optional)**; references; figures, photos with notes; tables with notes; short biography** (information on the scientific works of the authors).

The full manuscript should not be more than 6 pages including figures, photos and tables. Settings of the word document are: 3 cm margin up and down, 2,5 cm margin left and right. Paper size: A4. Letter size 10 pt, type: Times New Roman. Lines: simple, justified.

TITLE, AUTHOR

The title of the article should be short and objective.

Under the title the name of the author(s), workplace, e-mail address.

If the text originally was a presentation or poster at a conference, it should be marked.

ABSTRACT, KEYWORDS

The abstract is a short summary of the manuscript, about a half page size. The author should give keywords to the text, which are the most important elements of the article.

MAIN TEXT

Contains: materials and experimental procedure (or something similar), results and discussion (or something similar), conclusions.

REFERENCES

References are marked with numbers, e.g. [6], and a bibliography is made by the reference's order. References should be provided together with the DOI if available.

Examples:

Journals:

[6] Mohamed, K. R. – El-Rashidy, Z. M. – Salama, A. A.: In vitro properties of nano-hydroxyapatite/chitosan biocomposites. *Ceramics International.* 37(8), December 2011, pp. 3265–3271, http://doi.org/10.1016/j.ceramint.2011.05.121

Books:

[6] Mehta, P. K. – Monteiro, P. J. M.: Concrete. Microstructure, properties, and materials. *McGraw-Hill*, 2006, 659 p.

FIGURES, TABLES

All drawings, diagrams and photos are figures. The **text should contain references to all figures and tables**. This shows the place of the figure in the text. Please send all the figures in attached files, and not as a part of the text. **All figures and tables should have a title**.

Authors are asked to submit color figures by submission. Black and white figures are suggested to be avoided, however, acceptable.

The figures should be: tiff, jpg or eps files, 300 dpi at least, photos are 600 dpi at least.

BIOGRAPHY

Max. 500 character size professional biography of the author(s).

CHECKING

The editing board checks the articles and informs the authors about suggested modifications. Since the author is responsible for the content of the article, the author is not liable to accept them.

CONTACT

Please send the manuscript in electronic format to the following e-mail address: femgomze@uni-miskolc.hu and epitoanyag@szte.org.hu or by post: Scientific Society of the Silicate Industry, Budapest, Bécsi út 122–124., H-1034, HUNGARY

We kindly ask the authors to give their e-mail address and phone number on behalf of the quick conciliation.

Építőanyag – *Journal of Silicate Based and Composite Materials*, Quarterly peer-reviewed periodical of the Hungarian Scientific Society of the Silicate Industry, SZTE.
http://epitoanyag.org.hu